FTI-Initiative Vorzeigeregion Energie

2.Ausschreibung

Publizierbarer Endbericht

Programmsteuerung:
Klima- und Energiefonds

Programmabwicklung:
Österreichische Forschungsförderungsgesellschaft mbH (FFG)

Endbericht
erstellt am
14/11/2021

SANBA – Development of a low-temperature heating and cooling grid for the future
Smart Anergy Quarter Baden

Projektnummer: 868655

Ausschreibung	2. Ausschreibung Vorzeigeregion Energie
Projektstart	01.09.2018
Projektende	30.06.2021
Gesamtprojektdauer (in Monaten)	34 months
ProjektnehmerIn (Institution)	AIT Austrian Institute of Technology GmbH
AnsprechpartnerIn	DI Dr. Edith Haslinger
Postadresse	Giefinggasse 6; 1210 Vienna
Telefon	+43 50550 - 3608
Fax	+43 50550 - 6390
E-mail	edith.haslinger@ait.ac.at
Website	www.ait.ac.at

SANBA

Developing a simulation algorithm for a low-temperature heating/cooling grid for the future Smart Anergy Quarter Baden

AutorInnen:
Edith Haslinger, Robin Friedrich, Veronica Vana, AIT Austrian Institute of Technology GmbH
Veronika Turewicz, Gregor Götzl, Geologische Bundesanstalt
Karl Ponweiser, Viktoria Illyés, David Huber, Technische Universität Wien
Andreas Hammer, Montanuniversität Leoben
David Stuckey, Philipp Stern, Institute of Building Research & Innovation
Peter Biermayr, ENFOS

Gerhard Bartak, NÖM AG
Gerfried Koch, Stadt Baden
Richard Niederbrucker, geohydrotherm GmbH
Franz Vogl, David Bauernfeind, beyond carbon energy

Table of Contents

Table of Contents 4
1 Introduction 7
1.1 Low-temperature heating and cooling grids 7
2 Investigation area 9
2.1 History and background of the military camp “Martinek-Kaserne” 9
2.2 Scenarios for a future use of the “Martinek-Kaserne” and resulting research questions 10
2.3 Introduction into the design of the LTHC grid 12
3 Geoscientific site assessment and geothermal energy potential 14
3.1 Legal framework for geothermal energy use in Lower Austria 14
3.2 Hydrogeological and geothermal site information 14
3.2.1 Geological overview 14
3.2.2 Hydrogeological conditions 14
3.2.3 Hydrogeological 3D model 16
3.2.4 Geothermal potential and Thermal Response Tests 20
3.3 Numerical modelling of the BTES 24
3.3.1 Validation of the BTES model 25
3.3.2 Long-term simulation 28
4 Technical scenario assessment and system design 31
4.1 Energy demand of existing buildings 31
4.2 LTHC grid plan based on the three scenarios 33
4.2.1 MINI 34
4.2.2 MIDI 35
4.2.3 MAXI 37
5 Energy analysis of the dairy NÖM 39
5.1 Wastewater 39
5.2 Off-gas stream of the steam boiler plant 41
5.3 Waste heat from the recoolers of the cooling system for fresh products logistics (FRILO) 44
5.4 Chilling plant for production 45
5.5 Low pressure compressed air systems 46
5.6 Waste heat potential from the heat recovery of the stratified storage tank 46
5.7 Waste heat from the cooling circuit of high-pressure compressed air generation 47
5.8 Photovoltaic calculations 49
6 Thermo-hydraulic simulation of the LTHC grid 53
6.1 Pipe network and borehole heat exchangers 55
6.2 Energy Transfer Stations 58
6.2.1 Heat pumps 60
6.2.2 Heat exchangers 60

6.2.3 Buffer storage 61
6.2.4 Circulation pumps 61
6.3 Solar thermal energy 61
6.4 Photovoltaic & Battery Storages 62
6.5 Boundary conditions for the simulation 62
6.5.1 Temperatures 62
6.5.2 Thermophysical parameters of substrate and filling material 63
6.5.3 Demand profile 64
6.6 Design strategies for the anergy network and its components 64
7 Building technology assessment and system design 67
7.1 Characteristics of the Martinek military camp 68
7.2 Thermal-Energetic Investigation of the Existing Building 68
7.3 Structural components of the existing building stock 69
7.3.1 Exterior walls 70
7.3.2 Ceiling above upper floor 70
7.3.3 Ceiling above basement 70
7.3.4 Windows 71
7.4 Building damage documentation 71
8 Preservation and refurbishment concepts 74
8.1 Climate measures and preservation of indoor spaces 75
8.1.1 Moisture reduction of near-ground components 75
8.1.2 Salt reduction measures 76
8.1.3 Preservation of floors 77
8.1.4 Preservation of the exterior walls 77
8.1.5 Preservation of the windows 77
8.1.6 Salt reduction measures 78
8.1.7 Indoor climate measures and preservation of indoor spaces 78
8.2 Refurbishment measures 78
8.2.1 External insulation 80
8.2.2 External insulation of masonry with ground contact 81
8.2.3 Interior insulation 81
8.2.4 Thermal refurbishment of the windows 82
9 Economic assessment 83
9.1 Top-down evaluation approach through network figures 84
9.2 Bottom-up assessment approach on the basis of the capital value method 86
9.3 Further qualitative aspects 91
9.3.1 Benefits of the grid feed 91
9.3.2 Technical frame of the grid feed 91
9.3.3 Investment costs for the anergy network 91
9.3.4 Scale effects in the energy centres 93
9.3.5 The influence of learning effects 93
9.3.6 Failure reserve and redundancy 94

9.3.7 Cooling of buildings 94
9.3.8 Cost structure of anergy networks 95
10 Summary and conclusions 96
10.1 Summary of technical design of the LTHC grid 96
10.2 Summary of the available waste heat of the NÖM dairy 97
10.3 Economic Summary and Conclusions 98
11 Literature 100
12 Contact data 103
13 Annex 104
13.1 Geoscientific site evaluation 104
13.1.1 Geoelectric (DC) resistivity profiles 104
13.1.2 Profile sections used as data sources for the elaboration of the 3D model 104
13.2 Energetic evaluation of the scenarios 106
13.2.1 MINI 106
13.2.2 MIDI 108
13.2.3 MAXI 113
14 List of Figures 117
15 List of Tables 119

1 Introduction

1.1 Low-temperature heating and cooling grids

Low temperature heating and cooling (LTHC) grids are innovative approaches to meet the heating and cooling demand especially in urban areas. District heating systems face a transition of decreasing grid temperatures alongside the transition towards an increase in renewable energy use up to 100 % (Lund et al., 2014; Lund et al., 2017). LTHC grids were installed first in Switzerland around 10 years ago. In Austria, some research projects have dealt with the feasibility of those grids and in Vienna, there are two small LTHC grids in operation (Biermayr, et al., 2013; Götzl et al., 2017).

The topic of LTHC grids gains increasing attention particularly in urban areas in Austria, due to (I) the increasingly lower temperature demand of heating distribution systems in new buildings which often have a high building standard (passive house or similar); (II) energy efficiency measures in old buildings (thermal insulation, new windows etc.); and (III) the trend to decentralised heating and cooling grids with an increased share of renewables, supporting local or national climate and energy goals. The number of so-called local energy communities, especially in urban and sub-urban areas, where high-temperature district heating is not available or where the building and usage structure allows for low-temperature heating and cooling, is expected to increase substantially over the next years.

In general, the knowledge of the main components of LTHC grids is well developed. The actual challenge is not the design of the single components but rather the hydraulic and thermal interaction of all components with its high degrees of freedom. Standard procedures for the technical design of common district heating networks and geothermal installations are therefore not appropriate. For that reason, a fully dynamic simulation tool with coupled thermo-hydraulic processes is important for dimensioning the components and their interaction with the grid. In comparison to common district heating networks the flow direction is bidirectional. Hence, heat can be carried to and from the consumer, depending on the season and heating/cooling demand. The geothermal energy storage must balance the residuum of the actual energy demand of all users and should be designed with balanced annual heat load and discharge. Finally, a complex network with the interaction of many users and different load functions and constraints have to be considered in the system design. Additionally, the possible change of users or power loads must be taken into account and concepts for reliability have to be elaborated. In addition to the seasonal geothermal storage also technical thermal storages may play an important role, when a short time balance of heating and cooling is required or to optimize the heat pump operation time.

Furthermore, it is of advantage to use photovoltaic (PV) systems for the operation of the heat pumps and their impact will therefore be under investigation in this project.

LTHC grids are, technically speaking, networks of pipes, distributing water with temperatures in the range of 8 and 22 °C at most times (min. 2 and max. 30 °C) between individual buildings and/or groups of buildings. The water can be used for free cooling as well as cooling or heating with the help of heat pumps. Usually, the networks are connected to seasonal storage units for thermal energy (Figure 1) (Zach, 2016; Zach et al., 2016).

LTHC grids have the following main characteristics (Figure 1) (Zach et al., 2016):

- Low grid temperatures (4 - 30 °C) for supplying heat pumps (heating and cooling) as well as provision of free cooling capability, if the temperature level is suitable.
- Include seasonal underground storage of thermal energy, with balanced annual heat load and discharge.
- Implementation of available local low exergy heat sources (e.g.: waste heat, solar heat, geothermal resources, wastewater heat).
- Low carbon emission and low environmental footprint.

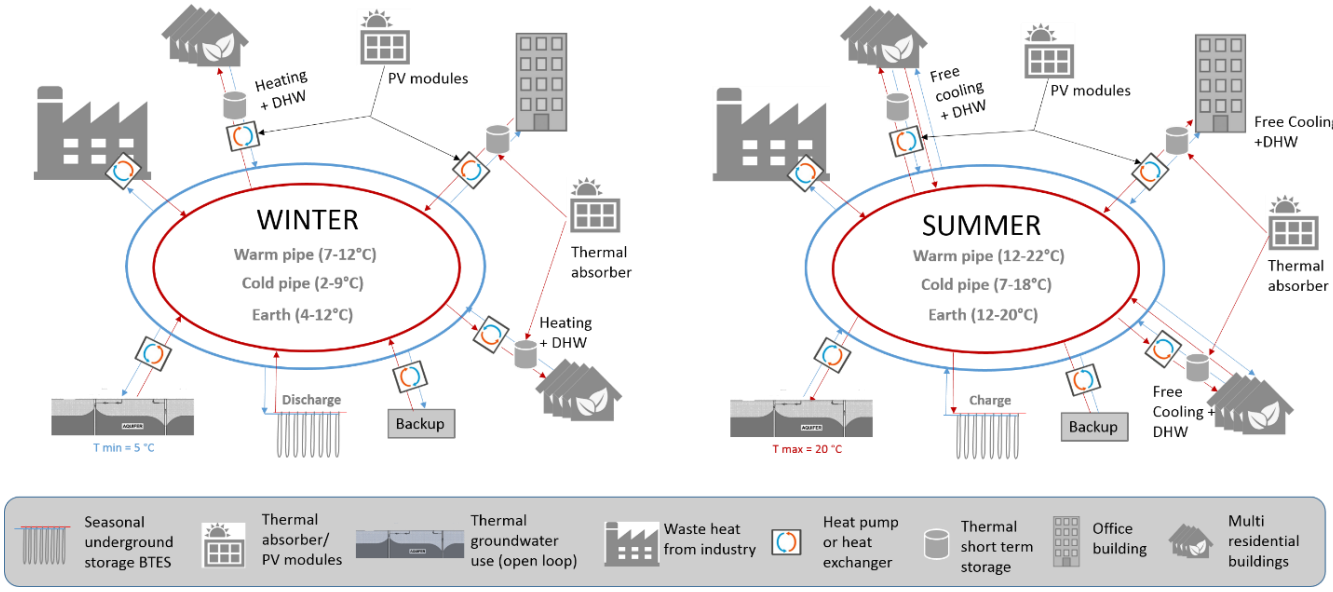

Figure 1: Illustration of the general concept of a low-temperature heating and cooling grid, its components, and the operating conditions in winter (left) and in summer (right).

2 Investigation area

2.1 History and background of the military camp “Martinek-Kaserne”

The former military camp “Martinek-Kaserne” was constructed by architect Leo Splett of the construction management of the German Luftwaffe during the war years 1938 to 1943 as antiaircraft defence base. After the Second World War, the camp was used by the Soviet Army and then by the Austrian Military until 2014, when the Military Camp was abandoned. The property owner is the Austrian Armed Forces with the Austrian Federal Ministry of Defence as superordinate institution.

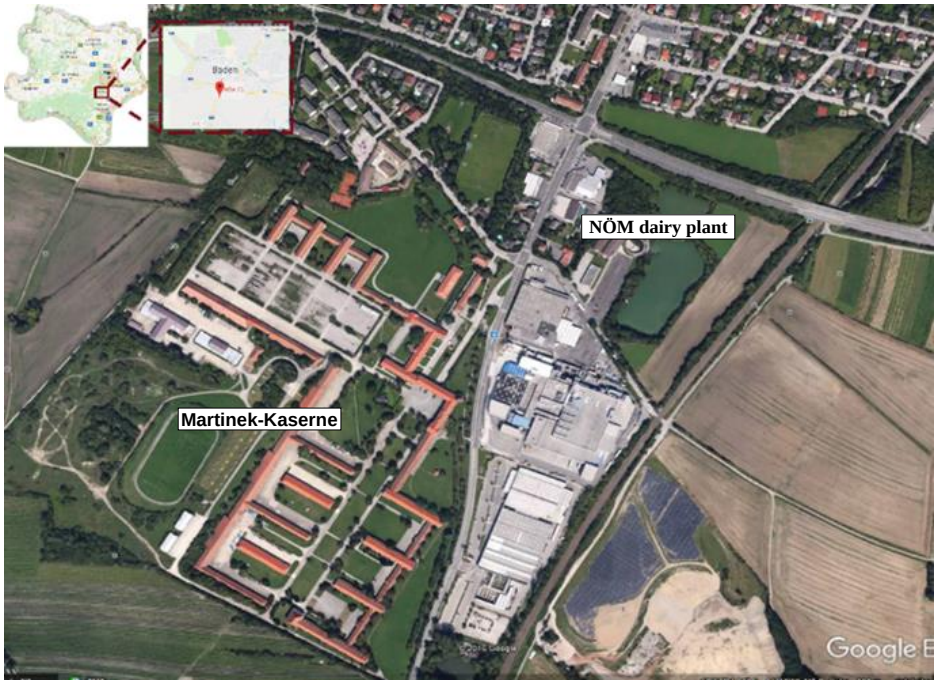

Figure 2: Satellite view of the “Martinek Kaserne” and the NÖM dairy plant (Google Earth)

The vast property with an area of 40 hectares with buildings protected by cultural heritage has been subject of several development plans over the years. Plans to sell the property to an investor were unsuccessful up to now, since the conditions of the buildings and the sheer size of the project has proven a challenge too big even for the most ambitious investors. Over the last years the main stakeholders, i.e. the Federal Ministry of Defence as property owner, the City of Baden, the Federal Monument Protection Agency, and the neighbouring municipality Sooß, which owns a small part of the “Martinek-Kaserne” property, have discussed several options for the future use of the area. Some areas of the former camp can potentially be developed with new buildings, whereas these developments have to be elaborated with the main stakeholders, mentioned before.

One of the biggest challenges of the project is the status of some of the buildings of the "Martinek-Kaserne". Since the abandonment in 2014, the condition of the buildings deteriorates very rapidly (Figure 3). In a meeting with the Federal Monument Protection Agency in April 2018, the representative of the Agency made a statement which summarizes the need for refurbishment measures concerning the buildings: *"One year of abandonment of the buildings has the same implications for the buildings as ten years of use".* This statement emphasizes the need for action, because every year of non-use deteriorates the buildings at an exorbitant rate. Independent of the future use of the buildings, there has to be a concept for refurbishment soon.

Buildings under cultural protection are subject to certain limitations in terms of thermal renovation and energy efficiency. From the provisions of monument preservation external insulation is usually not permitted, as they affect the appearance of the building massively. The focus is on measures that can increase energy efficiency without endangering their appearance or substance. Despite energy efficiency measures, buildings under protection usually have a higher heat load. Higher heat loads are provided by high flow temperatures of the heat distribution system. A LTHC grid works with low supply temperatures and usually requires customers to get accustomed to low supply temperatures to maximize the performance of the heat pumps.

2.2 Scenarios for a future use of the "Martinek-Kaserne" and resulting research questions

Over the past years after the abandonment, the "Martinek-Kaserne" has been subject to many development plans. The need for refurbishment of the buildings is given regardless of their future use. The refurbishment of the buildings that they are suitable for a low-temperature heating and cooling distribution system is a new aspect for the owner, the Federal Ministry of Defence. The Ministry itself carried out or ordered studies for a possible future use of the buildings. Three possible scenarios for planning and simulation of the LTHC grid for the "Martinek-Kaserne" were developed.

- Use of only the existing building stock with protected buildings ("Mini")
- Use of the existing buildings stock + 50 % of free area with new buildings ("Midi")
- Use of the existing building stock + 80 % of free area with new buildings ("Maxi")

The subsequent work for the design of the LTHC grid was done in close coordination with the stakeholders. The design and simulation of the grid was carried out independently of the future use, whereas a future use of the "Martinek-Kaserne" again merely as a military camp is excluded after talks with the stakeholders. The user and therefore load profiles of the buildings were assumed as mixed, with housing, commercial and office buildings, education etc., whereas we can work with preliminary studies of architects and developers as a guideline for the development of the scenarios.

Figure 3: Pictures of the interior of the buildings and the outside area. The central staff building with the main entrance and the round tower is well-preserved. The upper two pictures show the dining hall and the main meeting room in the round tower. In some pictures, the poor condition of the buildings – partially due to damage by water - even after only four years of abandonment and signs of vandalism can be seen.

2.3 Introduction into the design of the LTHC grid

To design the heating and cooling grid, in a first step, all available essential data from the site were gathered, whereas the available data can be classified as follows:

a. *Geoscientific data:* (hydro-)geological data, e.g. maps, data of boreholes, existing water rights; construction of test borehole, enhanced thermal response test (eTRT) measurements, soil and water examinations, geoelectric measurements;
b. *Technical data:* Possible components in the LTHC grid, technical and energetic specifications and boundary conditions;
c. *Building data:* Assessment of the existing building stock, load profiles etc.;
d. *Economic data:* Definition of essential cost components, price research etc.

ad a.: After the geoscientific data collection and the measurements at the borehole, a hydrogeological model was established, which was fed into a process model based on the software FEFLOW™ to assess the thermal interaction of three subsurface (solid soil and possible groundwater layers) with the seasonal heat storage.

ad b.: Following the three scenarios, the distinct energetic boundary conditions were developed for each scenario. Furthermore, the energy system of the NÖM dairy plant will be analysed to determine the energy potentials for the LTHC grid.

For the simulation of the LTHC grid new and communicating simulation tools were developed to cope with the complex situation of the area, consisting of different heat sources, protected and potential new buildings, different temperature levels and times of energy demand, different uses of the buildings, etc.

The simulation tool comprises:

(I) the heat recovery from the wastewater, cooling units and compressed air of the neighbouring NÖM dairy plant,
(II) integration of locally available renewable energy sources,
(III) energy storage aspects,
(IV) the special challenge of different building standards of the old listed buildings vs. newly built buildings with different usages (living, commercial, education), and therefore different supply temperatures and demand characteristics, and
(V) moderate cooling via Free Cooling.

ad c.: The existing building stock was assessed with regard to the renovation needs and the thermal requirement for refurbishment, in accordance with the monument protection standards. Subsequently, the free areas will be assessed for potential new buildings and usage, in order to generate realistic load profiles. For each scenario, the HVAC systems will be designed, including the energy transfer to the LTHC grid and the energy distribution within the buildings.

ad d.: On the basis of the available cost data, a method for a comprehensive economic assessment of the LTHC grid, considering environmental costs and benefits was developed. The calculations support the assessment of the competitiveness of LTHC grids with industrial waste heat and geothermal heat supply compared to fossil-fuel based grids and district heating.

3 Geoscientific site assessment and geothermal energy potential

3.1 Legal framework for geothermal energy use in Lower Austria

Heating and cooling facilities are subject to special rules in the Austrian Water Rights Act (Bundesministerium für Nachhaltigkeit und Tourismus, 2018). The thermal use of groundwater requires a permit in Lower Austria (Amt der NÖ Landesregierung, Gruppe Wasser, 2012). However, there are no groundwater reservoirs, which might allow the use of open loop systems for generating heat in the area of interest.

The installation of borehole heat exchangers (BHE) also requires a permit in Lower Austria within areas with confined and artesian confined groundwater conditions. The area of interest is located south of Baden where very complex confined groundwater conditions of thermal reservoirs occur. Therefore, it is strongly recommended to get in contact with local authorities. The selection of the drilling method, the grouting process, as well as knowledge of the geological and hydrogeological conditions in the subsurface are of great importance. It is crucial not to cause any hydraulic contact between different groundwater bodies. (Amt der NÖ Landesregierung, Gruppe Wasser, 2012) Furthermore, existing rights in the surrounding area have to be considered. The ÖWAV Guidance Document 207 (Österreichischer Wasser- und Abfallwirtschaftsverband, 2009) is recommended as state of the art in Lower Austria.

3.2 Hydrogeological and geothermal site information

3.2.1 Geological overview

The Martinek military camp is located south of Baden and thus situated near the western border of the Southern Vienna Basin. Most of the information about the geology was extracted from the 2006 published edition “Niederösterreich” (Wessely, 2006). It contains a comprehensive description of the geological conditions in Lower Austria. The basin is a syncline between the Alps and the Carpathian Mountains and the Pannonian Plain, and 50 km wide and 200 km long. The edge and basis of the basin consist of Triassic dolomites and limestones. The basin deposits are mainly characterized by marine and partly fluviatile sediments of the Miocene. The sedimentation was accompanied by tectonic processes and led to tilting and erosion of the sediments. A series of fault systems can be found in the basin. The main fault in our area of interest is the N-S striking Baden fault (Rögl, et al., 2008) (Figure 4).

3.2.2 Hydrogeological conditions

The hydrogeological conditions in the area of interest are predominantly characterized by a shallow quaternary groundwater reservoir, in the top 10 to 20 m, and deeper thermal water reservoirs.

There are smaller spring protection areas for the thermal waters in Baden and Bad Vöslau. Baden has 15 thermal water sources like the 'Josefsquelle', which supply the facilities with sulfurous thermal water. The water in Bad Vöslau is used for mineral water bottling and health resorts and is among others supplied by the drilling sites VÖ 6 and VÖ 7 (Figure 4). The sources are related to an extensive hydrodynamic circulation system. The Triassic carbonates, consisting of dolomites and limestones, are the reservoirs of these waters and overlying Badenian fine-grained sediments act as impermeable barriers. Fractures and thrust faults like the Baden Fault system cause the better permeability where waters can emerge on the surface. The waters in Baden come directly from the carbonates, which reach the surface in the area and in Bad Vöslau via cracks. (Rögl, et al., 2008) (Elster, et al., 2016).

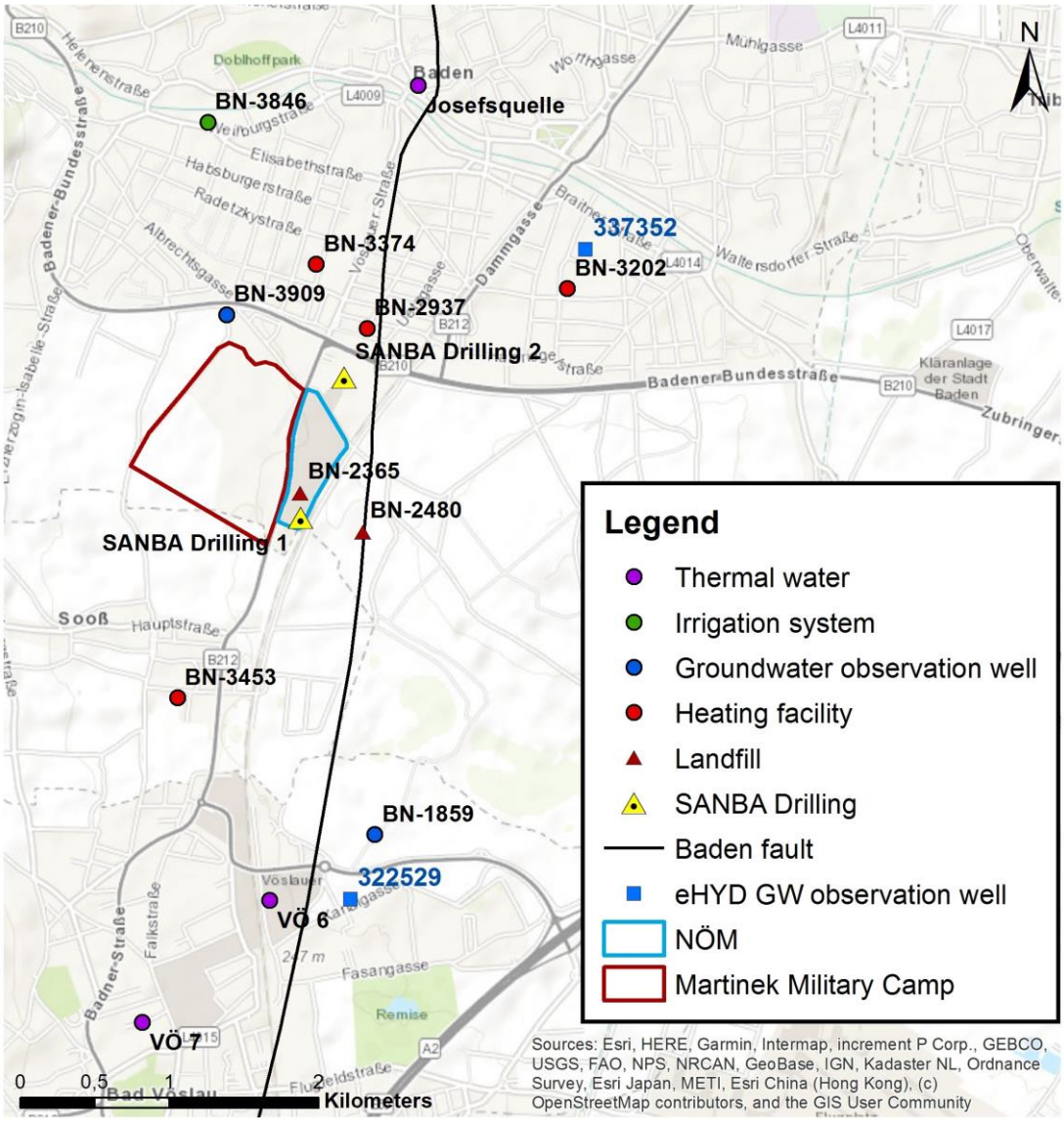

Figure 4: Locations of water facilities (irrigation system, groundwater observation well and heating facility) and landfills recorded in the water register, groundwater observation wells from the hydrographic service of Lower Austria (eHYD), drilling sites 'Josefsquelle', VÖ 6 and VÖ 7, and locations of the project drillings (SANBA Drilling 1 and 2) at the site of the NÖM plant.

All well systems recorded in the water register (irrigation system, groundwater observation well and heating facility) and the groundwater observation wells from the hydrographic service of Lower Austria

(eHYD) only penetrate the shallow quaternary groundwater reservoir. The district authority of Baden provided all information about the facilities from the water register. The aquifer covers areas of Vienna, Lower Austria and Burgenland (1228 m^2). Gravel and fine to medium sand layers act as the unconfined porous aquifer and the underlying Badenian fine-grained sediments act as impermeable barriers in the area of interest (BMLFUW, 2006). It may occur that the shallow quaternary waters mix with the thermal water reservoirs, for example at the thermal water springs in Baden. Hydraulic conductivity ranges between 0.0002 m/s and 0.1 m/s which means there are moderate permeable to highly permeable conditions. Characteristics of the aquifer, like groundwater flow direction, hydraulic conductivity and groundwater level, were measured at some locations in our area of interest. In summary, it can be said that the general groundwater flow direction goes from west to east. The lowest annual minimum groundwater level was 221.47 m.a.A. (4.6 m below ground level) and the highest annual maximum value was 222.71 m.a.A. (3.36 m below ground level) (eHYD, downloaded on 07.05.2019). The thickness of the aquifer ranges between 5.3 and 7 m. Furthermore, only very low groundwater inflow was observed at depth of 15 to 16 m during the flush drilling of the project drilling (SANBA Drilling 1). Since our area of interest is located at the edge of this shallow quaternary groundwater reservoir, there are many local inhomogeneities and only moderate permeable conditions (pump tests: 0.00015 m/s and 0.0003 m/s).

3.2.3 Hydrogeological 3D model

In order to estimate the resources for generating and storing heat based on shallow geothermal methods (borehole heat exchangers and thermal groundwater use) the knowledge of the subsurface conditions up to the maximum depth (in this project: 180 m) of planned installations is required. In that regard, subsurface characteristics like the lithological build-up, hydrogeological conditions and thermal properties are very important.

To establish a hydrogeological subsurface model of the site, all information available from literature and archives (lithological borehole profiles, hydrogeological cross sections and existing water permits in the closer vicinity of the site) were collected and subsequently compiled to a geological cross section (Figure 5) during the reporting period.

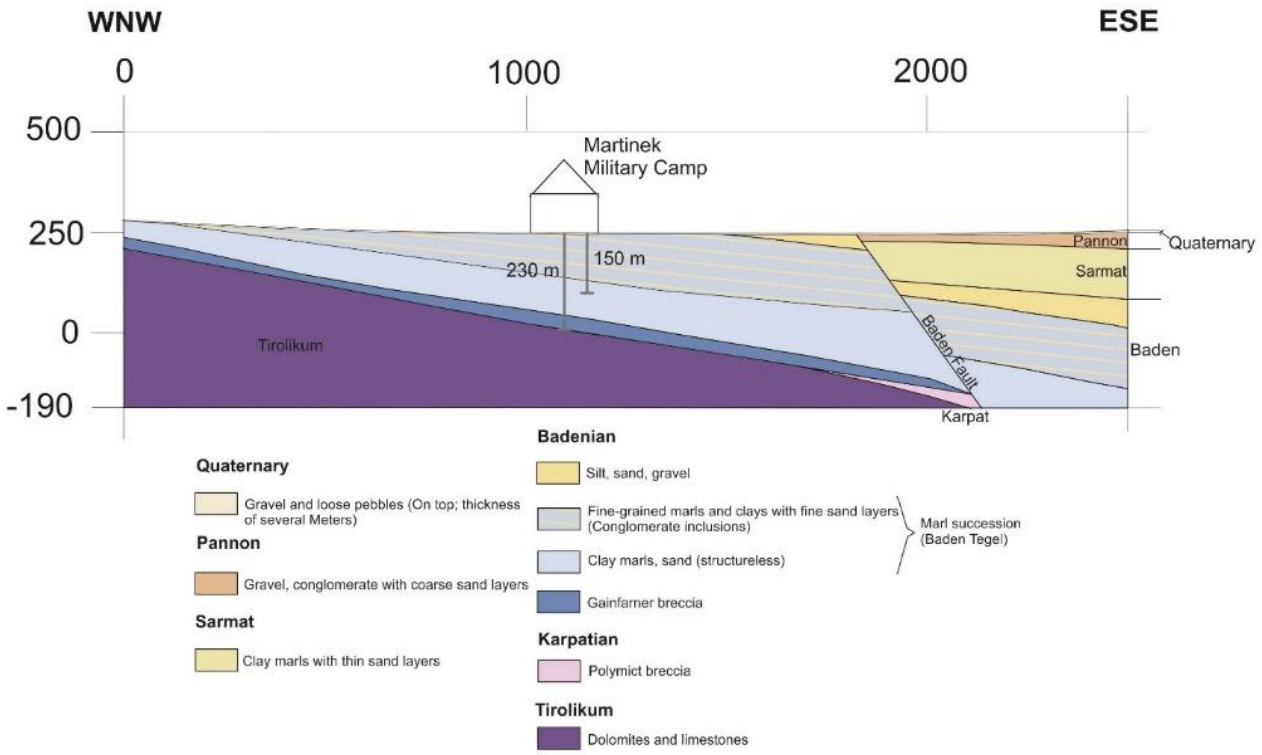

Figure 5: Geological cross section at the Martinek former military camp in Baden

To assess the underground and to plan the two exploratory drillings described later in the chapter, two geoelectric (DC) resistivity profiles have been measured. The campaign was executed between April and June 2019 and focused on resolving the resistivity in depths up to 150 meters. In general, the subsurface at depths up to 150 meters below the military camp is dominated by fine grained-, partly sandy marls and clay dominated marls of the Vienna Basin. Groundwater bodies are only expected in the uppermost 10 to 20 meters and might not allow the use of open loop systems for generating heat due moderate hydraulic conditions. At the base of the marl layers, we expect conglomerates and breccia, which might be connected to a regional thermal water system in the Vienna Basin. These layers, which might appear in depth layers between 170 and 250 meters must not be drilled during the installation process of closed loop systems to avoid any damage of the aquifer through leakage or contamination by drilling mud.

The compiled geological cross section was afterwards evaluated by the results of the DC resistivity campaign in late spring 2019 (Figure 6). In addition to the data from literature and archives, the geoelectric campaign revealed a zone of increasing resistivities in depths between 80 and 100 meters, which may indicate interbedded sand- or conglomerate layers, which dip in Northern direction. These layers might bear an additional aquifer, which could be either used for generating heat or might reduce the thermal storability of the site.

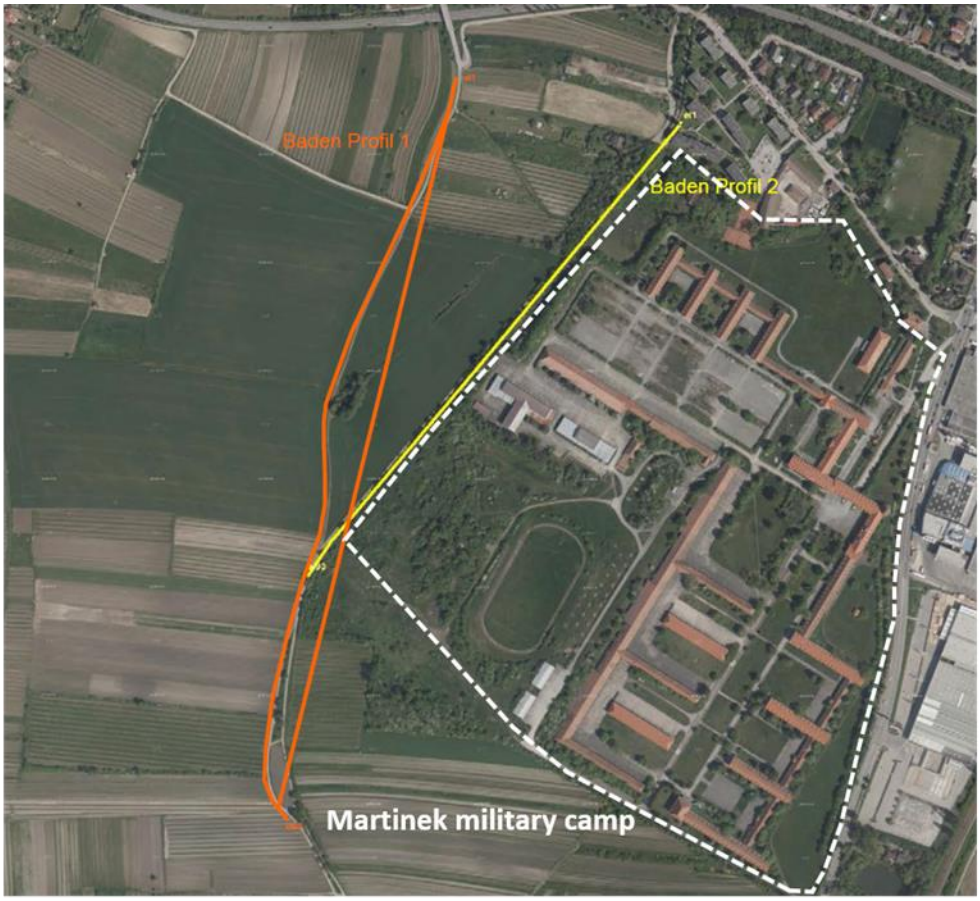

(1) Location of the geoelectric DC resistivity measurement profiles

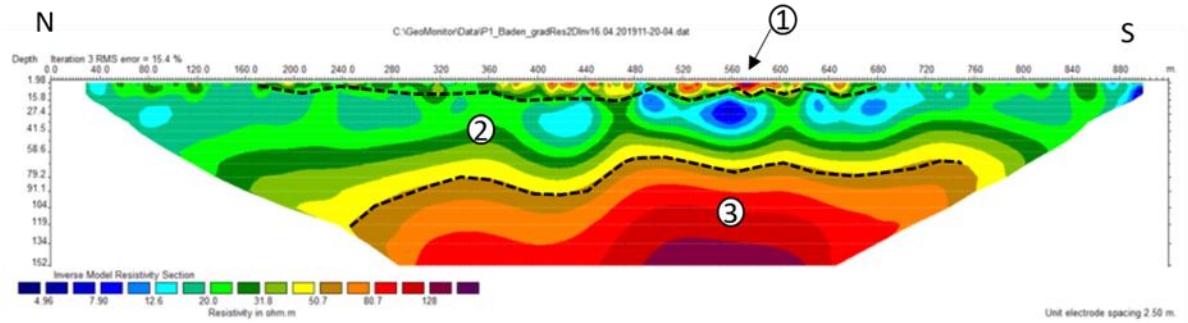

(2) Results of the resistivity measurement along profile 1

Figure 6: Location and results of the DC resistivity measurement at the Martinek military camp in Baden. The results indicate three main zones: (1) shallow gravel-based aquifer in the uppermost 10 meters; (2) clay and marl dominated zone and (3) a zone of increasing resistivity indicating higher sand contents or interbedded conglomerates.

In a first step, all existing geoscientific data from literature and archives were collected and assessed. This includes information like maps, lithological borehole profiles, hydrogeological cross sections, existing water permits in the closer vicinity of the site, groundwater observations and known contaminations. Additional information of the underground was gathered by field and laboratory measurements. Two exploration wells with a depth of 150 m (flush drilling) and 30 m (core drilling) were drilled at the site of the NÖM plant in spring and autumn 2020 (Figure 7).

Figure 7: 150 m flush drilling (left) and 30 m core drilling (right) drilled at the site of the NÖM plant in spring and autumn 2020

Samples were taken every 2 meters along the 150-meter drilling to allow recording of the geological profile, and mineralogical measurements.

The entire drilling depths of both project drillings can be characterized by fine grained, clayey and silty, mainly dark grey sediments, which can be allocated to the marl succession of the Lower Badenian ("Baden Tegel") of the Vienna Basin. In addition to the fine-grained material, the uppermost 10 m contain small and large fragments, which are probably carbonatic components belonging to the Quaternary. The N-S running Baden Fault displaces the Badenian sediments against Pannonian and Sarmatian depositions. These strata consist of gravel, conglomerate with coarse sand layers (Pannon) and clay marls with thin sand layers (Sarmat) (Brix, et al., 1982). All drilling sites, which are located on the west side of the fault, penetrate a series of Badenian sediments (Langhian, Middle Miocene) (Wagreich, et al., 2008; Wessely, et al., 2007).

The Badenian sediments consist of alternating marine and fluviatile facies. The subsurface below the military camp is dominated by fine-grained deposits ("Baden Tegel"), which indicate a generally quiet offshore depositional environment. The lower Badenian sediments belonging to the lower marl-rich part contain clay marls and partly interbedded gravel layers of different thickness. These layers were merged to one thick layer within the Baden Tegel in the 3D model (Figure 8), which presumably are the zone of increasing resistivity in depths between 80 and 100 m of the geoelectric (DC) resistivity profiles. The Vöslau conglomerate belongs to facies of the basin margin with fluvial input and is composed of gravel and sand layers. Another facies of the basin margin with fluvial input is the Gainfarner breccia, which consists of dolomitic components and belongs to Lower Badenian. It can be found in VÖ 7 with a

thickness of around 55 m (Wessely, et al., 2007). The edge and basis of the basin consist of Triassic dolomites and limestones (Gegenhuber, 2007).

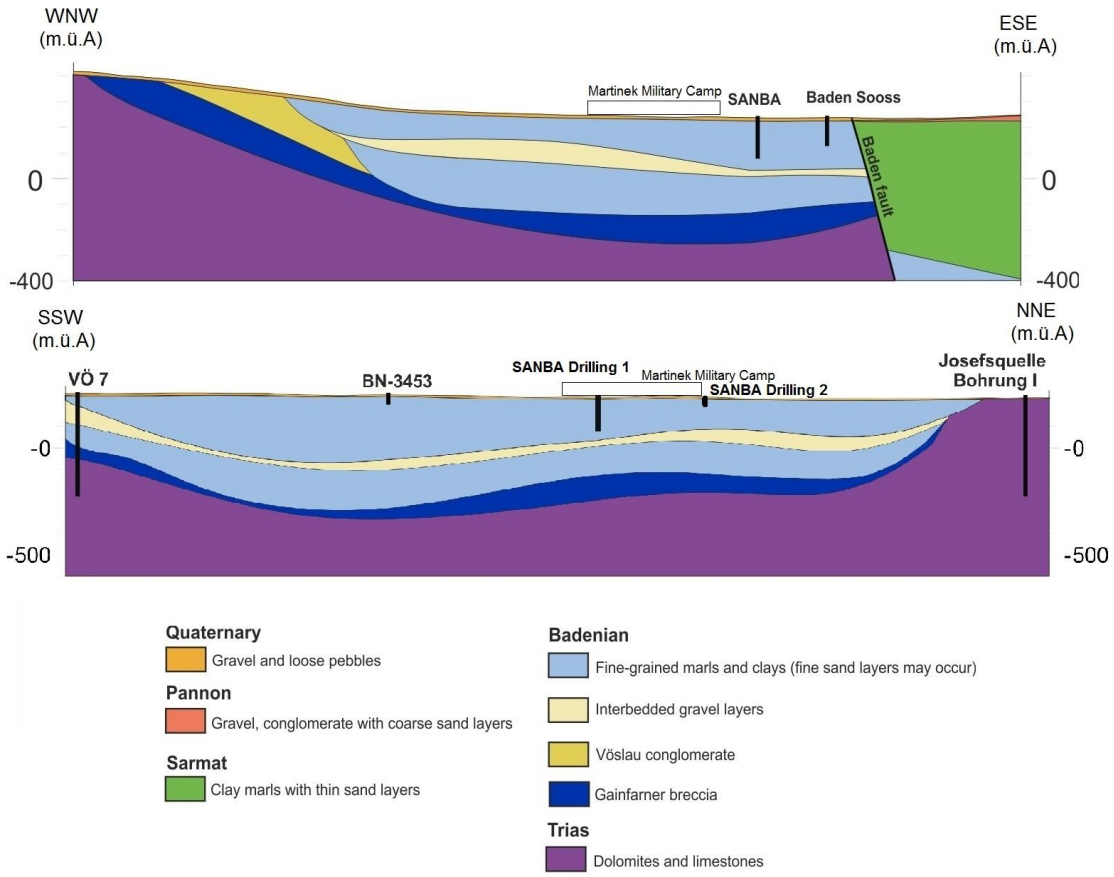

Figure 8: Cross section 1 (above) and 2 (below) of the elaborated hydrogeological 3D model.

3.2.4 Geothermal potential and Thermal Response Tests

The use of geothermal energy is based on the heat exchanger principle by taking thermal energy from the subsurface and bringing it to the surface where this thermal capacity can be used for heating, and the other way around for cooling purposes. This can be implemented in a closed loop system by borehole heat exchangers with a circulating fluid as the heat transfer medium or in an open loop system where groundwater is used as the heat transfer medium. The resulting thermal capacity depends on the volumetric heat capacity of the medium, the flow rate and the temperature difference between inlet and outlet of the medium (VDI 4640 Blatt 5, 2016). The temperature level of inlet and outlet, in turn, depends on the underground temperature. Furthermore, the thermal conductivity of the underground plays an important role as it determines how fast the thermal energy is transferred. Hence, obtaining this subsurface information is crucial for dimensioning of geothermal systems.

A borehole heat exchanger was installed in the drilling at the NÖM site including the installation of distributed measurement sensing (DTS). A conventional (April 2020) and an enhanced (June 2020)

thermal response test were performed at the borehole heat exchanger to gain knowledge of thermal properties, like the underground temperature and thermal conductivities of the underground. Based on the analytical line source method a depth-averaged effective thermal conductivity of 1.7 W/m/K and a thermal borehole resistance of 0.10 mK/W were evaluated by the conventional test, and a depth-averaged effective thermal conductivity of 1.77 W/m/K and a thermal borehole resistance of around 0.40 mK/W were evaluated by the enhanced test. The mean underground temperature of the profile, which was measured before the enhanced thermal response test, is around 13.3 °C.

Based on the analytical line source method a depth-averaged effective thermal conductivity of 1.70 W/(mK) and a thermal borehole resistance of 0.10 mK/W was evaluated by the conventional thermal response test (Figure 9). The depth-dependent thermal conductivities that were evaluated by the enhanced thermal response test and the lithological profile of SANBA Drilling 1 are shown in Figure 4. Most of the values vary between 1.5 and 2 W/(mK). The measurements show a depth-averaged effective thermal conductivity of 1.77 W/(mK) and a thermal borehole resistance of around 0.40 mK/W.

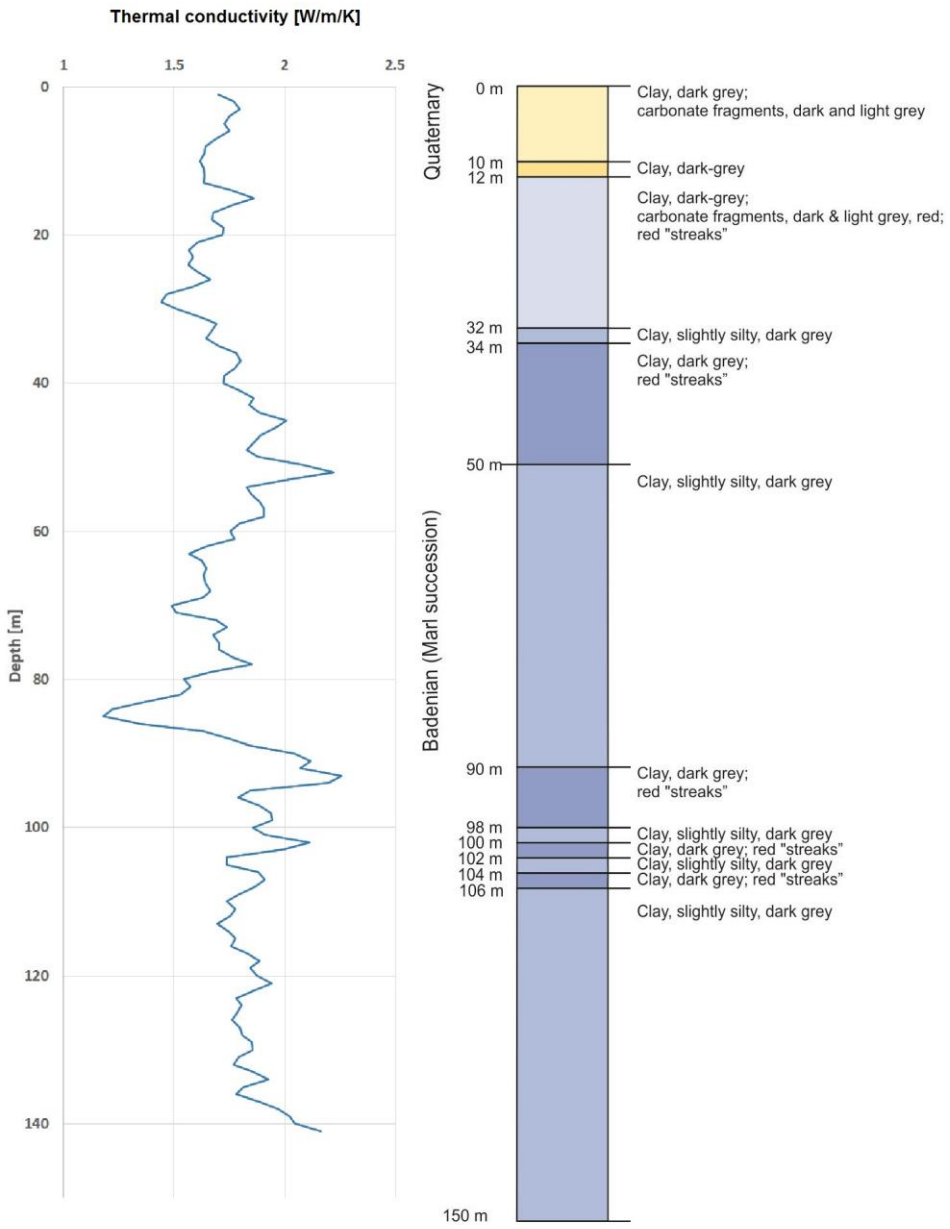

Figure 9: Evaluated depth-dependent thermal conductivities by enhanced thermal response test (left) and lithological profile of SANBA Drilling 1 (right).

The underground temperature was measured before and after the enhanced thermal response test (eTRT) along the borehole at the NÖM site (Figure 10). It can be seen that the near-surface underground areas, as well as the temperature of the shallow aquifer are influenced by the periodically varying surface temperature. The mean temperature value along the profile is around 13.3 °C.

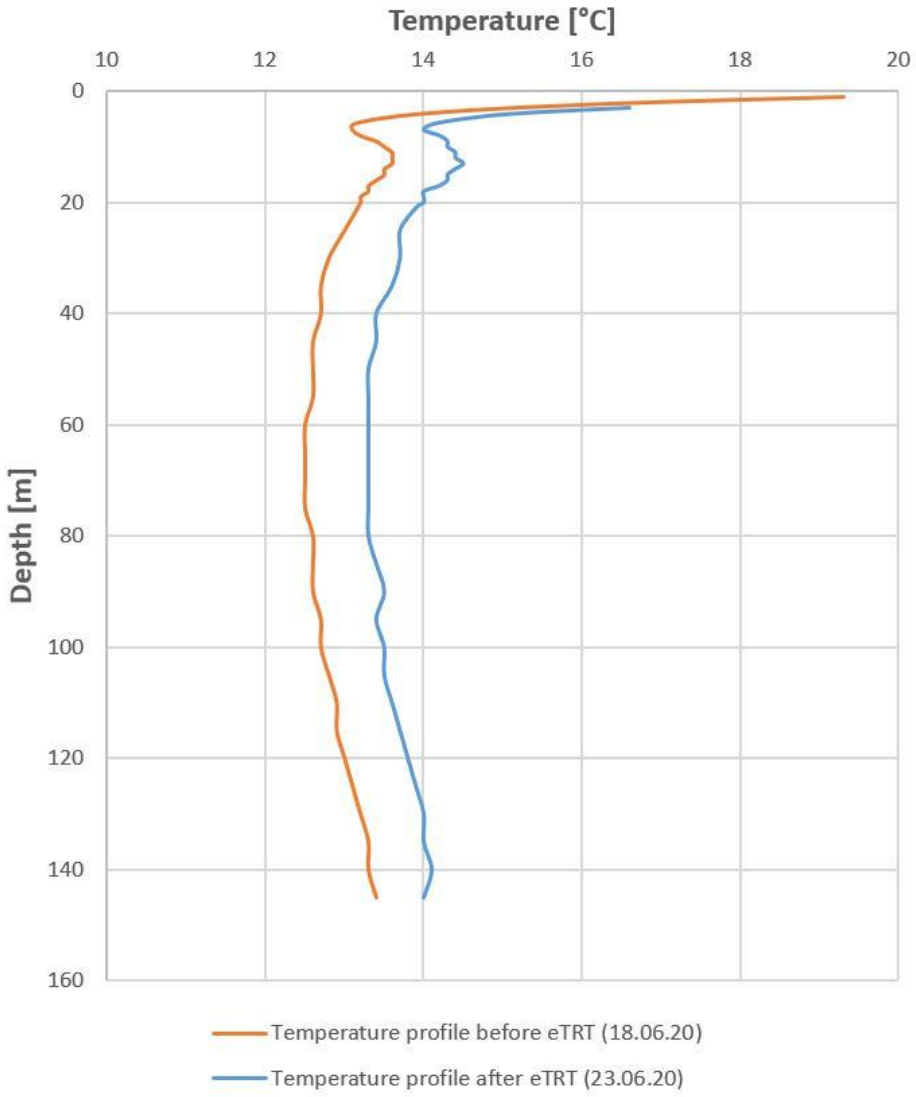

Figure 10: Temperature profiles of the underground measured before and after the enhanced thermal response test.

Furthermore, based on the information collected the shallow subsurface was assessed with regard to geothermal resources and limitations of the utilization of shallow geothermal methods (borehole heat exchangers and thermal groundwater use). Groundwater bodies, which are only expected in the uppermost 10 to 20 meters, might not allow the use of open loop systems for generating heat due to local inhomogeneities and only moderate permeable conditions. No limitations are known for the installation of closed loop systems up to the planned depth of 150 meters. Resources like the usable capacities (estimated value of 33 W/m) and energy available in place (estimated value of 93 kWh/m^{2}a) for heating, cooling and seasonal storage of heat were estimated based on analytic calculations (ÖWAV rule sheet 207).

The shallow quaternary groundwater body might not allow the use of open loop systems for generating heat due to local inhomogeneities and only moderate permeable conditions. No technical and legal

limitations are known for the installation of closed loop systems up to the planned depth of 180 m. There are no smaller spring protection areas for the thermal waters in our area of interest. However, since the layers of the Gainfainer breccia might be connected to the regional thermal water system and presumably appear at least in-depth layers around 350 m, these layers must not be drilled during the installation process of closed loop systems to avoid any damage of the aquifer through leakage or contamination by drilling mud (Gegenhuber, 2007).

The analytical estimation by the ÖWAV rule sheet 207 (2009) was used for the evaluation of the geothermal energy potential using borehole heat exchangers with regeneration. The volumetric heat capacity of the underground has a smaller influence on the thermal response of the subsurface, which was reliably estimated with a value of 2.2 MJ/m³/K (SIA-Norm 384/6, 2010). The norm capacity was determined with a value of 33 W/m and the energy available in place with a value of 93 kWh/m^{2}a. In general, this analytical estimation is valid for one borehole heat exchanger, a small field of borehole heat exchangers and for larger fields only when regeneration is applied. The energy available in place was estimated with the aid of a borehole heat exchanger length of 150 m, 1850 operating hours and a required area of 100 m^2.

3.3 Numerical modelling of the BTES

The borehole thermal energy storage (BTES) is a central element of the simulation tool since it is used for load balance. Numerical simulations were performed in order to validate the programmed geothermal module of the dynamic tool of the entire heating and cooling grid, and to determine the influence of the installations to the underground. For this purpose, the 3D hydrogeological subsurface model was fed into a process model based on the software FEFLOW^{TM} (Figure 11). The model was simplified with a depth of around 360 m, which comprises only the area of the Martinek military camp. The shallow quaternary groundwater body was not considered in the model due to local inhomogeneities, only moderate permeable conditions and low thicknesses. The BTES consists of 96 borehole heat exchangers (double-U-tube, depth: 180 m) with a borehole distance of 4 m.

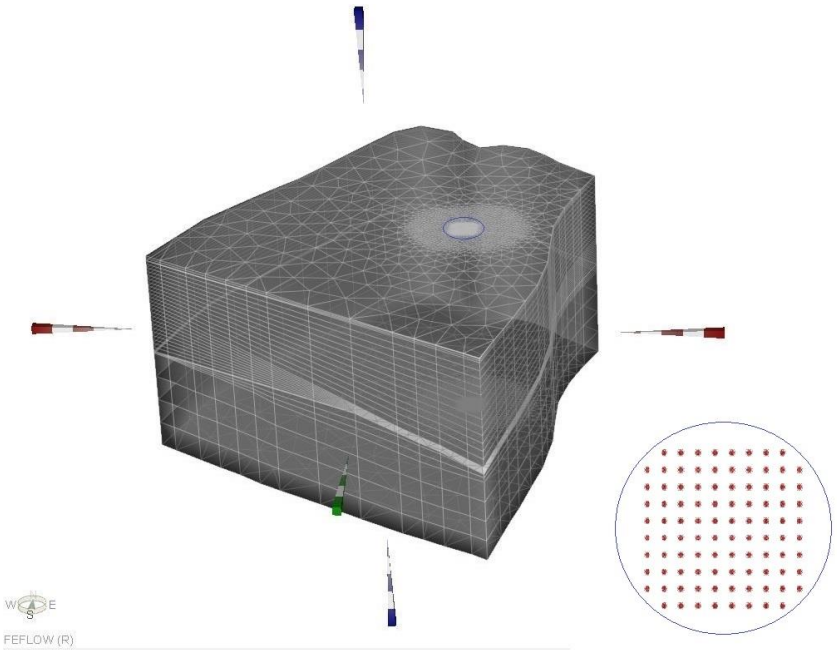

Figure 11: 3D subsurface model, which was used for the numerical simulations with the software FEFLOW™. The circle represents the location of the BTES and the borehole heat exchanger (BHE) positions are shown at the bottom right.

3.3.1 Validation of the BTES model

In order to verify the reliability of the simulation results of the tool, the programmed BTES model was validated by using the already well-established software FEFLOW™. The finite element program is able to simulate heat transport processes in the underground and model geothermal heating systems (DHI-WASY GmbH, downloaded on 12.01.2021). For this purpose, numerical simulations were performed with the tool and FEFLOW™ using identical initial and boundary conditions, as well as the same input data, massflow of the fluid and the inlet temperature into the BTES. The resulting outlet temperatures of the BTES were then compared for each time step.

At first, a homogenous subsurface model with a depth-averaged effective thermal conductivity of 1.75 W/(mK), a depth-averaged thermal capacity of 2.2 MJ/m3/K and a constant ground temperature of 15 °C were chosen. Furthermore, the same simplified input data, massflow of the fluid and the inlet temperature into the BTES for one year, were used. Throughout the validation process, the resulting outlet temperatures of the BTES was compared for each time step (time interval of 1 hour). The values of the thermal resistances of the FEFLOW model were adjusted in such a way that a mean annual relative deviation of less than about 0.64 % and a mean annual absolute deviation of less than about 0.04 °C was achieved. Larger deviations can only be observed when input values abruptly change (Figure 12). The highest resulting local deviations are between 10 and 40 %, but they decrease again to less than 1 % after only a few minutes. A possible reason can be the different time discretization for solving the systems of both models. The programmed tool uses constant time intervals of one hour, whereas FEFLOW uses an automatic time-step control scheme, which is a Predictor-corrector scheme (Diersch, et al., 2009).

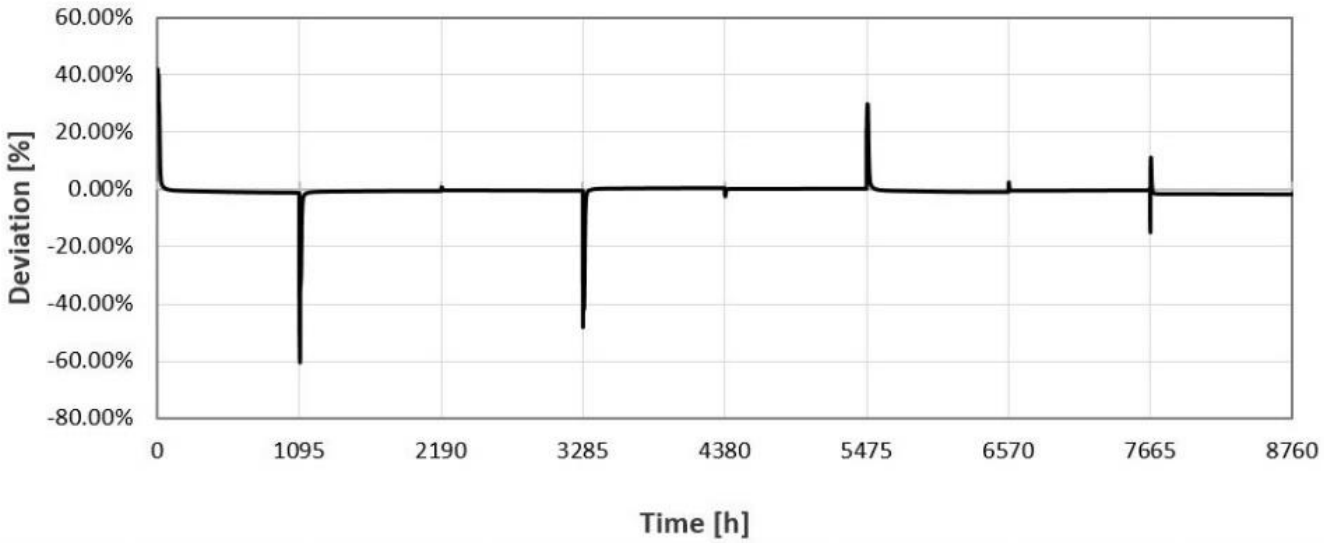

Figure 12: Relative deviations between the simulation results of the tool and FEFLOW with the simplified input data.

A further validation was performed by using the developed time-dependent load profiles of the MINI scenario. Massflow of the fluid and the inlet temperature into the BTES for one operating year were used as input data as shown in Figure 13. This time an interval of 6 hours was used, due to long computing times. Furthermore, the temperature boundary conditions were changed and typical ground temperatures from a test reference year, which are not constant over the year, were used in the near-surface area. In a depth of 15 m, a constant ground temperature of 10 °C was chosen. The temperatures below are determined by a geothermal gradient of 3 °C/100m. The resulting outlet temperatures of both models are shown in Figure 13. Comparing the results, a mean annual deviation of less than about 2.44 % and a mean annual absolute deviation of less than about 0.35 °C can be observed. The higher deviation, compared to the validation with the simplified input data, can be explained by the many abrupt changes of the input values. Nevertheless, the small overall deviations show a good correspondence of the simulation results and thus the validation's success.

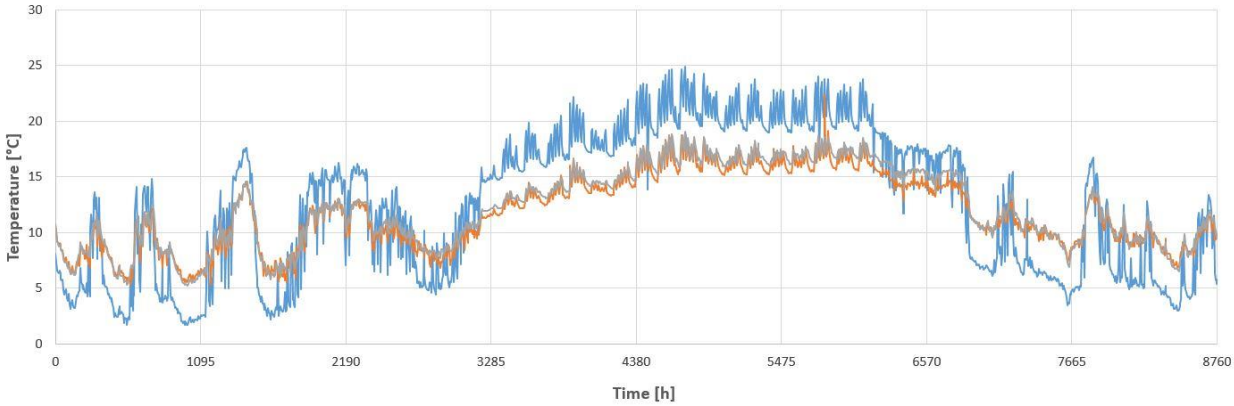

Figure 13: Inlet temperature into the BTES as input data (blue), the resulting outlet temperatures of the programmed tool (orange) and FEFLOW (grey) for one operating year of the MINI scenario using the homogenous subsurface model.

A heterogeneous subsurface model with depth-dependent effective thermal conductivities and thermal capacities was used for a final validation and a long-term simulation to determine the thermal environmental impact (see chapter 4.2.2).

Table 1 gives an overview of the depth ranges and chosen thermal properties. The thermal conductivities of the first 120 m are based on the measured effective thermal conductivities of the project drilling at the site of the NÖM plant (see chapter 4.1.4). All the other values of the underground are based on literature data from SIA-Norm 384/6 (2010). Typical ground temperatures from a test reference year, which are not constant over the year, were again used in the near-surface area. The other temperature boundary conditions are based on the temperature profile of the underground measured before the enhanced thermal response test (Figure 9). In a depth of 15 m, a constant ground temperature of 10.8 °C was chosen. The temperatures below are determined by a geothermal gradient of 2 °C/100m.

Table 1: Overview of the depth ranges and chosen thermal properties for the heterogeneous subsurface model which was used for the final validation and long-term simulation.

Depth range [m]	Thermal conductivity [W/(mK)]	Volumetric heat capacity [MJ/(m^{3}K)]
0 – 6	1.75	2.3
6 – 15	1.68	2.2
15 – 24	1.65	2.2
24 – 33	1.58	2.2
33 – 42	1.76	2.2
42 – 60	1.91	2.2
60 – 69	1.65	2.2
69 – 78	1.68	2.2
78 – 87	1.45	2.2
87 – 96	1.99	2.2
96 – 105	1.90	2.2
105 – 114	1.80	2.2
114 – 120	1.83	2.2
120 – 185	2.60	2.1
185 – 360	1.75	2.2

The developed time-dependent load profiles of the MINI scenario were also used for the final validation (Figure 14). The resulting outlet temperatures of both models are shown in Figure 9. Comparing the results, a mean annual deviation of less than about 3,80 % and a mean annual absolute deviation of less than about 0,54 °C can be observed.

The small deviations of this final validation process show again a good correspondence of the simulation results and thus the validation's success.

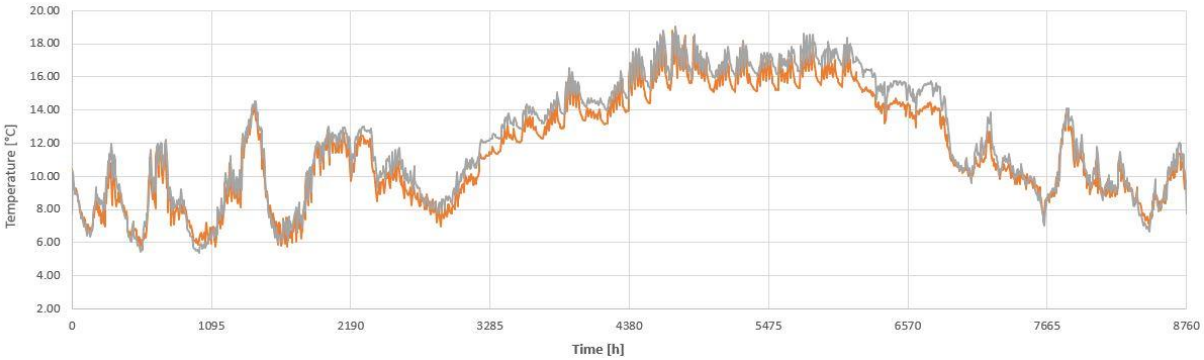

Figure 14: The resulting outlet temperatures of the programmed tool (orange) and FEFLOW (grey) for one operating year of the MINI scenario using the heterogeneous subsurface model.

3.3.2 Long-term simulation

Finally, a long-term simulation with a time period of 10 years was performed using the heterogeneous subsurface model. In order to determine the thermal environmental impact simplified heat load capacities and massflow of the fluid into the BTES were used as input data as shown in Figure 15. The results of the final validation process were used to determine the heat load capacities.

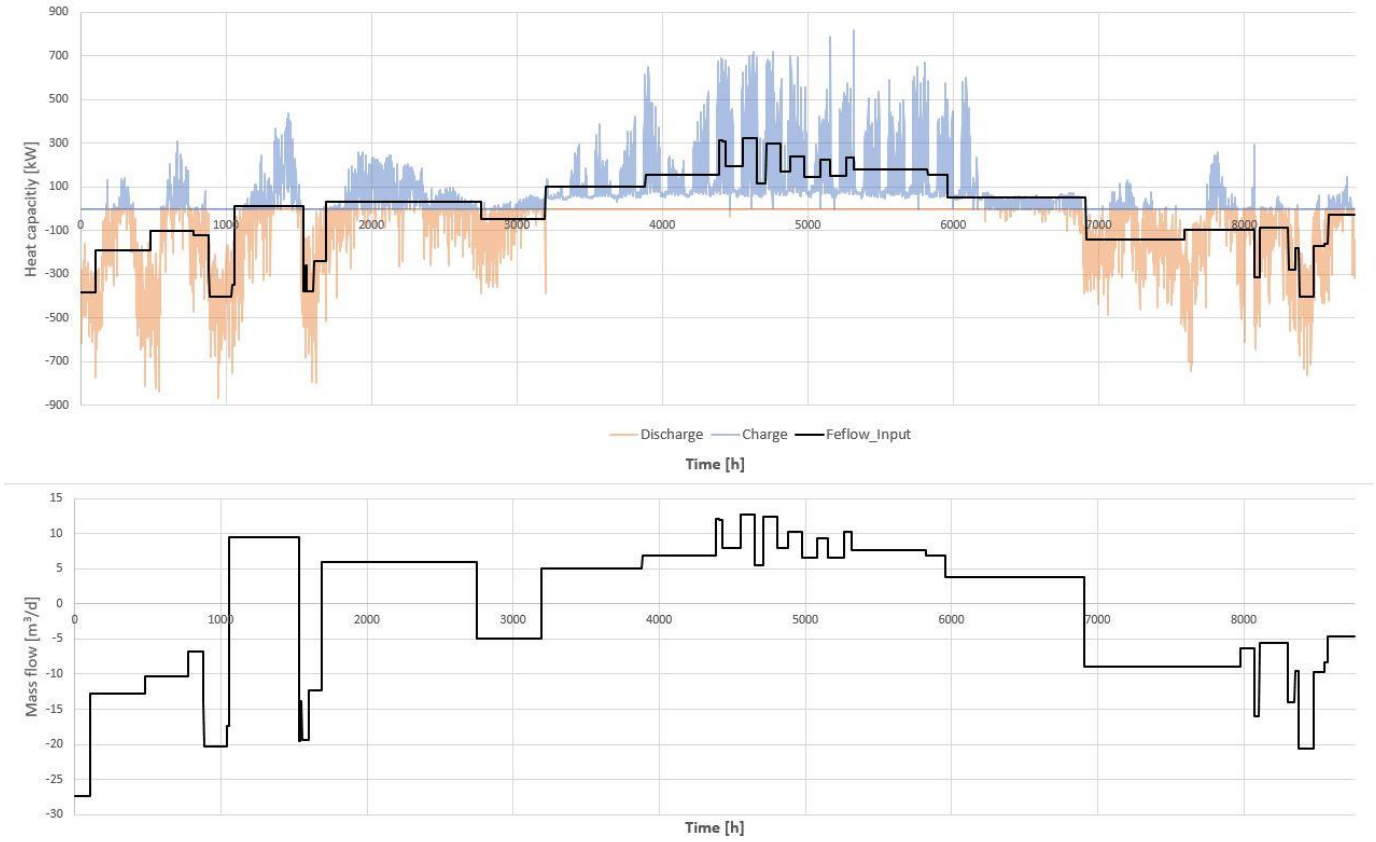

Figure 15: Simplified heat load capacities (black curve, above) and mass flow for each borehole heat exchanger (black curve, below) as input data for the long-term simulation.

Figure 16 shows vertical sections of the subsurface model with temperature distribution in the tenth simulation year during the cooling (charging) period and during the heating (discharging) period. It can be seen that the thermal environmental impact is very limited locally. Moreover, comparing the different temperature curves which are obtained at various locations at the surface in the model when the BTES is charged and discharged, it is very clear that the thermal influence is spatially limited to a few meters and seasonal influences can be primarily observed (Figure 16).

About 630 MWh/a are charged and discharged within the BTES in a yearly cycle. The BTES is not entirely balanced to zero. It is discharged more than it is charged by 12,8 MWh/a. Assessing the accumulated heat flows over the entire tenth simulation year, it can be observed that overall, there is a deviation of 12 MWh in the annual balance in the direct surrounding of the BTES, and around 13 MWh are lost at the surface.

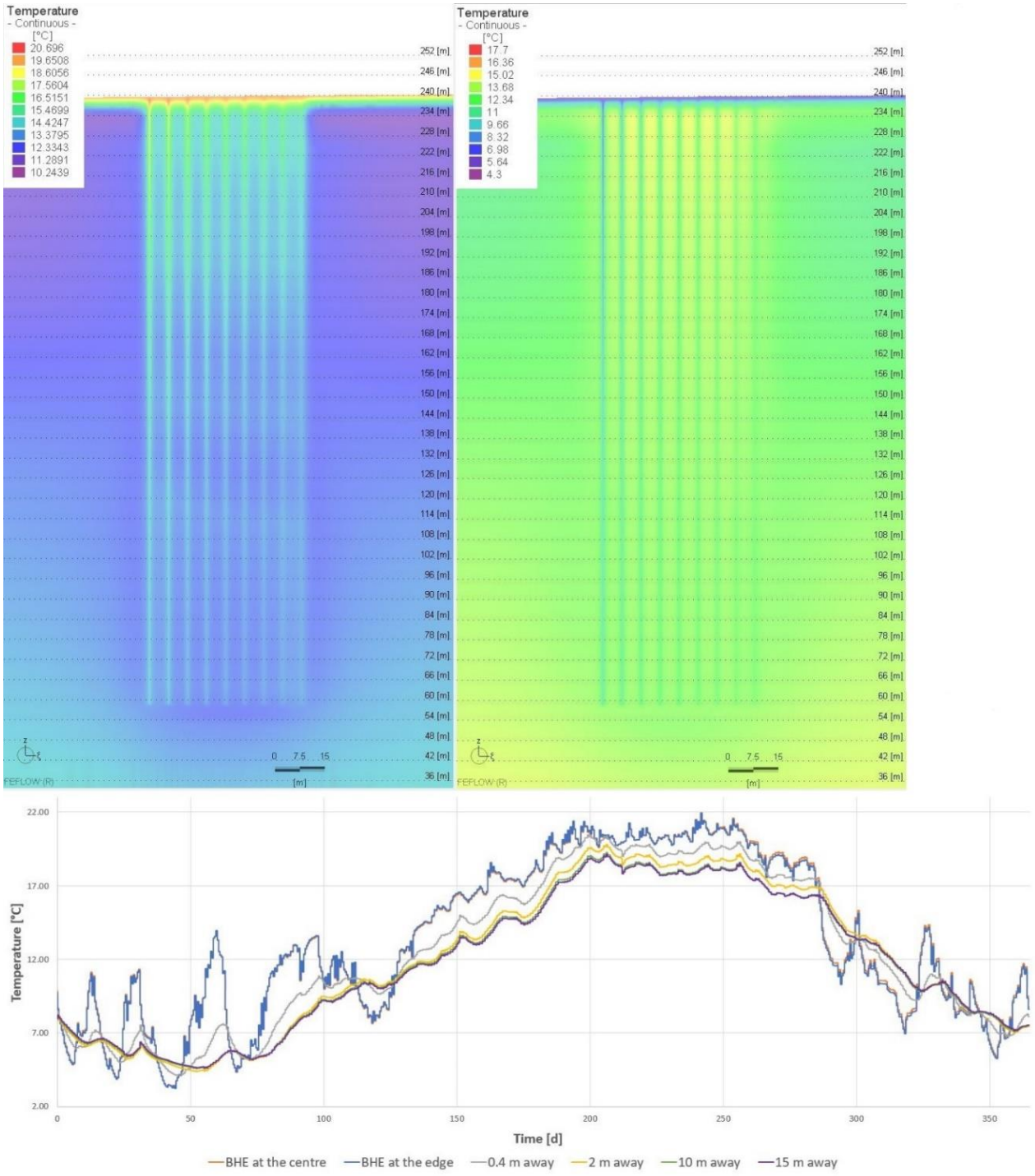

Figure 16: Vertical sections of the subsurface model in the tenth simulation year are shown above at two different times: During the cooling (charging) period (top left) and during the heating (discharging) period (top right). Temperature curves at various locations in the model when the BTES is charged and discharged are shown below.

4 Technical scenario assessment and system design

As mentioned in subchapter 2.2, the technical design of the LTHC grid followed three utilization scenarios, which differed mainly with respect to the degree in which the free areas of the military camp are used for new buildings in the future:

- Use of only the existing building stock with protected buildings (“Mini”)
- Use of the existing buildings stock + 50 % of free area with new buildings (“Midi”)
- Use of the existing building stock + 80 % of free area with new buildings (“Maxi”)

The future use of the buildings – different for each scenario – was classified into seven categories, as can be seen in Table 2.

Table 2: Categories for future utilization of buildings

	Refurbished housing stock	**Newly built house**
Residental	r-old	r-new
Office	o-old	o-new
Education (school, campus)	e-old	e-new
Archive	a-old	-
Gastronomy, event, shops	ges-old	ges-old
Hotel	-	h-new
Supermarket	-	s-new

4.1 Energy demand of existing buildings

On the basis of the listed building components, building geometry, orientation and usage profile, the energy performance certificate results in the characteristic values shown in the following Table 3. It should be noted that the demand quantities according to the energy performance certificate correspond approximately with the calculated demand quantities from the heating cost billing.

Table 3: Energy demand of the existing building stock according to the energy certificate.

HWB_{SK}	222	kWh/m²a
$HEB_{SK,HEATING}$	266[1]	kWh/m²a
WWWB	6	kWh/m²a
$HEB_{SK,WW}$	11[2]	kWh/m²a
HEB_{SK} (Usable energy and distribution losses)	277	kWh/m²a
HEB_{SK} (incl. boiler efficiency 85%)	326	kWh/m²a
HEV according to the heating bill	365	kWh/m²a.

HWB_{SK}	space heating demand in local climate
$HEB_{SK,HEATING}$	energy demand for space heating in local climate
WWWB	heating demand for warm water
$HEB_{SK,WW}$	energy demand for heating of warm water in local climate
HEB_{SK}	energy demand for space heating and warm water in local climate
HEV	energy consumption for space heating and warm water

In the years 2008 to 2012, an average of 425.000 EUR/a worth of natural gas was purchased[3]. In the same period, the gas price for consumers with a consumption of more than 10 GWh/a was 28 EUR/MWh[4]. This results in an average gas consumption of 15.0 GWh/a for heating and hot water. With an assumed conditioned area of 41.040 m² GFA (corresponds to 40 % of the total GFA), this results in a heating energy demand (HEB) of 365 kWh/m²a.

As a next step, first calculations of the yearly energy consumption based on the gross floor areas in the three scenarios lead to first estimations on the energetic feasibility of the three scenarios as well as design strategies for the anergy grid and its components (Table 4: Preliminary values of scenarios).

Table 4: Preliminary values of scenarios

	MINI	**MIDI**	**MAXI**
Gross floor area refurbished building stock	65.333 m²	69.770 m²	58.220 m²
Gross floor area newly built	-	80.500 m²	144.177 m²
Yearly energy consumption heating	1,94 GWh/a	4,90 GWh/a	7,21 GWh/a
Yearly energy consumption domestic hot water	-	0,94 GWh/a	1,36 GWh/a
Yearly cooling demand	1,40 GWh/a	3,53 GWh/a	5,34 GWh/a
Pipe length anergy grid	2.341 m	2.868 m	3.545 m

[1] Corresponds to the HWB_{SK} according to the energy certificate plus 20% distribution losses (empirical value)
[2] Corresponds to the WWWB according to the energy performance certificate plus 90% distribution losses (empirical value)
[3] MIMZ, 2012, Immobilien Report 2012
[4] E-Control, 2017, development of industrial prices

4.2 LTHC grid plan based on the three scenarios

For the three scenarios, the number and position of prosumers and therefore number of domestic heat systems as well as their required components (art of heat pumps, hot water storage tanks, etc.) were assigned. The length and position of the pipes and the possible positions of the borehole thermal energy storage in the LTHC grid were set in a first attempt as presented in Figure 17.

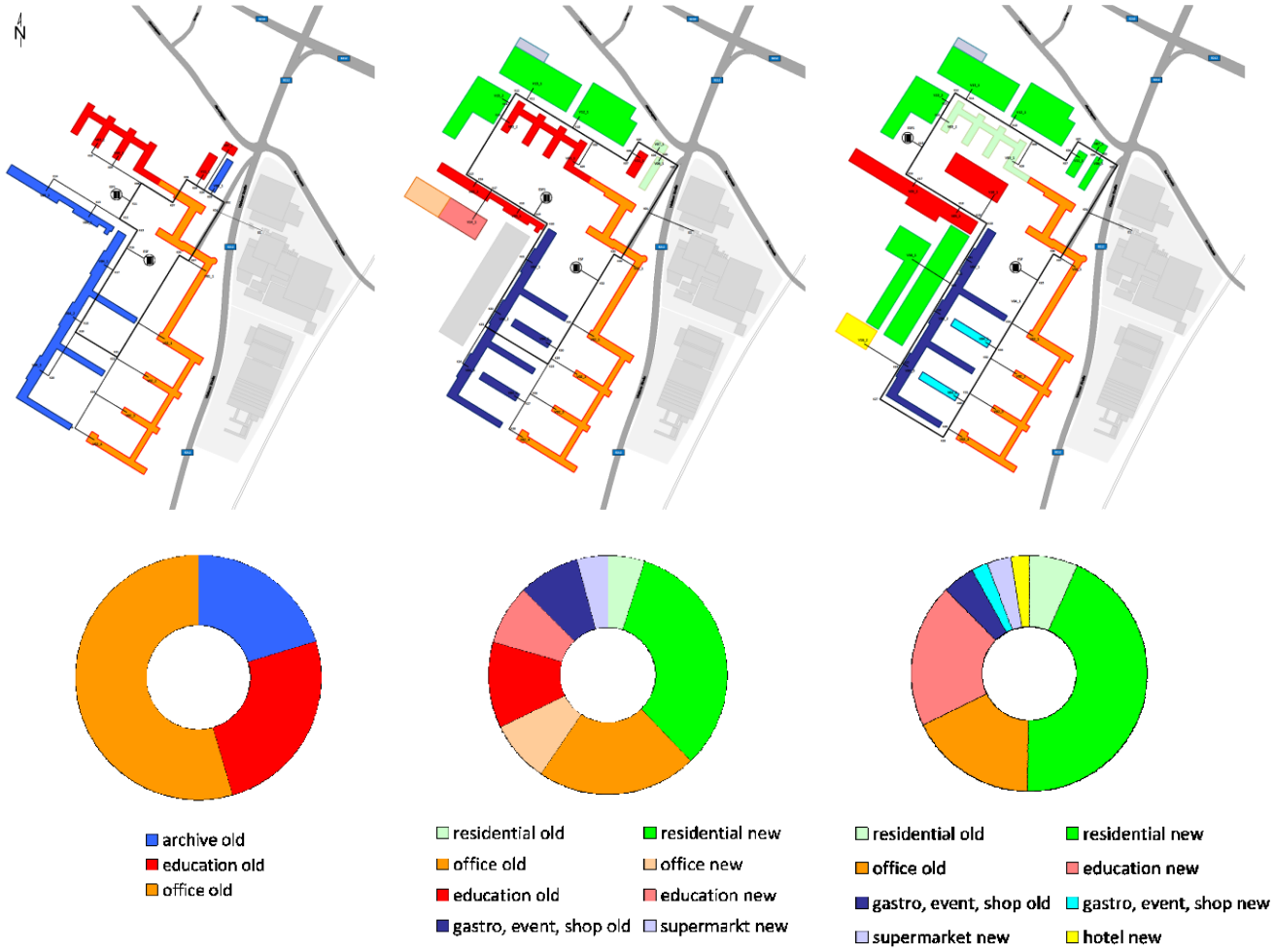

Figure 17: Grid plan of three scenarios, left: MINI, middle: MIDI, right: MAXI

In the following three subchapters, the grid plans, the building-specific data and the usage categories for each scenario are shown in more detail.

4.2.1 MINI

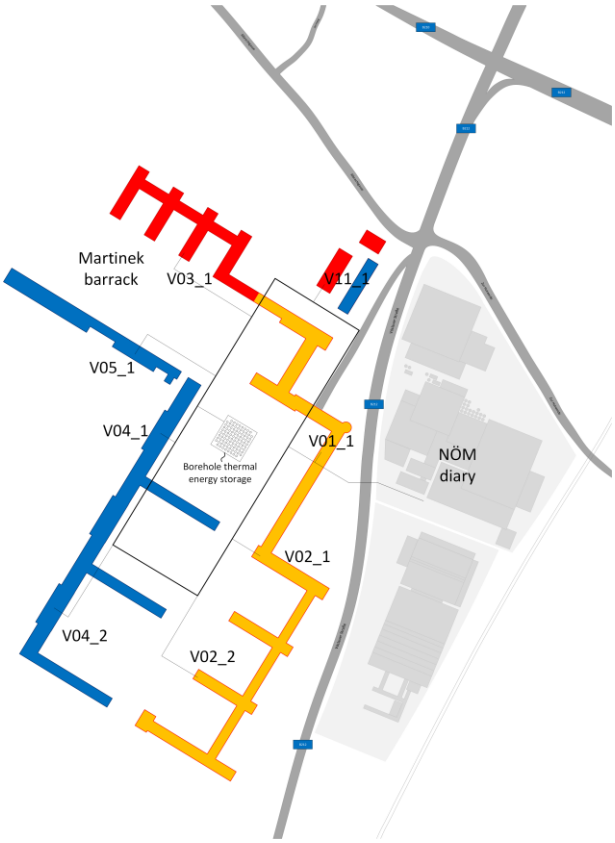

Figure 18: Subareas relevant for scenario development - MINI

Table 5: Building-specific data for scenario MINI

Prosumer	Usage	Condition	GFA m²
V01_1	Office	refurbished	11357
V02_1	Office	refurbished	12264
V02_2	Office	refurbished	12251
V03_1	Education	refurbished	13716
V04_1	Archive	refurbished	4445
V04_2	Archive	refurbished	4445
V05_1	Archive	refurbished	3730
	Education	refurbished	1606
V11_1	Education	refurbished	713
	Education	refurbished	1064
			65590

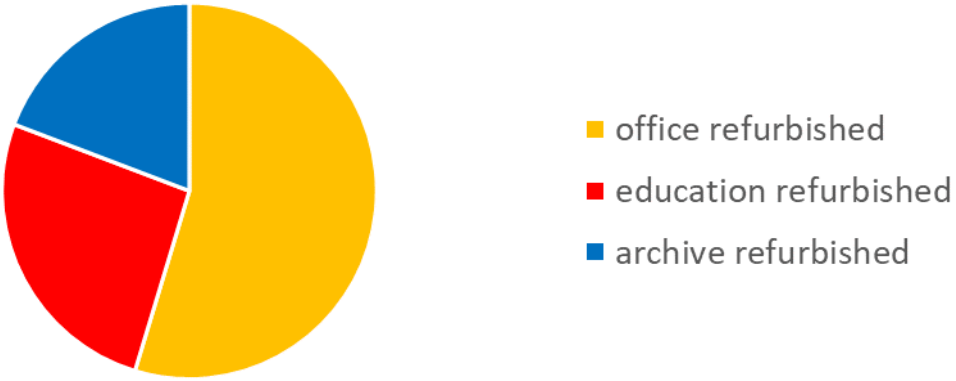

Figure 19: Breakdown by usage category for scenario MINI

4.2.2 MIDI

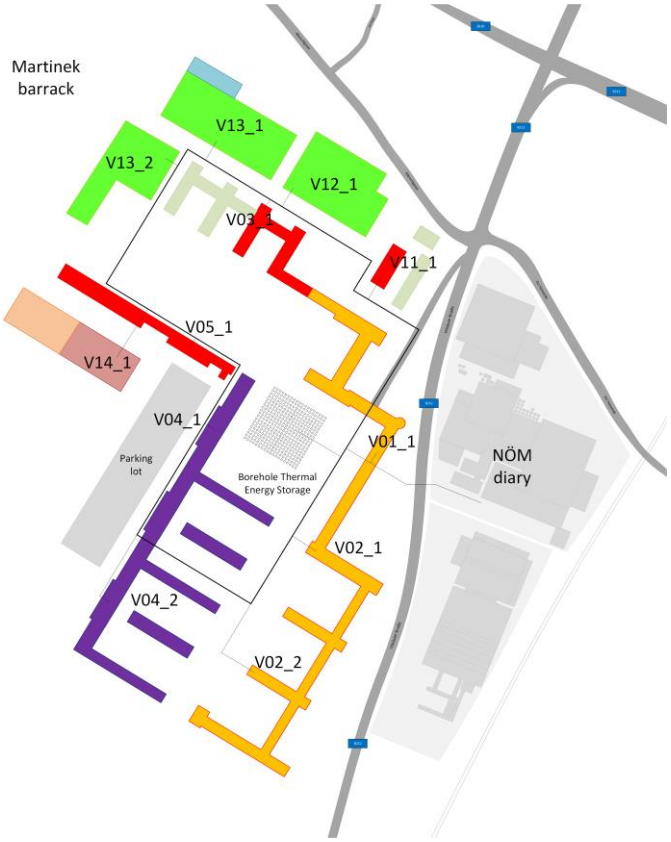

Figure 20: Development-relevant subareas for scenario MIDI

Table 6: Building-specific data for scenario MIDI

Prosumer	Usage	Condition	GFA m²
V01_1	Office	refurbished	11357
V02_1	Office	refurbished	12264
V02_2	Office	refurbished	12251
V03_1	Education	refurbished	6858
	Residential	refurbished	6858
V04_1	Gastro / Event / Shop	refurbished	4445
V04_2	Gastro / Event / Shop	refurbished	4445
V05_1	Education	refurbished	3730
V11_1	Education	refurbished	1606
	Residential	refurbished	713
	Residential	refurbished	1064
V12_1	Residential	new	30000
V13_1	Residential	new	15000
	Supermarket	new	7000
V13_2	Residential	new	15000
V14_1	Education	new	13500
	Office	new	13500
			159590

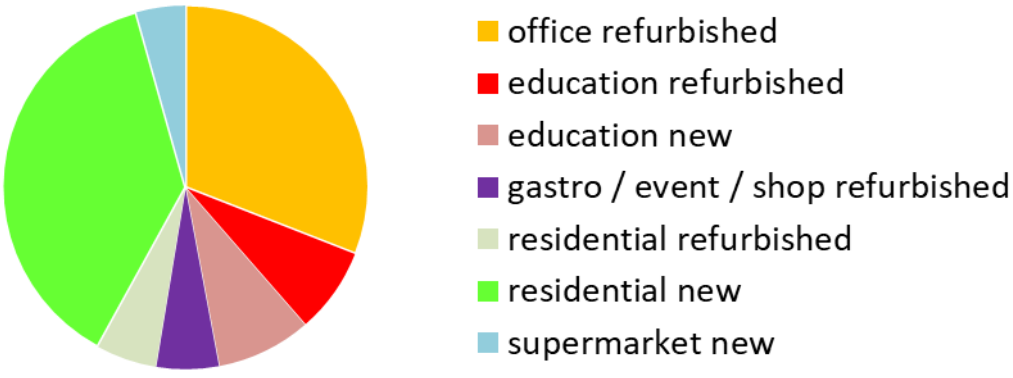

Figure 21: Breakdown by usage category for scenario MIDI

4.2.3 MAXI

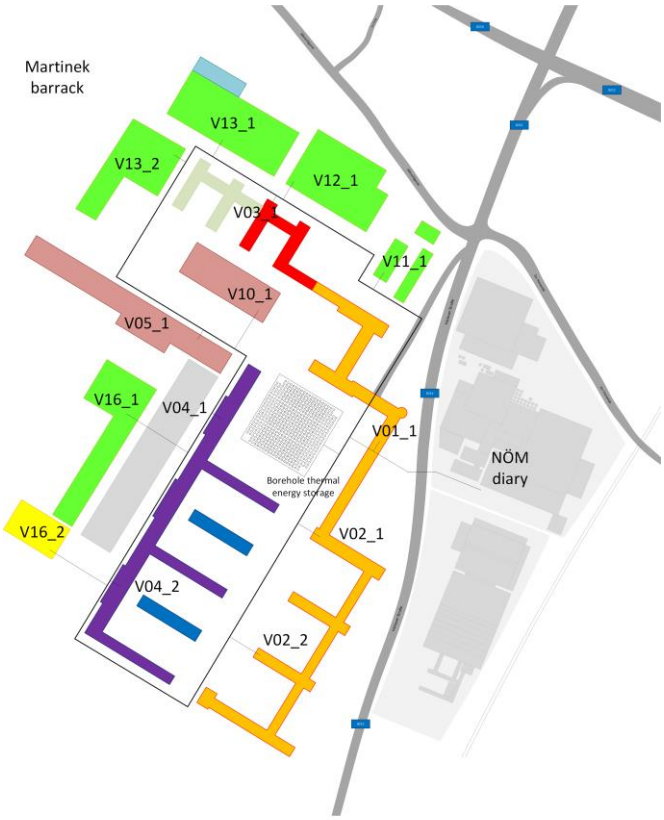

Figure 22: Development-relevant subareas for scenario MAXI

Table 7: Building-specific data for scenario MAXI

Prosumer	Usage	Condition	GFA m²
V01_1	Office	refurbished	11357
V02_1	Office	refurbished	12264
V02_2	Office	refurbished	12251
V03_1	Education	refurbished	6858
	Residential	refurbished	6858
V04_1	Gastro / Event / Shop	refurbished	4918
	Gastro / Event / Shop	new	2200
V04_2	Gastro / Event / Shop	refurbished	3971
	Gastro / Event / Shop	new	2200
V05_1	Education	new	15000
V10_1	Education	new	25000
V11_1	Residential	new	6000
V12_1	Residential	new	30000
V13_1	Residential	new	15000
	Supermarket	new	7000
V13_2	Residential	new	15000
V16_1	Residential	new	20000
V16_2	Hotel	new	5000
			200877

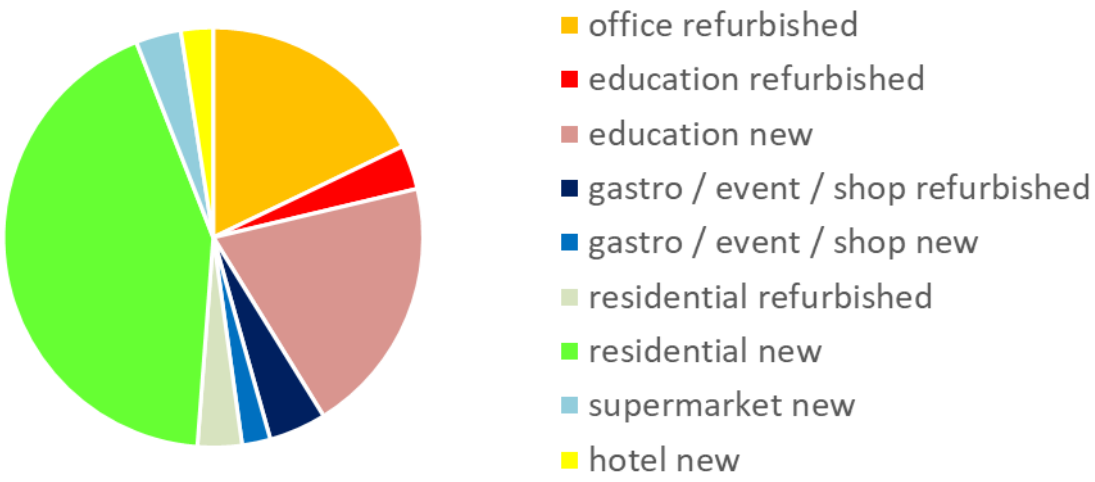

Figure 23: Breakdown by usage category for scenario MAXI

5 Energy analysis of the dairy NÖM

The determination of the waste heat potentials of the dairy NÖM forms an important basis for the dimensioning and simulation of the planned neighbouring anergy network. In order to determine the waste heat and energy efficiency potentials of a plant and to analyse the energy system, the data of the existing energy flows must be determined in a first step.
In the case of the examined dairy NÖM these are waste heat from the following areas: From air compressors (high pressure and low pressure), from cooling units, from the wastewater from the various cleaning processes, from the off-gas stream of the steam boiler plant as well from the existing heat storage tanks (Figure 24). In addition to the here illustrated 70°C heat storage tank there is also still another 50°C heat storage tank, which is not represented here however, because the heat is used all year round internally.

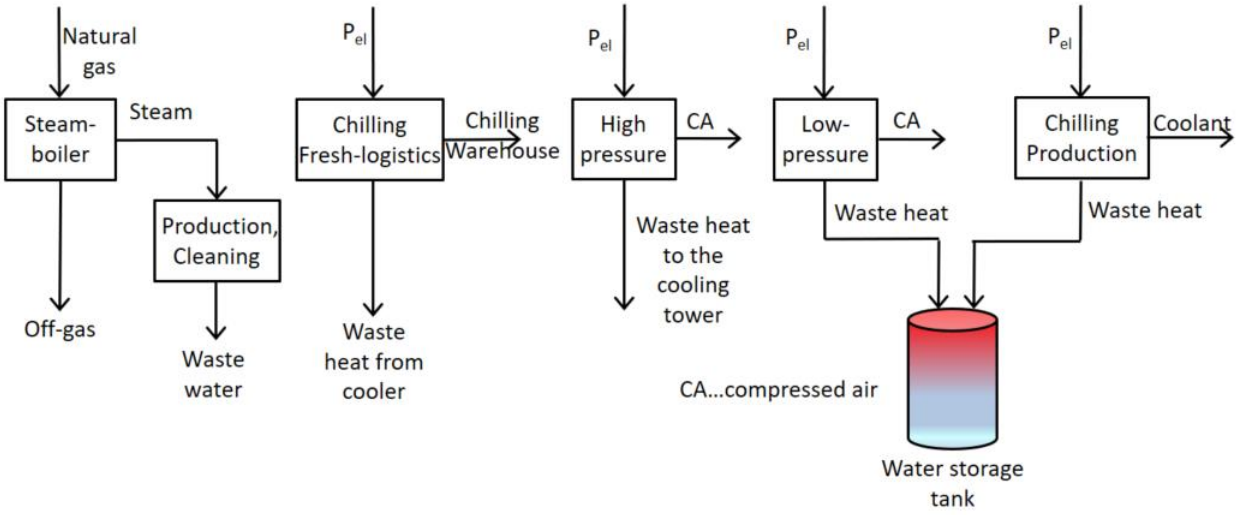

Figure 24: Overview of the identified waste heat potentials

5.1 Wastewater

Wastewater is produced during the cleaning process of the plant and consists of chemical cleaning and rinsing, carried out by CIP (Cleaning in Place). The sequence of a CIP cleaning process is divided into several steps such as pre-rinsing, alkaline cleaning, rinsing, acid cleaning, rinsing and disinfection. This is a crucial energy consumer of a dairy. The thermal energy for cleaning is provided by steam.

The accumulating waste water of the dairy comes from the waste water streams from the CIP cleaning process of 4 lines. The measurement data and first calculations during the first analysis showed that only 2 lines provide sufficient water quantities. For this reason, only these lines are analysed and included in the results. The heat quantity of the waste water was calculated with reference to a minimum cooling

temperature of 25 °C. The exergetic evaluation was carried out with reference to the reference temperature of the anergy network at the different seasons.
The data of temperatures as well as flow rates could be read out from the internal process control system. The temperature curves of the wastewater flows from the CIP process were analysed over a period of more than 1,5 years, with the following Figure 25 showing one month as an example.

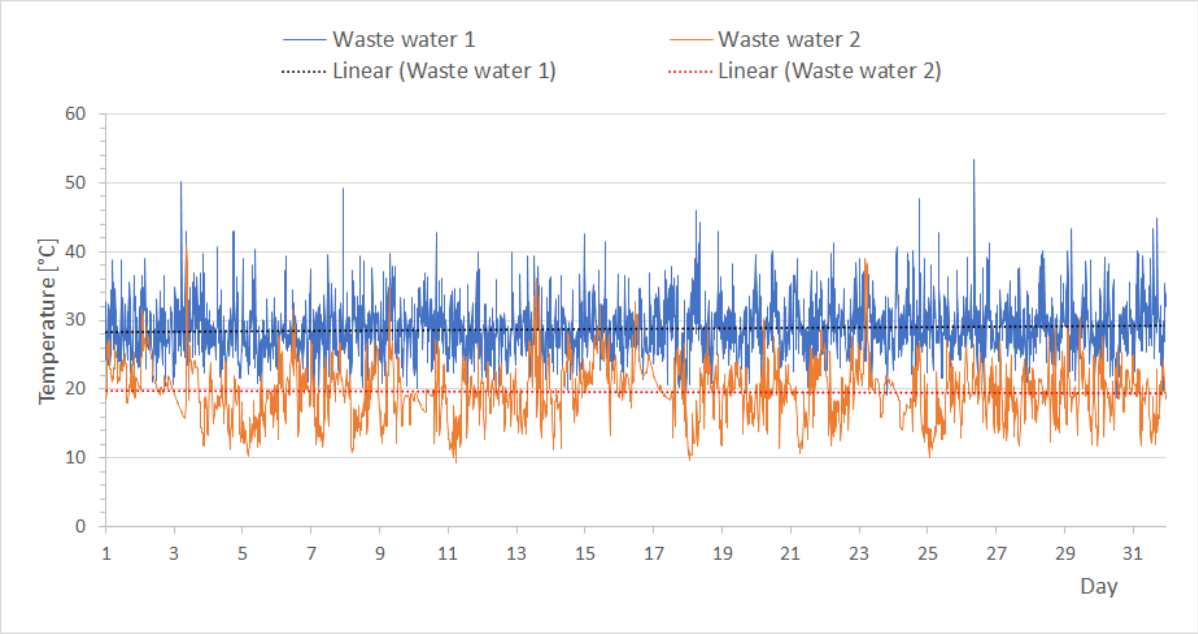

Figure 25: Temperature curve of the two wastewater streams from the CIP processes over a period of one month. The dotted lines show the linear trend of the two temperature curves.

As seen in Figure 25, the temperatures are relatively constant, which is a consequence of the numerous daily rinsing processes. This is of great importance for the use of waste heat. It can also be seen that the temperature curve of wastewater stream 1 is at a significantly higher level, about 12 K higher than the wastewater temperature of wastewater stream 2.

Furthermore, the volume flow rates of both wastewater flows were evaluated over a period of 7 months. It was found that wastewater flow rate 1 is about five times as much as wastewater flow rate 2. It is also of importance here that the volume flows are relatively constant due to the numerous daily rinsing processes. Of particular interest here is the achievable waste heat recovery. The waste heat output is 9,3 %, compared to the average natural gas input and given as a percentage. The assumed cooling temperature is 25 °C.

If the cooling temperature is lower, it is possible to recover more power. However, in this case, it is limited by the temperatures of the low-temperature heating and cooling grid and especially the limitation due to biological issues.

It can be seen in Figure 26 that in summer months the available heat capacity of the wastewater is slightly increased. This is due to a larger production capacity of milk and thus to an increased utilization

of the production lines.

The averaged exergy factors of the wastewater for the different meteorological seasons are between 5,4% and 7,0% and also depend on the assumed seasonal temperatures of the anergy network. If the wastewater is cooled down below 25 °C, however, it must be taken into account that biological deposits can form in the wastewater pipes (biofouling). For this reason, the initially considered extraction of waste heat from wastewater was no longer pursued.

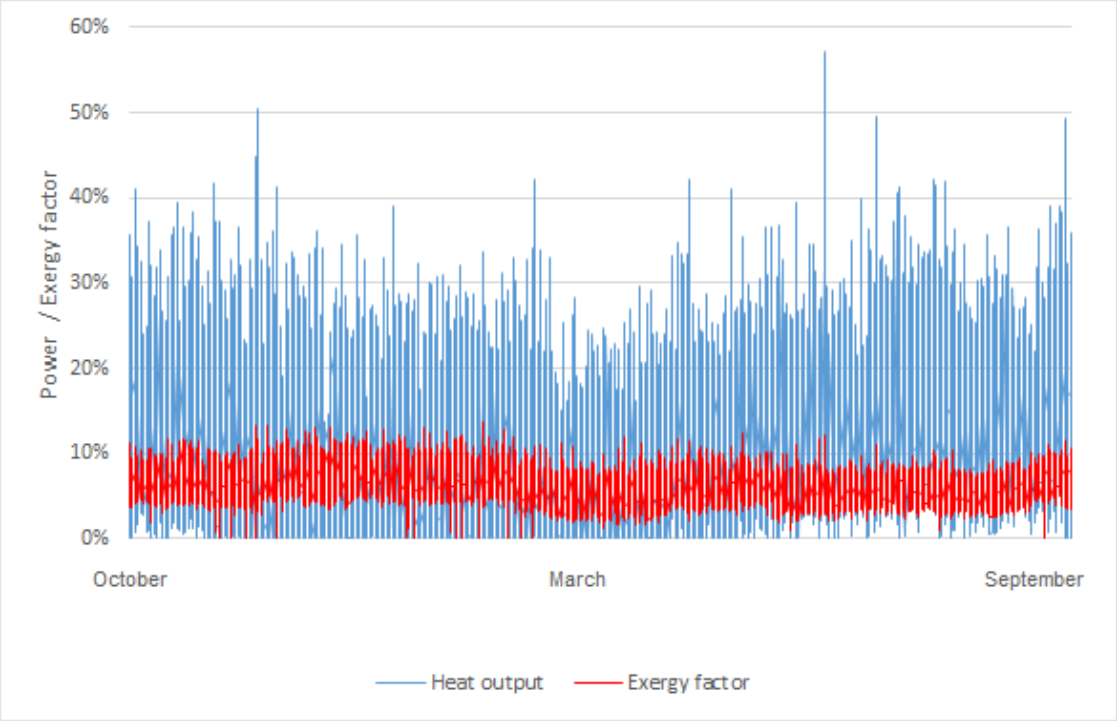

Figure 26: Curves of the heat output and the exergy factor for the wastewater.

5.2 Off-gas stream of the steam boiler plant

A redundant system with two water tube boiler units (Figure 27) is used to generate process steam for production process. The main plant, a Bosch company boiler, has a thermal capacity of 9,5 MW and produces 14,5 t/h of steam.

Two off-gas stream heat exchangers are installed to preheat the fresh and feed water. Approximately 60% of the steam used is returned from production to the boiler plant in the form of condensate. The rest is supplied with fresh water. The fresh water is preheated from about 12 °C to 85 °C. The Off-gas stream temperature of the Bosch boiler system (after the preheating heat exchanger) is about 64°C and thus slightly above the condensation temperature of about 58 °C.

Figure 27: Boiler plants for process steam generation [Picture: Edtmayer]

The data of the gas consumption as well as the off-gas temperatures could be read out from the internal process control system.

Off-gas stream of the steam boiler plant

Cooling the flue gas down to 30 °C can result in condensation of about 80 % (source: Energielexikon) of the water vapor. The waste heat potential of the off-gas condensation and sensible heat is 7,0 % compared to the average input of gas and electricity (see the trend in Figure 28). This would offer the possibility of preheating the combustion air for the gas burner, resulting in savings of natural gas. Thus, the heat could be used directly on site and transport, which leads to losses, would be eliminated. However, lack of space makes the installation of a combustion air preheating hardly possible.

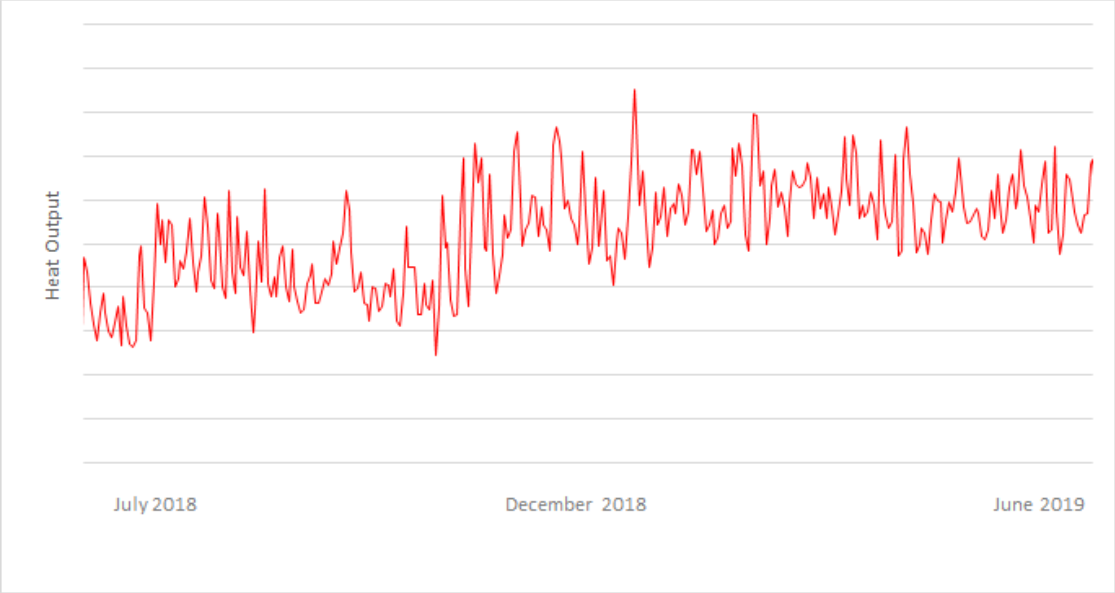

Figure 28: Trend of heat output from Off-gas stream July 2018 to June 2019.

In the exergy analysis, Figure 29 shows the changes of energy or exergy from the use of primary energy in the form of natural gas to the condensate stream. The field of steam generation describes the energy loss through the flue gas and the exergy loss during steam production and the associated increase in entropy. When the steam is throttled from 10,5 bar(g) to 7,5 bar(g), there is only a small loss of exergy. The energy level during throttling remains constant.

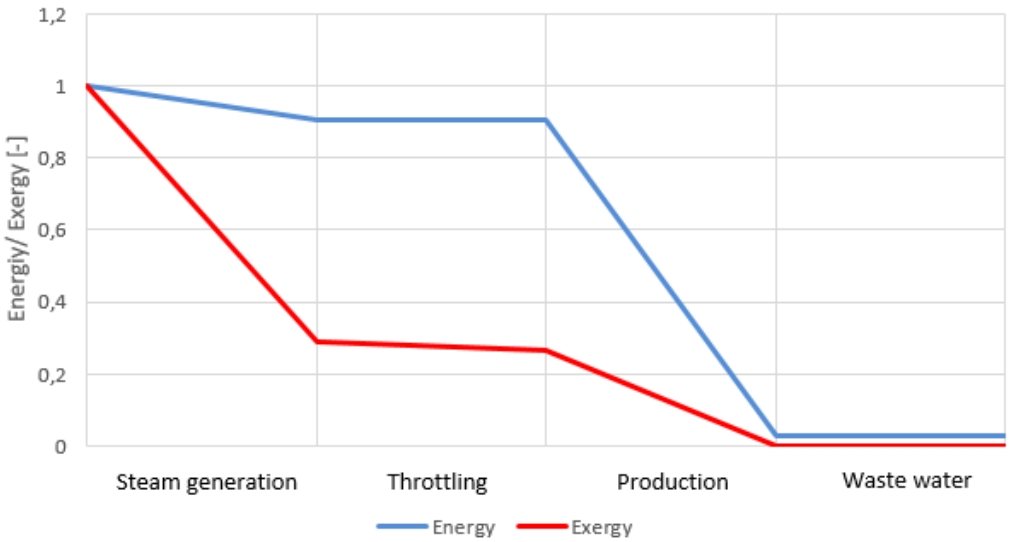

Figure 29: Changes of the energy or exergy level from steam production to wastewater.

As the steam or already condensed steam passes through the production lines, there is both exergy and energy loss to the environment. In the wastewater flow, energy and exergy reach their minimum.

5.3 Waste heat from the recoolers of the cooling system for fresh products logistics (FRILO)

The temperature in the cooling system for the warehouse of fresh products logistics FRILO is kept constant at 3 °C to 4 °C. The cooling is supplied from four refrigeration plants via a collecting pipe to distribution substations, which in turn serve the air coolers located on the site, which is called the cold brine circuit. The waste heat generated by the four refrigeration plants is lead to table chillers on the roof of the building via a common collection pipe and is released into the environment. A part of the waste heat is decoupled via a heat exchanger shortly after the refrigeration units and is fed to the individual cooling units for defrosting. The defrosting of the cooling units is necessary to prevent freezing and thus to maintain the functionality.
Time-resolved data regarding the electrical power consumption of the refrigeration systems as well as temperature data of the flow and return pipes of the hot and cold brine circuits are available. In order to determine the heat output or heat quantity emitted, the volume flow had to be measured at the collector pipe of the warm brine circuit using ultrasonic measurement (Figure 30).

Figure 30: Ultrasonic flow measurement at the cold brine line (left) and the warm brine line (right).

From the measurement series from November 2019 to January 2020, the ratio factor $f_{Q,FRILO}$ between heat output and electrical power input was determined. Using this power factor, a performance profile for the heat output as a percentage of the nominal cooling output of the units for the year 2019 was extrapolated.

After this first series of measurements, the ultrasonic flowmeter continued to operate at the measuring point for several months in order to validate the first series of measurements. Furthermore, a more precise determination of the factor $f_{Q,FRILO}$, the ratio between heat output and electrical power input at the chillers, should be carried out.

Waste heat from the drycoolers of the cooling system for fresh products logistics (FRILO)

The waste heat potential of the drycoolers is 7,3 % related to the average input of gas and electricity. Furthermore, the trend of the exergy factor of the waste heat for the year 2019 is shown, whereby the reference temperatures refer to the assumed seasonal temperatures of the anergy network (Figure 31).

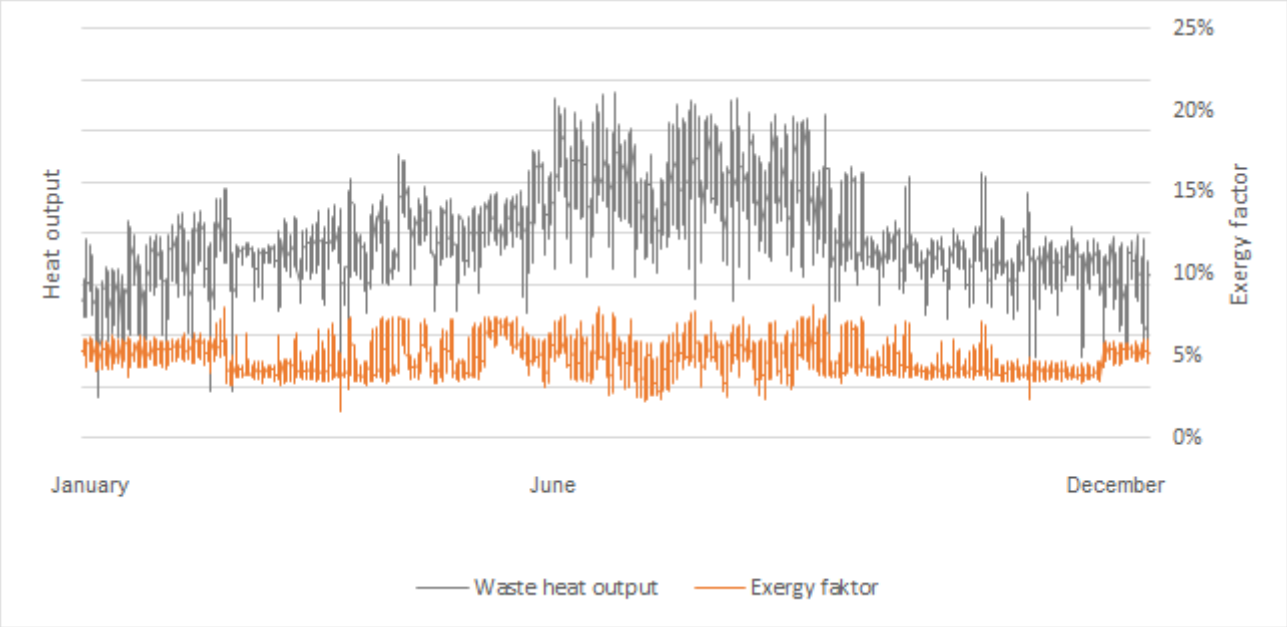

Figure 31: Trend of heat output and exergy factor of fresh products logistics FRILO for the year 2019.

The flow measurement was operated further until November 2020 and a higher ratio factor $f_{Q,FRILO}$ between heat output and electrical power input could be determined, which allows to expect an even greater amount of waste heat. The reason for this is probably the improved sealing of the refrigerated hall of the fresh product logistics, which reduces the influx of humid outside air and thus fewer defrosting processes.

This waste heat source was selected to supply the LTHC grid of this project because both a constant, sufficient supply of energy and a relatively short connection to the LTHC grid are possible.

5.4 Chilling plant for production

For cooling in the production lines three refrigeration units are used, which provide ice water for product cooling. Thereby cold is produced at a very low temperature level between 0°C and 1°C. The waste heat from the cooling systems for production is already stored in an integrated heat recovery storage tank (75°C) and is therefore not discussed in further detail.

5.5 Low pressure compressed air systems

The low-pressure network is fed by three screw compressors. Compressed air is required in many areas of the company's production. Pneumatic actuators of the products filling-station as well as the CIP-cleaning system are supplied here. As with the chilling system of product cooling, the waste heat from the low-pressure air compressors is already stored in the 75 °C heat storage tank. The low-pressure air system was therefore not considered further.

5.6 Waste heat potential from the heat recovery of the stratified storage tank

The 75-degree water storage tank has potential for further heat extraction. The storage tank is fed with the waste heat from the low-pressure compressed air systems and chilling machines for cooling of production process. Additional use of the waste heat would be desirable, due to too small voulume the waste heat occasionally has to be released via air coolers to ensure cooling of the compressed air and refrigeration units.

The stored heat is mainly used to heat the office buildings in winter. The heating system of the office buildings is supplied by a heat exchanger with a capacity that covers about 70 % of the maximum heating capacity for the office space. Since no measured data was available, the waste heat potential and the heat output profiles were determined indirectly with the help of the heating degree-days and the time-resolved outdoor temperature data from PVGIS database. The exergetic evaluation of the heat output is carried out with reference to the water temperature of the storage tank of 75 °C and the reference temperature of the anergy network in the individual seasons.

The storage tank is loaded with waste heat from the low-pressure compressed air systems and product chillers and mainly supplies the office buildings with heating energy in winter. The time-resolved trend of the freely available heat output and the exergetic share for the year 2017 are shown in Figure 32. This results in an average yearly waste heat of 1,1 % related to the average input of gas and electricity.

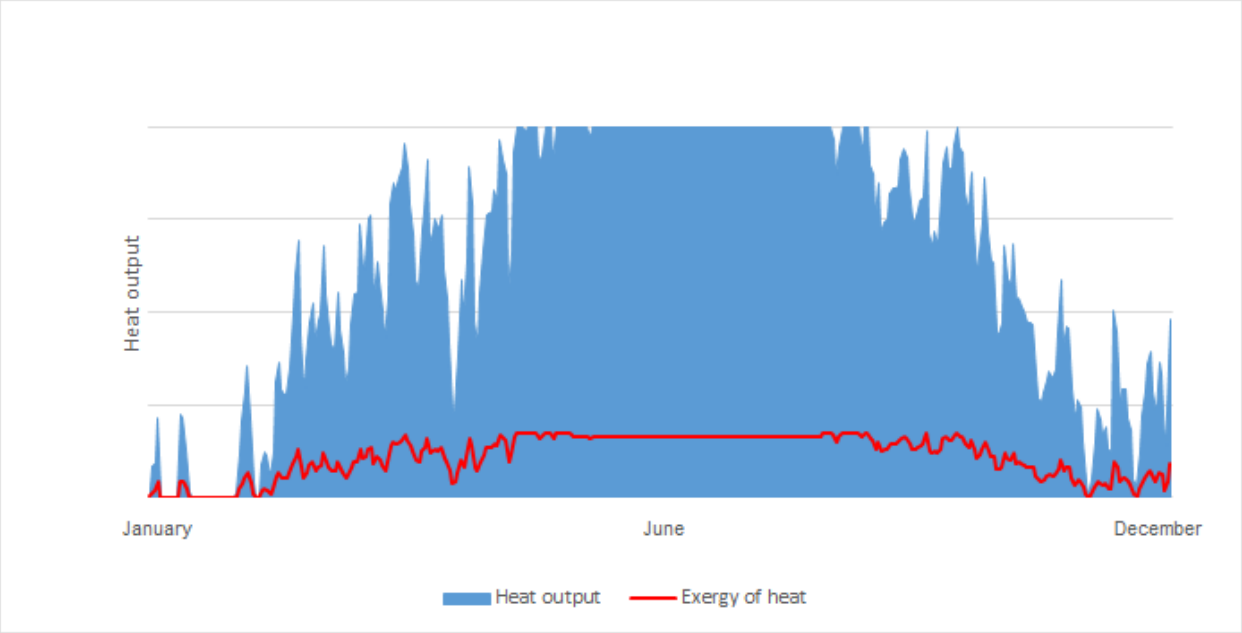

Figure 32: Illustration of the available heating power and its exergetic part.

The plateau in Figure 32 is caused by the limited capacity of the existing heat exchanger for heat extraction from the heat storage tank. The profile of the exergy follows that of the available heating power. Due to the constant power of the heat exchanger, which is available during the summer months, the exergy is also kept at a constant level. The exergy factor however remains more or less constant throughout the year due to the constant storage temperature.

5.7 Waste heat from the cooling circuit of high-pressure compressed air generation

Two Atlas Copco high-pressure compressors type AC Crepelle D46 and one LMF EcoPET high-pressure compressor are available for the compressed air high-pressure network. There is mainly one of the AC units in operation to provide the compressed air. The second AC unit serves as backup. The LMF compressor is switched on when there is an increased demand or is also used as a replacement for the AC system.
The high-pressure air compressors feed into the compressed air network at a pressure of 30 bar(g). The high-pressure air is required to inflate PET bottle blanks. The waste heat generated by the compressors is transported to table coolers and cooling towers on the roof of the dairy via a glycol-water circuit.
Time-resolved data on the electrical power consumption of the high-pressure air systems was available for the year 2019. In the course of an energy audit in 2015, measurements of the compressed air flow over a period of two weeks were carried out. In order to obtain further flow rate data, measurements were also made using clamp-on ultrasonic measuring equipment (Figure 33).

Figure 33: Measurements on the HDD systems: Atlas Copco (left) - LMF (right)

The flow measurements on the LMF-compressor did not yield any results, because signal errors occurred due to strong vibrations of the pipelines. As value for the flow rate the flow rate of the pump according to the data sheet was used. Due to the irregular operation of the high pressure compressed air system, a factor between absorbed electrical power and emitted cooling power was used. This power factor is used to create a profile of the heat output for all three high-pressure compressed air systems.
The calculation of the exergetic efficiency η_{ex} of the compressor, considering the exergy of the waste heat, was done with the following equation:

$$\eta_{ex} = \frac{\dot{m} \cdot c_p \cdot (T_2 - T_1) + \dot{m} \cdot T_{atm} \cdot \left(R \cdot \ln\left(\frac{p_2}{p_1}\right) - c_p \cdot \ln\left(\frac{T_2}{T_1}\right)\right) + Q_{ab} \cdot \left(1 - \frac{T_R}{T}\right)}{P_{el}}$$

As mentioned before, the flow measurements on the LMF-compressor did not yield any results, because signal errors occurred due to strong vibrations of the pipelines. As value for the flow rate the flow rate of the pump according to the data sheet was used. This results in an average waste heat output of 1,6 % related to the average input of gas and electricity.

The power profile for the year 2019 is shown in Figure 34.

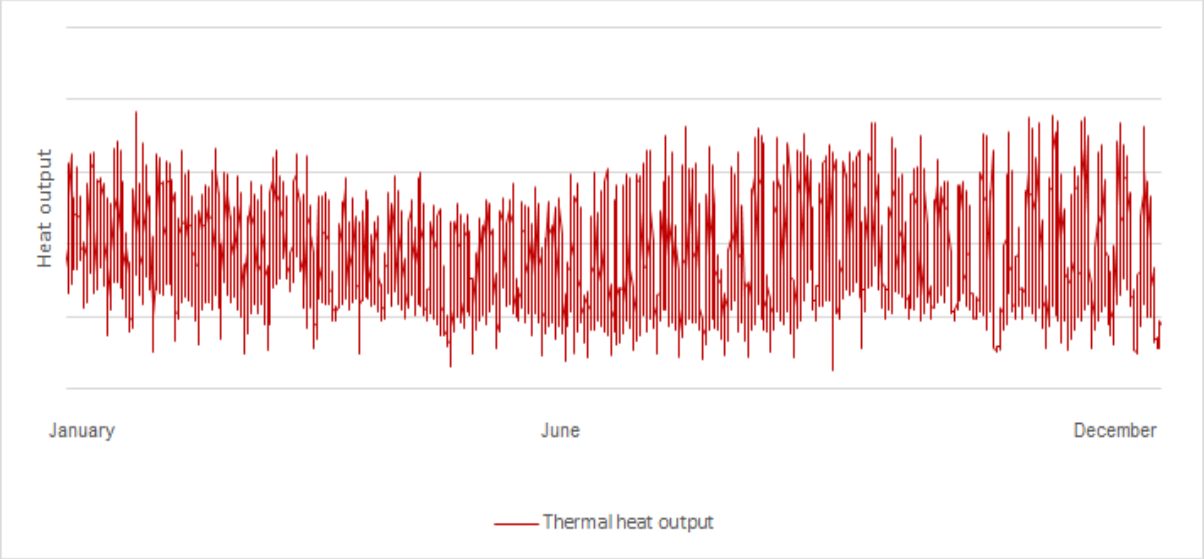

Figure 34: Profile of heat output of high-pressure compressed air systems for the year 2019.

53,2% of the exergy can be used in the compressed air after the compressor, which is driven by electric current (100% exergy). The remaining 46,8% is in the form of heat. This waste heat can be evaluated exergetically. Figure 35 shows the exergy respectively anergy flow of this compressed air system.

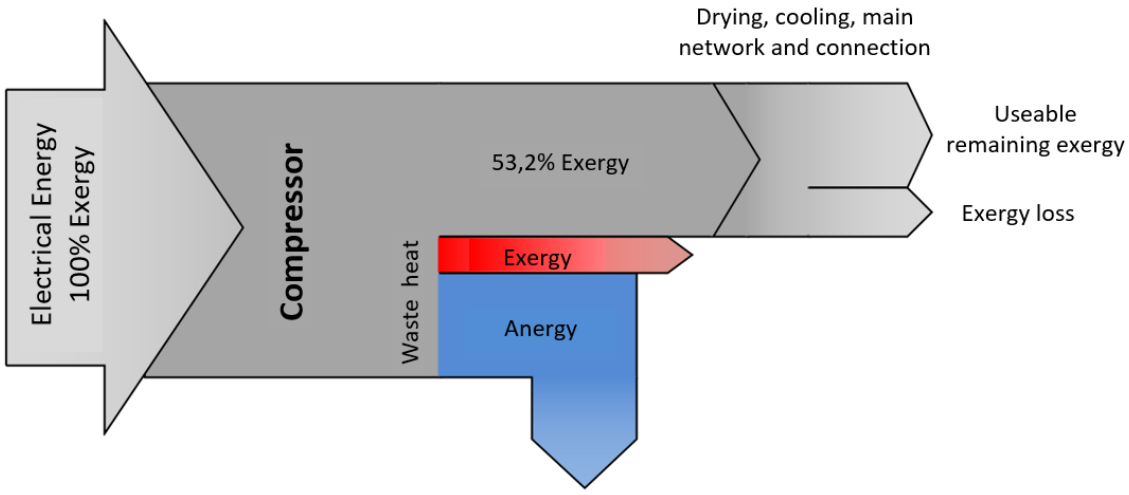

Figure 35: Sankey diagram to illustrate the exergy or anergy flow of a compressed air system.

5.8 Photovoltaic calculations

The numerical values of global irradiance used for the analysis come from the PVGIS data system (Photovoltaic Geographical Information System) of the European Commission, which was largely calculated from satellite data. The data refers to the exact location of the dairy (geographical longitude 16.23° and geographical latitude 47.99°) and is resolved at hourly intervals. Values for relative global

irradiation and ambient temperature are available for the period from 2006 to 2016.

A value of 30° was assumed for the inclination β of the surface of the PV module. Furthermore, an orientation of the modules to the south was assumed and thus an azimuth angle α of 0°. To determine the electrical output of the PV cell, the single diode model with series and parallel resistance was used, using the method of Villalve, Gazoli et. al. which does not neglect the series resistance (Figure 36).

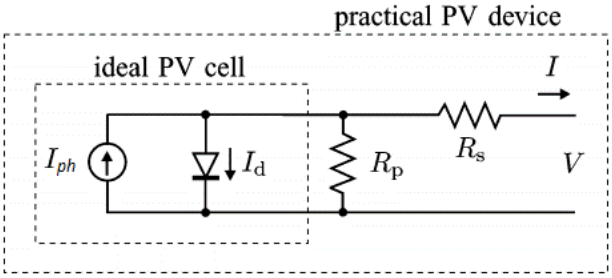

Figure 36: Circuit diagram of a PV cell / diode model [source: HABBATI, Bellia ; RAMDANI, Youcef ; MOULAY, Fatima]

The model was implemented with the software Matlab/Simulink, so that the P-V curves for different irradiances and temperatures could be calculated. Based on these curves, a regression model could be created in which irradiation and temperatures are used as variables. Since PV collectors only supply direct current, the efficiency of an inverter was also taken into account in this model. This is not a fixed value, but a function over the entire power range, whereby the function was determined from measurements of a real device.

After the specific solar data had been determined, the yields over a longer period of time had to be determined. The selection of suitable roof areas was carried out together with responsible persons at NÖM. The chosen areas can be seen in Figure 37.

Figure 37: Suitable roof surfaces of the NÖM dairy [source: Google Earth]

These selected roof surfaces are sufficiently stable to support the additional weight load by the PV

modules and their pedestals. These two areas were measured using Google aerial images with the associated measuring tool. Light wells and skylights integrated in the surface were of course subtracted. This results in a total area of 5434 m².

The modules would be aligned to the south and provided with an inclination of 30° by means of stands. The inclination results in shading losses, which can be determined by calculations of Quasching/Hanitsch: For the selected area utilisation factor f = 0,333, the relative shading losses are 4,8%. The efficiency of the inverter was calculated via a polynomial, which was determined via measurements on a real inverter. Furthermore, the degradation of the modules must also be taken into account in real operation, as they are subject to ageing during operation. This degradation was assumed to be 0,5% per year (source: Kiefer, Farnung, Müller).

Figure 38 shows the results of the simulation of the specific daily average power. It can be seen that the electrical power in 2011 is about 12 % higher than in 2016. According to the results for the years 2011 to 2016, the efficiency of the PV module considered here is 17,3 % on average, which is slightly higher than the specified value.

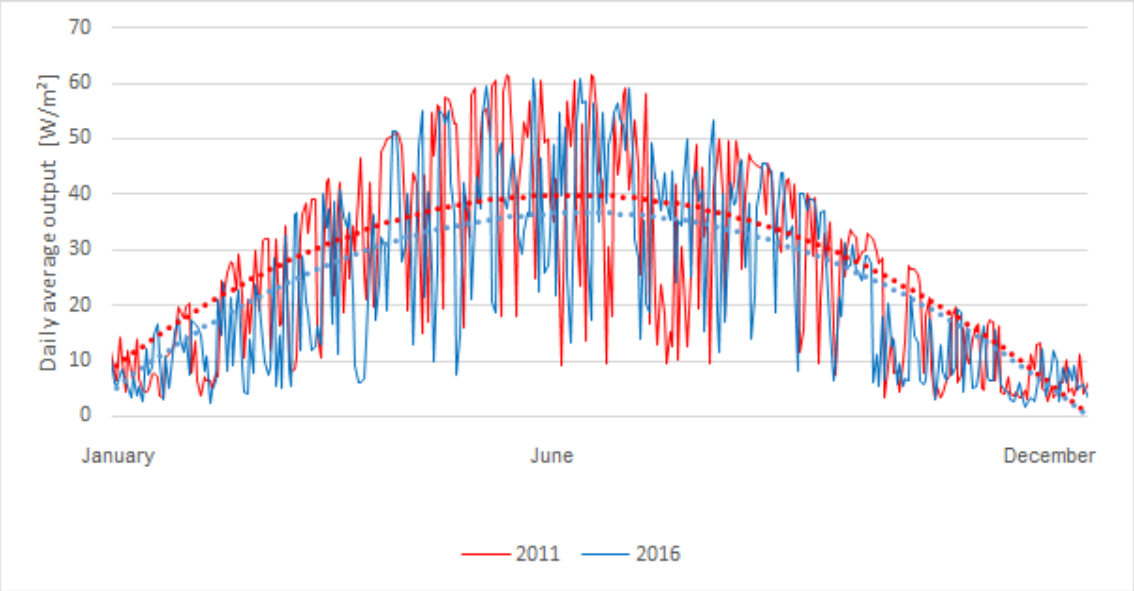

Figure 38: PV performance profiles for the location of the NÖM dairy in Baden near Vienna according to the method of Villalva, Gazoni et. al.

The profile shows the typical pattern of irradiance and associated electrical output power with increased power in the sunny summer months and low power in the dark winter months.

The following Table 8 shows the annual energy yields with the above assumptions (orientation, inclination, shading, inverter losses) and total roof area of 5434 m². The years with the lowest (2016) and highest (2011) energy yields in the period under consideration from 2006 to 2016 were taken into account.

Table 8: Energy yields of the years 2016 and 2011 with consideration of inverter, shading and degradation.

	2016		2011	
	Specific energy [kWh/m²a]	For selected area [MWh/a]	Specific energy [kWh/m²a]	For selected area [MWh/a]
Model only	199,89	361,8	224,43	406,2
Consideration inverter	186,96	338,4	210,24	380,5
Consideration shading losses	177,98	322,1	200,15	362,2
Degradation 5 years	173,58	314,1	195,20	353,3
10 years	169,28	306,4	190,37	344,5
15 years	165,09	298,8	185,65	336,0
20 years	161,01	291,4	181,06	327,7

6 Thermo-hydraulic simulation of the LTHC grid

The thermo-hydraulic simulation of the LTHC grid was carried out on the basis of the developed scenarios and all the data from the waste heat measurements in the NÖM dairy plant as well as on the geoscientific assessment.

The simulations covered hydraulic and thermal simulations of the three grid scenarios and the borehole thermal energy storage (BTES) as well as the connected heat pumps and the corresponding water based thermal energy storages, located in the energy transfer stations of the buildings. The BTES and the anergy network is modelled according to Nagler[5]. The heat transport equation leads to a linear equation system, which was solved in MATLAB® in a resolution of 15 minutes. Output parameters of the simulation are network pressures, mass flows and temperatures.

The simulation tool used in this project is based on Nagler´s (2018) low-temperature heating/cooling grid (NT-WK) simulation tool. The thermal and hydraulic simulation program TEGSim (**T**hermal **E**nergy **G**rid **S**imulation) is a stand-alone tool that does not require external computational software to model and simulate the main system components. TEGSim was programmed entirely in the MATLAB® simulation environment, and can simulate the following components:

- pipe network
- Geothermal heat storage tank
- Energy transfer stations with
  - heat pumps,
  - heat exchangers,
  - circulation pumps and
  - sensible thermal accumulators.

With the pipe network´s help, the fluid´s thermal energy in the pipes can be made available to any number of prosumers through a closed two-pipe system. The term prosumer is composed of **pro**ducer and con**sumer**. The pipe system, consisting of one hot conductor and one cold conductor, can thus be supplied with or discharged from thermal energy bidirectionally. At the energy transfer stations, the prosumers can be provided with energy from the pipe network to feed the heat pumps at different temperature levels (domestic hot water 65 °C, heating 35 °C). The required cooling energy can be provided either by using reversible heat pumps (Active Cooling) or directly by free cooling (Free Cooling). In this case, energy is supplied to the fluid in the pipe network (Free Cooling / Active Cooling) or removed (Heating / Service Water).

[5] J. Nagler: Design Criteria for GCHP-Systems with Seasonal Storage (Anergienetze); PhD-Thesis, TU Wien, Institute for Energy Systems and Thermodynamics, 2018.

The main input parameters for the simulation are the pipe network´s predefined topology and the prosumers' load curves at the energy transfer stations. If, as in most cases, additional energy is needed for the annual thermal balancing of the system, the load curve of a heat source must be specified. In a first step, TEGSim automatically estimates the pipe diameters based on the maximum flow rate and considering hydraulic factors (pipe dimension, pressure drop per meter of pipe). However, a manual adaptation of the pipe diameters according to technical-economic criteria such as price per diameter, installation costs, and efficiency is recommended in most cases. If sensitive thermal storage tanks (hot water tanks) are present within the energy transfer stations, they can be generically dimensioned based on technical-economic criteria for initial simulations. The user can also configure all active and passive components, their specific properties, performance data of heat pumps, circulation pumps, and many more. The geothermal heat storage can also be pre-dimensioned by the developed algorithms for a yearly balanced operation. If desired, the storage sizes can be adjusted by the user. Furthermore, geometries and operation modes of the borehole heat exchangers are available to choose from CX, 1U, or 2U borehole heat exchangers with different flow and arrangements of the U-tubes (for 1U and 2U borehole heat exchangers).

The developed simulation tool calculates the thermal and hydraulic operating conditions for given boundary conditions. Due to the complexity of the power distribution network, a thermal-hydraulic calculation method was designed, see Figure 39, which allows both the calculation time and the required storage capacity to be kept as low as possible. Compared to the transient thermal simulation, the hydraulic simulation of the network calculates in a quasi-stationary manner. Due to the period of one year to be simulated, a time step size of 60 minutes was applied for the hydraulic simulation. The variables resulting from the iterative hydraulic simulation, such as pressure and velocity field, serve as boundary conditions for the subsequent transient thermal calculation. For the selected time step size, the hydraulic quantities are kept constant. In the transient thermal simulation, the main task is to calculate all temperatures in the pipe network and the geothermal reservoir. The time step size of the thermal simulation is set to 30 minutes by default. After completing the thermal calculation, new boundary conditions are set for the hydraulic simulation. In the developed thermohydraulic calculation method, two thermal calculation steps are performed within each hydraulic calculation step.

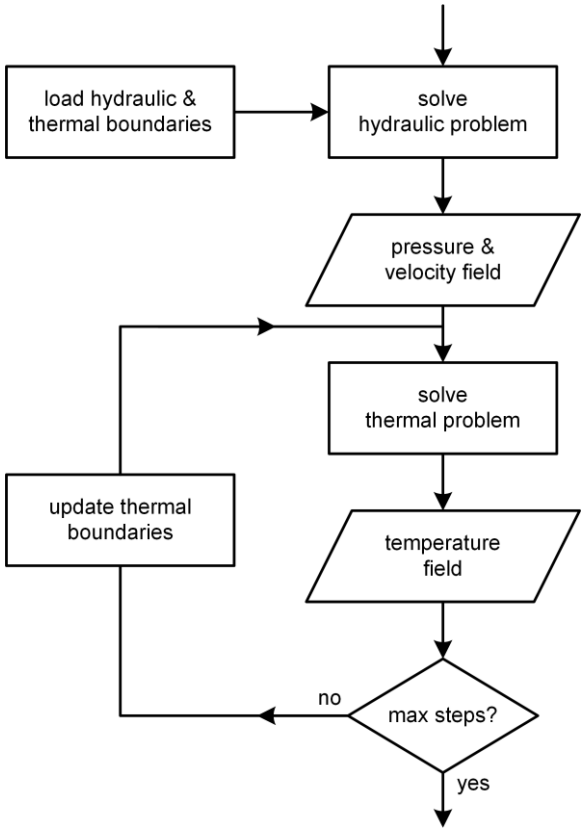

Figure 39: Flowchart of the thermal-hydraulic calculation scheme for one hydraulic calculation step and a user-defined number of thermal calculation steps.

We developed the program was to simulate the varying temperature level of complex energy distribution systems and confirm the proposed concept´s long-term suitability. It is necessary to consider the whole range of time-dependent load profiles and boundary conditions for reliable simulation results.

6.1 Pipe network and borehole heat exchangers

In a first step, TEGSim estimates the pipe diameters according to the maximum heat output to be transported. A practica method for reducing pumping work and investment costs is adjusting the maximum pressure drop per meter of pipe. In the SANBA project, a specific pressure drop of 150 Pa/m was chosen. Since this means that the pipes are designed for the maximum load, manual adjustment of the lines diameters according to technical and economic criteria such as price per diameter, installation costs, and pipe friction losses is inevitable. The quasi-stationary hydraulic calculation was carried out following existing methods and the work of Nagler (2018) and Bothe (2016). The topology of the network is represented by an incidence matrix known from graph theory. The system equations are set up according to the QH - method. In the QH - method, an equation is set up for each pipe string as a function of the volume flow in the pipes Q and the pressure heads in the nodes H, whereby the equations are formulated with the variables pressure p and velocity u. Therefore, a subsequent conversion of the simulation results is not necessary. For the pressure losses due to pipe friction Δp_f, the Darcy-Weisbach equation is used. These pipe friction losses depend on the pipe friction coefficient λ,

the density of the fluid ρ, the pipe length L, the characteristic pipe diameter d, and the flow velocity u in the pipes. Geodetic height differences ∆h and the resulting pressure differences ρg∆h are calculated by extending the Darcy - Weisbach equation according to equation (1)

$$p_1 - p_2 = \frac{\lambda \rho L}{2d} u^2 \pm \rho g \Delta h = \Delta p_f \pm \rho g \Delta h. \quad (1)$$

For modeling the thermal behavior of the pipe network, a 2D-resistance-capacity model (2D - RCM) for 1U-pipe BHE according to Bauer (2018) is used, see Figure 40. The calculation can consider the thermal conductivities and capacities of the different layers of the soil. Inside the tubes, the heat transfer coefficients are calculated according to the flow regime and the properties of the heat transfer medium. The heat transfer medium is assumed to be incompressible. The calculation of the thermal resistances inside the BHE is partially performed using empirical approaches from Bauer (2018) and the 1st order multipole method of Claesson and Javed (2019). The fill material is divided into two equal parts, each with a node where the temperature (T_f1, T_f2) is calculated. The node of the borehole wall is connected to the soil by thermal resistances and capacitances. The surrounding ground is modeled axisymmetrically with n concentric annular surfaces. These are coupled to the borehole wall employing thermal resistances and capacitances.

In the application presented here, the pipes between the borehole wall and the outer edge of the computational domain (outer diameter: 2.4 m) were divided into nine circular rings of equal thickness. From a programming point of view, it makes sense to discretize each pipe with the same number of axial and radial elements. The discretization was chosen so that the maximum axial cell thickness does not exceed 1 m. Based on the pipe lengths, each pipe was divided into 225 equidistant elements. Based on the general transport equation, the nodes of each layer can be connected to form a two-and-a-half-dimensional model of the BHE and the surrounding soil. Within the pipes, heat transfer by conduction and convection is considered. In solid components such as the pipe, fill material, and soil, on the other hand, only conduction is possible. The thermal model is fully unsteady using the implicit formulations of the 1st order forward differences in time and the 1st order upwind scheme in space. The axial and radial discretizations were evaluated and optimized in terms of computational time and accuracy. The reader can find further details on the transport equations in Huber (2020).

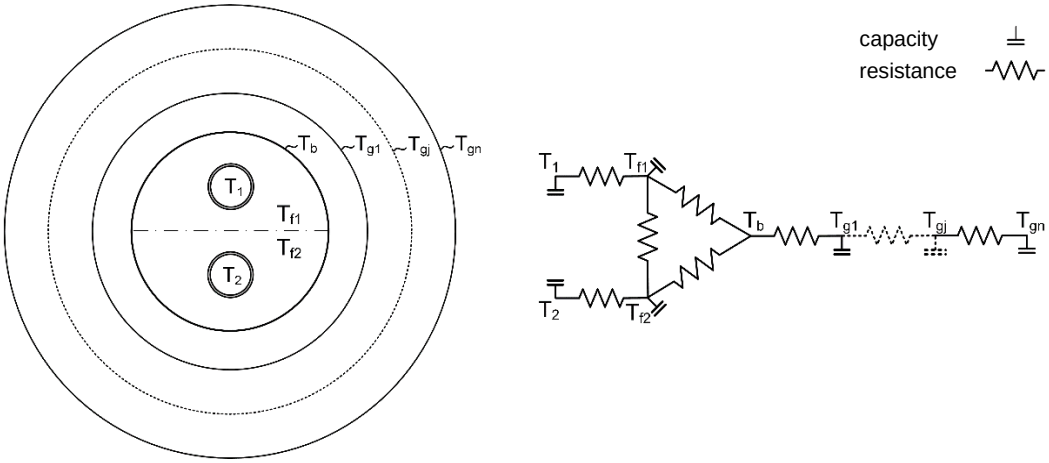

Figure 40: RCM for a segment of the pipe network and the surrounding soil with the calculated temperatures: T_1, T_2... Temperature of the fluid in the pipes, T_{f1}, T_{f2}...Temperature of the filling material, T_b... Temperature of the borehole wall, T_g... Temperature of the surrounding soil. Adapted from Bauer (2018).

The Borehole Thermal Energy Storage (BTES) consists of several 2U BHE connected in parallel or series. TEGSim can simulate CX-, 1U- and 2U-tubes. Only the 2U - tube BHE relevant for the SANBA project will be discussed in more detail in the following. The temperature field and the pressure drop are calculated analogously to one of the pipe networks.

The hydraulic calculation of the BTES mainly aims at the determination of the pressure losses. Since all BHE within the BTES have the same mass flow passing through them, it is sufficient to calculate the pressure loss for only one pipe BHE. Analogous to the pipe network, the flow within the BTES is also considered to be incompressible. The friction-induced pressure loss between BHE inlet and outlet is determined with the Darcy - Weisbach equation, see equation (2).

$$\Delta p_{Sonde} = \frac{\varrho u^2}{2}\left(\frac{\lambda L}{d} + \zeta\right) \qquad (2)$$

A pressure loss coefficient ζ considers the change in flow direction at the BHE base. The pipe friction coefficient λ is calculated depending on the flow regime. For laminar flows (Re<2300), the Hagen - Poiseuille equation is used. The pipe friction coefficient must be estimated iteratively in the transition and fully turbulent region. The Colebrook - White - equation is used in the transition region, and the Nikuradse - equation in the fully turbulent region.

The thermal calculation of the BTES is broadly analogous to the pipe network. In contrast to the pipe network, however, different BHE can be used. Therefore, for the thermal behavior of the BTES, 2D - ERMs for CX, 1U, and 2U - pipe BHE were calculated according to Bauer (2018). In contrast to the work of Nagler (2018) thermophysical parameters such as density, heat capacity, and thermal conductivity of the soil can be taken into account as a function of depth. The presented model can thus be better adapted to the local conditions. Figure 41 shows the RCM used for a 2U - pipe BHE. There is radial and

vertical heat conduction in the soil. The RCM used by Nagler (2018) for a 1U tube BHE considers the vertical heat conduction within the transport equations, but the ground below the BHE is not modeled. As the BHE depth decreases, the influence of the modeled soil below the BHE increases. Therefore, the authors considered the soil below the BHE in the development of TEGSim. For this purpose, the borehole was extended to the lower edge of the calculation area and connected to the surrounding soil with one node per circular ring and layer. The thermophysical parameters of the extended borehole were also adapted to those of the soil. With this procedure, TEGSim can calculate the thermal behavior in the area of influence of the pipe BHE more precisely.

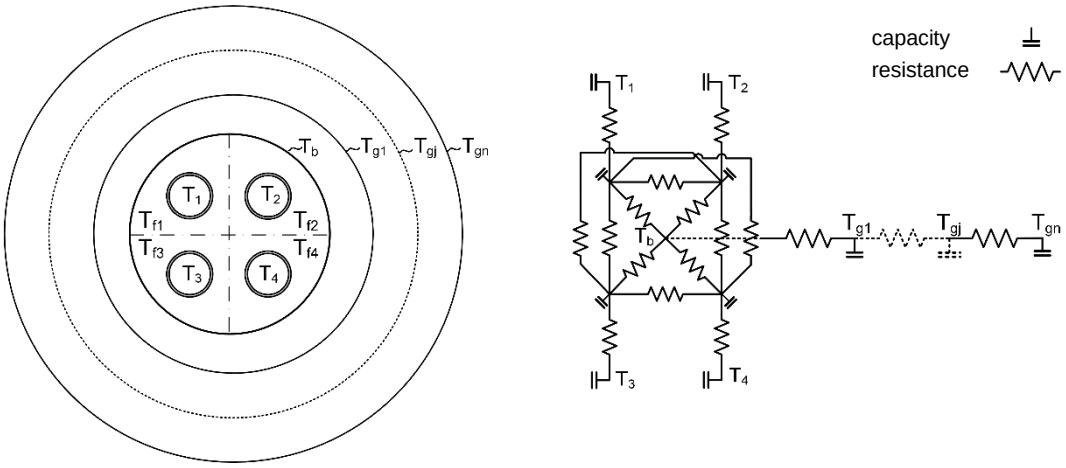

Figure 41: RCM for a segment of a 2U pipe BHE and the surrounding soil with the calculated temperatures: T... Temperature of the fluid in the pipes, T_f... Temperature of the filling material, T_b... Temperature of the borehole wall, T_g... Temperature of the surrounding soil. Adapted from Bauer (2018).

The individual drillings in the BTES are aligned equidistantly in the x and y-directions. The distance between the BHE is typically in the range of a few meters. The adjacent BHE thermally influence the BHE in the center of the BTES. In contrast, the BHE at the edge are only partially influenced by the neighboring BHE. The superposition of the calculation results from one BHE to all other BHE would violate the model assumption of identical boundary conditions. The reciprocal influence of the quadratic BHE field is taken into account by a global procedure using Kelvin´s line source theory. Thus, the temperature at the radial boundary layer of the simulated BHE is adjusted every 24 hours, see Nagler (2018).
The equations of the pipe BHE, the pipe network, and the boundary conditions are accumulated as a linear system of equations in a matrix and solved for each thermal time step. Therefore, all nodal temperatures within the pipe BHE and the pipe network are known for each thermal simulation time step.

6.2 Energy Transfer Stations

With the help of Energy Transfer Stations (ETS), prosumers can be supplied with energy for heating (H) and domestic hot water (DHW) via heat pumps, FC directly from the grid, and active cooling (AC) via

reversible heat pumps. The ETS connects the prosumers to the low-temperature heating/cooling network (ultra-low temperature district heating - ULTDH). Depending on the prosumers, the tasks of the ETS are:

- Provision of hot water for H
- Provision of hot water for DHW
- Provision of cold water for FC or AC

In addition, the following components are in the ETS: heat pumps, heat exchangers, hot water storage tanks, circulation pumps, and valves. Since not all prosumers have the exact requirements for DHW, H, and C, different types of ETS are usually necessary. However, they all consist of the same kind of components except for a different number and size of heat pumps and hot water storage tanks.

Figure 42 shows the schematic hydraulic diagram of a fully equipped ETS. Depending on the requirements, various components can also be omitted. For example, an office or school building with low hot water demand does not require a heat pump for hot water preparation. The required hot water is provided highly efficiently by using decentralized electric instantaneous water heaters. The modeling of the ETS, particularly the modeling of the circulation pumps, heat exchangers, and hot water storage tanks, was kept simple to reduce complexity and computational time. A more detailed model would have little impact on the simulation results. In the models used here, pressure losses within the ETS occur only due to pipe friction. Due to the short pipe lengths within the ETS, it was assumed that pipe friction losses only occur when flowing through the heat exchangers. Using ζ-values, these can be taken into account analogously to equation (2). Hence, the pressure loss changes the pressure boundary condition between the ETS and the pipe network at the transfer point.

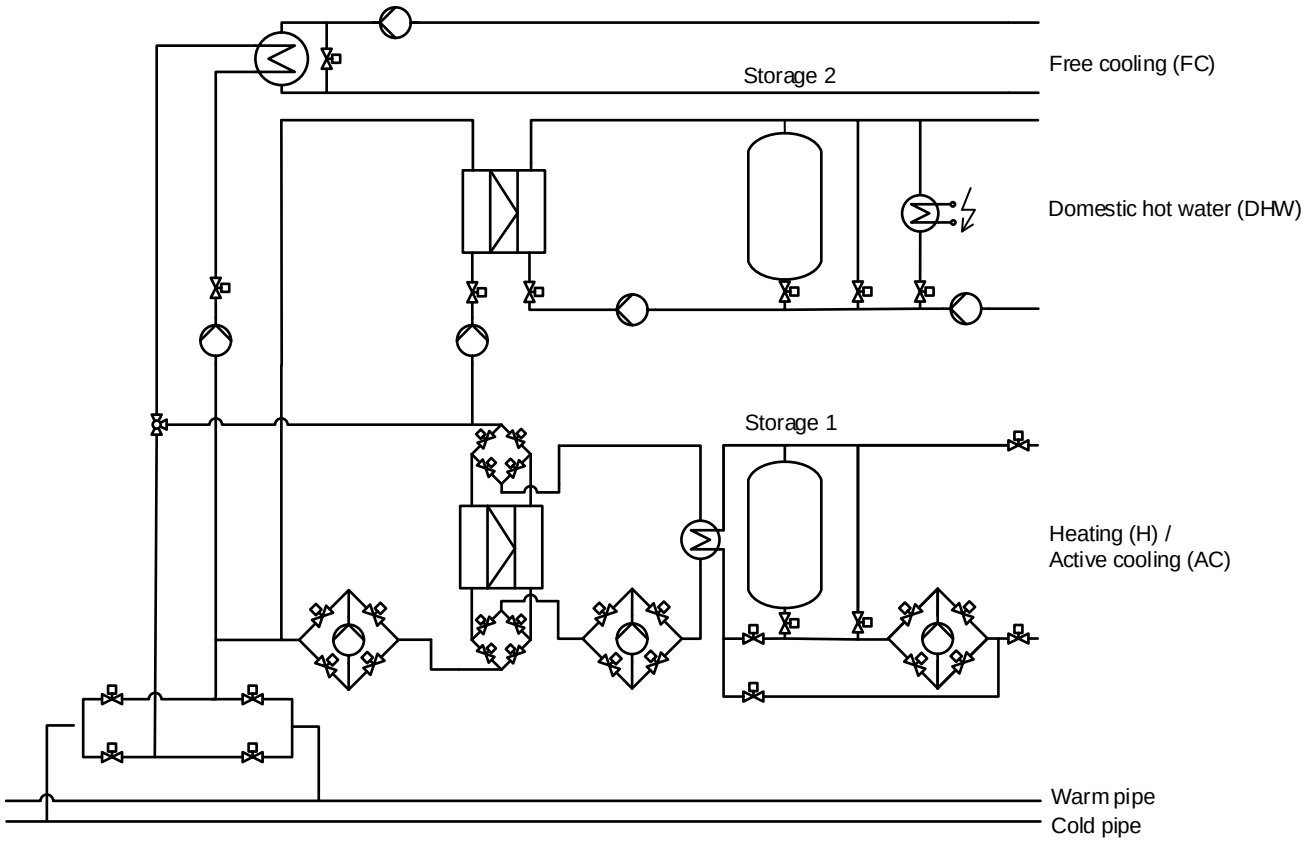

Figure 42: Schematic hydraulic diagram of a fully equipped ETS and its main components: Heat pumps, heat exchangers, circulation pumps, hot water tanks, and valves.

6.2.1 Heat pumps

The temperature difference between the inlet and outlet of the heat pumps is fixed at 4 K. Manufacturer-specific models with specified COP values and performance classes are implemented. The temperature dependency of the COP values of the heat pumps is taken into account by manufacturer-specific COP values for two temperature levels (35 °C for H and 63 °C for DHW). TEGSim can generically determine the number of heat pumps needed by specifying specific maximum and minimum loads from a set of predefined heat pumps. It has been shown that the source temperature for prosumers (e.g.15 °C) varies only slightly. A more detailed calculation of the COP values requires more computation time, while the impact on the resulting electrical energy demand is negligible.

6.2.2 Heat exchangers

The temperature difference between the inlet and outlet temperature of the heat pumps was set to a user-defined value of 4 K. Table 9 shows the defined temperature differences at the different heat exchangers. These temperature differences can always be achieved by adjusting the flow at the heat

exchangers depending on the load. Detailed modeling of the heat exchangers is not beneficial due to the long computation times as accuracy improves negligibly.

Table 9: Temperature differences and pinch point at the different heat exchangers

Heat exchanger at position	Temperature difference K
NÖM	4
FC	5
AC	5
H	5
DWH	5
Pinch FC	2
Pinch AC	2
Pinch H	2

6.2.3 Buffer storage

In a first approach, TEGSim estimates the capacity of the storage tanks in such a way that the heat pumps only have to be designed for 80% of the peak load. This guarantees an economically reasonable dimensioning of the manufacturer-specific devices. In addition, TEGSim selects the storage tank sizes within predefined storage tank volumes. This makes it possible to implement commercially available storage sizes without having to adjust the storage size to manufacturer-specific sizes iteratively. The water storage tanks are modeled with two temperature levels, a one-dimensional thermocline and a state of charge. In evaluating the results, it was found that the water storage tanks are frequently charged and discharged, and the idle times of the charging cycles are in the range of a few hours, justifying the simple model.

6.2.4 Circulation pumps

Each of the ETS has several circulation pumps depending on the configuration. The pumps are controlled in such a way that a user-defined temperature difference, e.g. 4 K, at the heat exchangers can always be guaranteed. The pressure losses of the components within the ETS are taken into account by manufacturer-specific zeta values. The dimensioning of the circulating pumps is done in post-processing based on the pressure differences and the required mass flows.

6.3 Solar thermal energy

The energetic potential of solar thermal plants was evaluated using a simulation tool developed at the Institute of Energy Technology and Thermodynamics at the Vienna University of Technology. However, the economic viability of solar thermal plants is not given under the present conditions. Such a plant is

not necessary since the feed-in by the NÖM can cover the demand to balance the BTES on an annual basis. In cases where there is no industrial waste heat source, the use of solar thermal can be an economically viable and highly efficient system for energy feed-in.

6.4 Photovoltaic & Battery Storages

The electricity demand of the heat pumps can be covered at least partially by photovoltaics. Simulations with different inclinations and orientations prove considerable potential as all roof surfaces of the new buildings could be equipped with photovoltaic modules. Due to the temporal discrepancy between supply and demand, the use of electrical storage (Battery Storages) is necessary. However, it has been shown that the high costs of the required electrical storage and photovoltaic modules do not offer an economic advantage. Therefore, the overall economic concept does not include the use of photovoltaics and electrical storage.

6.5 Boundary conditions for the simulation

The simulation results are significantly influenced by the imposed boundary conditions. The main boundary conditions are described in more detail below.

6.5.1 Temperatures

Dirichlet boundary conditions are imposed for the borehole heat exchangers and the pipe network considering the geothermal temperature gradient and a test reference year (TRJ) data set. The TRJ dataset includes ground temperatures at a depth of 0,1 m, 0,2 m, and 0,5 m for the market town of Gumpoldskirchen in Lower Austria. The temperature at a depth between 0,5 m and up to the beginning of the undisturbed soil temperature was solved using the one-dimensional heat conduction equation. Newmann boundary conditions have been imposed at the top and Dirichlet boundary conditions at the bottom. The undisturbed ground temperature occurs at a depth of 15 m in the studied area and is 10.8 °C. Above a depth of 15 m, the constant geothermal temperature gradient is 0,02 K/m. Figure 43 shows the schematic temperature curve down to a depth of 30 m for different seasons.

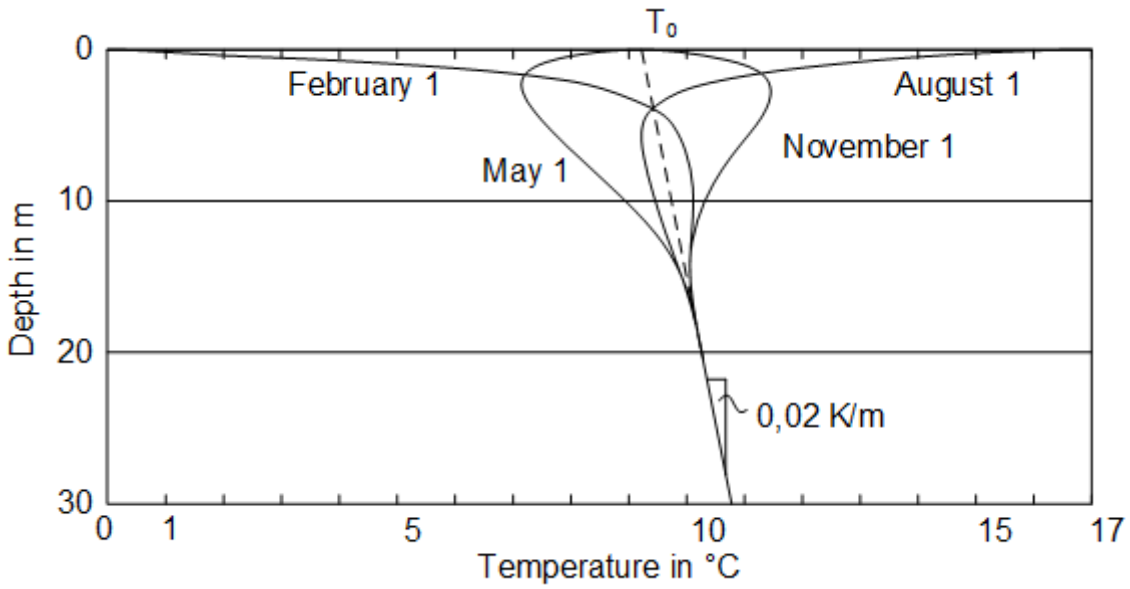

Figure 43: Schematic temperature curve down to a depth of 30 m for different seasons, according to Huber (2020).

6.5.2 Thermophysical parameters of substrate and filling material

Natural variations of the geological layers in the catchment area of the borehole heat exchangers entail deviations of the thermophysical parameters (density, thermal conductivity, and specific heat capacity) of the subsurface. Depth-dependent thermophysical parameters were used. Since the subsurface surrounding the BHE was modeled rotationally symmetrical, only horizontally running geological layers can be considered. An inclination or an asymmetrically decreasing thickness of the geological layers cannot be considered. Thus, for the presented simulations, the different geological layers have all been assumed to lie ideally horizontally. The depth-dependent thermophysical parameters are listed in Table 10.

Table 10: Tiefenabhängige thermophysikalische Parameter des Untergrunds

Depth m	density kg/m^3	Heat conductivity W/(m K)	spec. heat capacity J/(kg K)
6	1900	1,748	121,53
15	2400	1,677	916,67
24	2400	1,652	916,67
33	2400	1,583	916,67
42	2400	1,756	916,67
51	2400	1,915	916,67
60	2400	1,908	916,67
69	2400	1,647	916,67
78	2400	1,681	916,67

87	2400	1,452	916,67
96	2400	1,990	916,67
105	2400	1,901	916,67
114	2400	1,796	916,67
120	2400	1,828	916,67
121	2300	2,600	913,04
185	2300	2,600	913,04

The thermophysical parameters of the soil surrounding the pipe network are almost constant due to the existing homogeneity of the top layer of soil. For the simulation of the soil surrounding the pipes, the thermophysical parameters shown in Table 11 have been used.

Table 11: Constant thermophysical parameters of the subsurface in the catchment area of the pipe network

Density kg/m^3	Heat conductivity W/(m K)	Spec. heat capacity J/(kg K)
1500	1,5	1500

6.5.3 Demand profile

The simulated energy grid distribution network is significantly influenced by the demand profiles imposed at the energy transfer stations. The demand profiles of the different scenarios, therefore, form essential boundary conditions for the simulations carried out using TEGSim. Within the scope of this project and the developed scenarios, operation without an external heat source cannot be covered economically from the BTES due to the high peak loads. The use of waste heat from the NÖM, as envisaged by the consortium, therefore contributes significantly to the economic success of the overall concept. Unlike the load profiles of the buildings, the load profile of the waste heat source is based on measured values.

6.6 Design strategies for the anergy network and its components

Table 12 summarizes the main design strategies of the different components.

Table 12: Design strategies for the anergy network and its components

Component	Design strategies
Pipe network	
Topology	– Shortest possible cable lengths
	– Laying under buildings or roads leads to significantly higher costs
Pipe diameter	– Design for maximum capacity leads to oversizing

	– Analysis of annual duration curves of flow velocities to minimize pressure losses over long periods of time
	– Standard pipe dimensions offer price advantages
Pipe material	– Long-term resistant and easy to install pipe material such as polyethylene (PE)
	– Poor thermal conductivity of PE reduces thermal losses
	– Bar material reduces transportation costs compared to roll material
	– Easy processing and low weight of PE offers price advantages
	– Common pipe material offers price advantages
	– Conditional pressure resistance of PE, but sufficient for SANBA
Pipe insulation	– Insulated pipes reduce thermal losses
	– At fluid temperatures close to the ambient temperature, the influence of insulation is negligible.
	– The more significant the temperature difference between the fluid in the pipe and the environment, the greater the input on heat losses
	– Increased costs due to pipe insulation
BTES	
BHE type	– CX tube BHE have high short-circuited heat flux between flow and return
	– Positioning of the core tube in the annular gap is difficult; off-center core tube position increases the short-circuit heat flow
	– 2U tube BHE are only conditionally better suited than 1U tube BHE
	– 2U tube BHE are state of the art
BHE geometry	– standard dimensions d 32 and d 40 offer cost advantages
	– Minimum BHE spacing approx. 4 m; smaller BHE spacing cannot be realized due to unwanted borehole deflection
BHE depth	– Depending on the local geology
	– Depths greater than 200-300 m are unfavorable from an energy point of view
ETS	
Heat pumps	– Design according to manufacturer-specific performance classes
	– Integration of specific COP values for the calculation of the electrical energy demand
	– Design according to maximum load does not make sense as this

	leads to frequent cycles of the heat pumps; better two small heat pumps than one large one
Hot water tank	– Design according to manufacturer-specific volumes – Modeling with two temperature levels and one thermocline is sufficient for frequent loading and unloading.
Circulation pumps and valves	– Design based on maximum pressure head and flow rate in post-processing – Neglecting flow resistances due to pumps and valves
Heat Exchangers	– Consideration of the pressure loss through manufacturer-specific pressure loss coefficients at the nominal point – Modeling of the heat exchanger by fixed temperature difference and pinch point – No iterative solution of the WT equations
Photovoltaic & Battery Storages	– Dimensioning to meet own demand is usually not economically viable – Feeding surplus electricity into the grid is usually not economically viable

7 Building technology assessment and system design

The state of the buildings of the Martinek Kaserne has been examined with two on-site inspections. It is obvious, that the condition of the buildings worsens rapidly with every year they are not in use. Thus, the renovation needs increase in parallel. Based on the monument protection, the blueprints provided by the Austrian Military and the perception of the conditions on-site thermal refurbishment measures, have been defined. The effect of every measure has been quantified using the methodology of the Austrian building energy certificate ("Energieausweis"). The following diagram shows the heating demand of the building stock in dependence of different thermal refurbishment measures.

As a groundwork for the dynamic thermal simulation the areas of the stock buildings which actually had been in use were determined. Additional areas within the building stock that could be used in the future were identified (e.g. conversion of attic stories, adding a second floor to part of the garages).
In advance of the detailed dynamic thermal simulation, the locally resolved load profiles for the anergy grid have been estimated and the supply temperatures for each HVAC component has been set.

For the estimation of the energy demand, the quality of the thermal envelope and the usage in dependence of the three utilization scenarios has been taken into account. The following diagram shows the heating and cooling demand for the three scenarios (Figure 44).

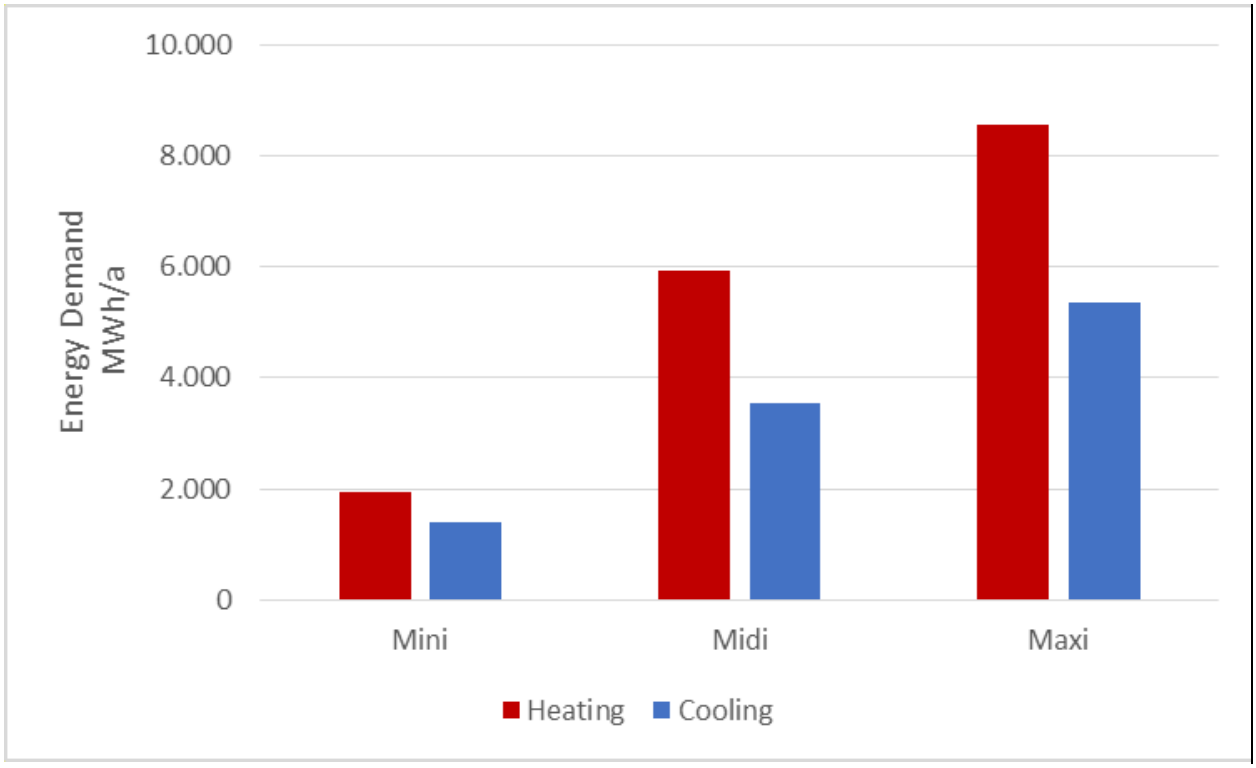

Figure 44: Energy demand for heating and cooling of the three utilization scenarios

This renovation concept is a guideline for the holistic consideration of the renovation of historical buildings using the Martinek Barracks as an example. In accordance with the concerns of cultural heritage preservation, the most necessary measures for increasing the thermal building standard and energy efficiency are dealt with and possible solutions are presented as examples. It does not claim to be complete and does not represent a planning service in the sense of the Civil Engineering Act[6].

7.1 Characteristics of the Martinek military camp7

Year of construction	1938 - 1941	
Total floor area:	418,900	m²
Built-up area:	80,900	m²
Number of buildings:	57	
Number of other buildings:	21	
Gross floor area (GFA):	102,600	m²
Net floor area (NFA):	72,900	m²
Usable floor area (UFA):	54,100	m²

7.2 Thermal-Energetic Investigation of the Existing Building

The buildings on the site are constructed in two different ways. The former crew buildings are of solid construction with solid brick walls and reinforced concrete ceilings, and the former garages are of lightweight timber-frame construction.

Energy performance certificates are available for the team buildings and parts of the garages. The different parts of the building have heating demand values, HWB_{SK}[8] , between 130 and 270 kWh/m²a (with an outlier of 899 kWh/m²a for one part of the garage). These values are based on default U-values and deviate significantly from the real values in some places. In order to carry out an energy demand survey with higher accuracy, a representative team building is defined for which the U-values are calculated on the basis of the real wall constructions. The heating energy demand of all crew buildings is derived from this representative crew building. The heating energy demand of the garage buildings is neglected in the following analysis, as these parts of the building were largely unheated.

[6] Federal Act on Civil Engineers (Ziviltechnikergesetz 2019 - ZTG 2019)

[7] *MIMZ, 2012, Immobilien Report 2012*

[8] space heating demand in local climate

7.3 Structural components of the existing building stock

The component structures are derived as accurately as possible from the as-built plans and, if necessary, supplemented by empirical values. For the assessment of the building stock, one buildings was analysed in detail.

Building 24 is a two-storey team building with a north/south orientation. As can be seen in the following Figure 45, it is embedded in the group of buildings and located in the south/east of the site. It measures 63.23 m in length and 13.50 m in width. It has a basement and the attic is not insulated. Due to its cubature and equipment, it can be seen as representative of the buildings on the site and allows conclusions to be drawn about the energy situation of the entire ensemble.

Figure 45: Aerial photograph of the ensemble with marking of the object 24

7.3.1 Exterior walls

The exterior wall construction, as shown in the following Table 13, is simplified for all exterior walls of the building in the energy performance certificate and has a U-value of 1.4 W/m²K.

Table 13: Existing exterior wall construction

	d [m]	λ [W/mK]	ρ [kg/m³]
Exterior plaster	0.040	0.870	1,800
Normal format brick	0.300	0.700	1,700
Interior plaster	0.040	0.800	1,800
Total	0.380		

7.3.2 Ceiling above upper floor

The structure of the top floor ceilings, as shown in the following Table 14, is described in a simplified form for all ceilings above ground floor level in the energy performance certificate and has a U-value of 1.4 W/m²K.

Table 14: Ceiling above upper floor of the existing building stock

		d [m]	λ [W/mK]	ρ [kg/m³]
Parquet		0.020	0.170	700
Formwork		0.030	0.150	600
Fill		0.030	0.150	1,800
Screed		0.050	1.400	2,000
Reinforced concrete - ceiling		0.200	2.300	2,400
Interior plaster		0.020	0.800	1,800
Total		**0.350**		

7.3.3 Ceiling above basement

The structure of the ceilings above the basement, as shown in the following Table 15, is simplified for all ceilings above the basement of the building in the energy performance certificate and has a U-value of 1.2 W/m²K.

Table 15: Ceiling above basement of the existing building stock

	d [m]	λ [W/mK]	ρ [kg/m³]
Reinforced concrete - ceiling	0.200	2.300	2,400
Screed	0.060	1.400	2,000
Fill	0.030	0.700	1,800
Formwork	0.030	1.150	600

Parquet	0.020	0.170	700
Total	0.340		

7.3.4 Windows

The two window sizes listed below are used for all windows of the study building with a U-value of 2.5 W/m²K (default value according to OIB Directive 6 Guideline 2015).

Table 16: Window stock

	Dimension [m]	Energy transmittance [-]	Glass share [%]
Exterior windows A	1.50 x 1.65	0.67	80
Exterior windows B	1.75 x 1.65	0.67	80

7.4 Building damage documentation

Figure 46: Damage patterns in different indoor spaces.

The ensemble is currently not in use. Windows have been destroyed by vandalism and some of the interior rooms are in a very poor condition. Under these circumstances, detailed measurements of the indoor climate would not be very meaningful.

During the use of the barracks, the groundwater level was actively lowered by means of pumps to prevent water from entering the basement rooms. After the barracks were closed down, these measures were discontinued, and parts of the cellars are currently under water (Figure 48).

Figure 47: Damage to ceiling and walls due to moisture ingress

Due to the considerable moisture ingress, walls and ceilings are in part severely impaired. The wooden floors, where present, are partly broken and severely damaged (.

Figure 48: Cellar room with considerable water ingress

Figure 49: Damage to parquet flooring

A large proportion of the building components are affected by moisture damage and salt efflorescence (Figure 50). A sampling for the analysis of the damaging salts was not carried out. In order to initiate such an investigation, there must be a defined task and the preservation of the monument must be coordinated.[9]

Figure 50: Interior with considerable moisture damage.

8 Preservation and refurbishment concepts

The preservation of the building structure and the conservation of monuments are at the centre of a sensible approach to the renovation or reutilization of listed buildings. The sooner the envisaged new uses correspond to the original purpose of the buildings and/or parts of the buildings, the easier and more economically feasible it is to resume utilization. A thorough examination of the existing substance and the possibilities for a new use are necessary in any case.

Parts of the Martinek military camp, for example, were originally used for training purposes, so it makes sense to continue using them in this way and thus fundamentally preserve the structure of the buildings concerned. The original catering facilities could also be used again as such and could be reactivated as a refectory and cafeteria. It also makes sense to reuse existing office space as such, whereby special attention should be paid to the interiors and their furnishings. Modern offices sometimes need a completely different infrastructure than how they were originally intended. Some of the former garages could be reused as such or adapted as commercial space. There are extensive basements throughout the site. The future use of these areas depends on how much of the existing moisture can be removed

[9] (Hebert & Österreich, 2015, S. 54)

after reactivation of the groundwater pumps. The use for storage is not foreseeable in the short-term; the dry attics are more suitable for this.

8.1 Climate measures and preservation of indoor spaces

The indoor climate is largely determined by the room volume and the nature of the envelope. Changes in the indoor climate always have an impact on the existing building substance, which must be taken into account. For example, changes in surface temperatures can cause condensation and mould to form. Measures to stabilise the indoor climate should be implemented in the preservation of historical monuments with minimal intervention in the historical substance and inert climate processes. From the point of view of monument preservation, passive measures (utilisation behaviour) should always be preferred to active methods (climate control). Temperature stability should be aimed for and extreme deviations, which can damage surfaces and inventory in the medium and long term, should be avoided or minimised.
The favoured passive measures for the preservation of historical monuments are

- Ventilation behaviour
- Seals on windows and doors
- Appropriate insulation and temperature control measures
- Spatially limited heat radiation without significant heating of the room air

Active systems include heating systems (such as air heating systems or surface heating systems), full air conditioning systems (HVAC systems) and combined systems. For the stabilisation of the indoor climate, systems for dehumidification (condensation systems and ventilation) are particularly useful in regard to the preservation of monuments.

8.1.1 Moisture reduction of near-ground components

The permanent lowering of the groundwater level, as was done during the use of the military camp, is associated with high costs for the operation and maintenance of the technical facilities. These costs must be weighed up against the utility value of the affected rooms, and restoration has to be weighed against controlled decommissioning.

Fundamental aspects of the approach to the elimination of masonry moisture in historic buildings are always the consideration of the technical necessity, the technical and economic effort and, above all, the protection of the existing substance. Dehumidification is a massive intervention in existing masonry and complete dehumidification is usually not possible in historic buildings. Therefore, the use of the building must primarily fit the substance; for example, residential use on the ground floor of a historic building with high wall moisture will inevitably result in damage.

Since hygroscopic moisture due to salt exposure and capillary mansonry moisture usually occur together, the latter is often less pronounced than assumed from an aesthetic point of view. A thorough professional consideration of all the fundamentals is therefore necessary.

In principle, the goal is not maximum moisture reduction, but rather a reduction of the building component moisture that is appropriate in regard to building physics, in order to prevent further damage, such as e.g. massive salt efflorescence on the surfaces. Maintenance deficiencies, such as the shutdown of the groundwater pumps in the case of the Martinek Barracks, must be remedied as a first step. The existing water drainage systems of e.g. roof-, surface water also have to be examined.
In a further step, the moisture reduction measures specified by the respective material should be optimised. Historic building fabric often consists of highly capillary materials, so moisture-reducing systems should be given priority over moisture-blocking systems.

Extract from the dehumidification systems in the standards for the preservation of historic buildings:

- Elimination of maintenance damage
- Dehumidification trenches with guaranteed drainage from the bottom of the trench
- Separation layers, diffusion-open for stone and mixed masonry, geotextile layer on the surface
- Clay layers, protective plasters, joint sealants based on naturally hydraulic limes
- Facing shells and ventilation trenches for ventilation
- Electro-osmotic systems
- Horizontal separation layers (injection, transection, drilling core methods, press-in sheets, wall replacement or wall underpinning)

In connection with increased moisture, damage to porous, mineral building materials by salts often occurs. The damage processes (e.g. salt efflorescence) on building material surfaces are to a certain extent inherent to the system and were historically remedied or covered up by maintenance measures. The goal of monument restoration is therefore not the maximum reduction of the salt content, but a reduction to a level that is justifiable from a conservation/restoration point of view and can be maintained in the long term.

8.1.2 Salt reduction measures

Knowledge of the respective source of input is important for the planning of measures. Common sources of harmful salts are soil, historic building material components, sanitary facilities, stables modern alkaline building materials or restoration agents. In connection with rising-up moisture, salts are often accumulated over long periods of time and often do not allow conclusions to be drawn at the surface about unusually high salt loads in the soil.

Salt reduction usually involves reducing moisture input (e.g. through drainage), eliminating salt sources (e.g. vault filling with animal faeces, fertiliser, etc.) and reducing the amount of salt (e.g. through sacrificial plaster or compresses). Another method is salt conversion (e.g. ammonium carbonate and ammonium oxalate) or stabilisation (e.g. barium hydroxide and lead silicofluoride), the former being preferable. Stabilisation through the introduction of stabilising agents such as silicon-containing or organosilicon compounds is not acceptable from the point of view of monument preservation. They do not have a salt-reducing effect but are unpredictable with regard to their mode of action. Salt reduction or

salt conversion are specific restoration measures and require expert supervision by stone or wall restorers and natural scientists.[10]

8.1.3 Preservation of floors

The historic soils of the Martinek Barracks are to be viewed in a differentiated manner. Most of the terrazzo floors in the access areas are in a condition that allows for them to be reused and confirms their worthiness of preservation. The parquet floors in the adjoining rooms have been severely damaged by moisture and are largely unsuitable for use. In addition, open areas show a black colouration of the subfloor, which suggests damage to the wood.

8.1.4 Preservation of the exterior walls

From the point of view of monument preservation, structural components such as exterior walls form the core of a listed building. As evidence of the design intentions and building techniques of individual historical epochs, they have historical source value of historical standards, building rules, building methods and building materials. The unaltered and authentic preservation of the building stock is a declared goal of the monument preservation. Interventions must be assessed with regard to the preservation of substance, the historical-aesthetic as well as the technical-constructive preservation and the effects on the building physics. Measures should be technically and aesthetically subordinate to the existing building stock and material continuity should be strived for. This may result in contradictions with currently applicable standards and regulations, which may require a more in-depth discussion. If necessary, it must be examined whether the standard can be adequately achieved or substituted by the sum of selective changes or whether the serviceability can be achieved by other measures (e.g. by changing the utilisation of the building).[11]
Significant external insulation is not permissible in regard to monument preservation. The possibilities of interior insulation were explored in thermal simulations and their results are presented in Chapter C.4.

8.1.5 Preservation of the windows

Windows and window constructions are significantly responsible for the appearance of buildings and monuments. The goal of preservation-oriented actions lies in the preservation of historically preserved windows and fenestration constructions, including the window glass and the fittings. In the context of the existing building substance and the preservation perspective to be achieved preservation measures are to be assessed and harmonised with the technical requirements. From the point of view of the preservation of historical monuments, window constructions are not to be considered as wearing parts. Material continuity is a prerequisite for the preservation of monuments.
In any case, energetic improvements are to be measured according to the utilisation and the associated room climate and building physics aspects. In order to increase the thermal resistance, subsequent seals, the change to coated single glazing or the construction of a second window level on the inside or outside are justifiable (composite or box construction, additional inner windows)[12].

[10] (Hebert & Österreich, 2015, S. 84)
[11] (Hebert & Österreich, 2015, S. 169)
[12] (Hebert & Österreich, 2015, S. 235)

8.1.6 Salt reduction measures

For the time being, salt reduction measures also include the reduction of moisture penetration. Some rooms in the basement are also flooded with groundwater and cannot currently be entered or used. Due to the strong entry of moisture into the historic masonry, large-scale salt efflorescence has occurred, resulting in considerable damage to the interior plaster. The lowering of the groundwater level for the affected basement floors by restarting the drainage pumps seems necessary for an unimpaired operation of the building. However, complete dehumidification cannot be expected even under these circumstances. Replacement space, for example for storage, could be created in the attic. Under these considerations, all further measures for salt reduction must be weighed up.

8.1.7 Indoor climate measures and preservation of indoor spaces

In addition to the exterior appearance, certain parts of the interior of the Martinek Barracks are also under a preservation order. This applies in particular to the representatively designed access areas such as stairways and corridors. Interventions in the existing building substance must be dealt with in regard to monument preservation at an early stage of planning and must be coordinated with the monument protection authorities.

Most of the parquet floors in the Martinek Barracks have been severely damaged or completely destroyed by moisture and cannot be restored. The broken surfaces also show that mould infestation of the subfloor and moisture penetration of the fill must be assumed. It is anticipated that the parquet floors cannot be preserved and that the floor structure up to the raw ceiling must be comprehensively replaced. The reconstruction has to be coordinated with the preservation authorities, but it also offers the possibility of implementing a floor construction in the course of the renovation that can also be used thermally by means of component activation (surface heating).

8.2 Refurbishment measures

In a preliminary analysis, areas were identified that could be changed in the course of a subsequent utilisation. The buildings in the area marked in red are listed monuments. All interventions on these objects must therefore be coordinated with the Federal Office for the Protection of Monuments. The buildings marked with "X" are not subject to such regulations and can be demolished.

Figure 51: Orthophoto of the barracks site with designated area of monument protection

Figure 52: Aerial view with buildings approved for demolition by the Federal Monument Protection Agency

The historical economic living conditions generally required a high level of resource efficiency and thus an energy-saving usage of historical buildings. This resulted in special construction methods and components (e.g. smokehouses, storerooms, tiled stoves, ventilation systems), which today represent important testimonies to historical building techniques and life culture. Adapted room management, for example through different temperature zones in the building, as well as the separation of functions, also contributed to an economical energy consumption.

The utilisation of the Martinek military camp under current requirements, but also the elimination of building deficiencies, make a thermal-energetic optimisation necessary. A thorough consideration of the effects on the building substance and the visual appearance of the monument is necessary. The holistic approach, which takes equal account of the building envelope, building technology and user behaviour, is of the utmost importance. The aim of the monument preservation is to develop fault-tolerant and reversible solutions that are always based on an analysis of the existing building and only increase energy efficiency to the extent that this is possible without significant detrimental changes to the existing building substance and appearance. Substantial interventions should be reduced to a minimum.[13]

In the following, possibilities for the thermal refurbishment of the Martinek military camp are explained regarding monument preservation.

8.2.1 External insulation

In general, exterior insulation results in a loss of the original appearance of the monument and the handcrafted surface. Regarding monument preservation, exterior insulation is therefore not justifiable.
In exceptional cases, exterior insulation with insulating plaster is possible under the following conditions.[14]

- The effect of insulation cannot be achieved by alternative measures.
- The application of the insulating plaster does not lead to any detrimental impairment of the historical aesthetic of the façade nor to the destruction of historically valuable plaster layers and wall surfaces.
- Whether and how existing plasters may be changed must be clarified by the Federal Office for the Protection of Monuments.
- In individual cases, preliminary examinations of masonry, plaster and paintwork are required as a basis for decision-making.
- Aggregates that conform to the material must be used (e.g. mineral aggregates for lime plasters).
- The long-term damage-free condition of the underlying masonry must be ensured.
- Plaster thickness, material composition and plaster surface are to be as close as possible to the original plaster. Connections, shapes and dimensions of the architectural elements (e.g. reveals, cornices, etc.) of the façade must correspond as closely as possible to the historical architectural concept.

[13] (Hebert & Österreich, 2015, S. 360)
[14] (Bundesdenkmalamt Hofburg, 2011, S. 12)

8.2.2 External insulation of masonry with ground contact

When converting the basement rooms of the Martinek Barracks, external insulation of masonry in contact with the ground can be of importance.
It is possible under the following conditions:[15]

- In the case of historic stone and brick masonry, the possibility of the masonry drying to the outside must not be prevented by insulation. The application of barrier layers must be avoided for reasons of reversibility (separating layer, installing ventilation).
- Long-term absence of damage must be proven.
- Detailed planning must be done next to the simultaneous formation of a drainage trench.
- If necessary, archaeological monitoring of the construction must be carried out.

8.2.3 Interior insulation

According to monument preservation, interior insulation is an appropriate means of improving the thermal requirements in individual cases while at the same time preserving the historical exterior appearance. For the Martinek Barracks, this method of improving the thermal envelope is preferable.
It is possible under the following conditions:

- The installation of the insulation must neither impair the historic aesthetic of the room nor destroy historically valuable plaster layers and wall surfaces.
- Before installing the insulation, the Federal Office for the Protection of Monuments must clarify whether the existing plaster may be removed, plastered over, pasted over or doweled.
- In individual cases, preliminary examinations of the masonry, plaster and paintwork are required as a basis for decision-making.
- Long-term absence of damage must be proven.
- Diffusion-open and capillary materials are preferable to diffusion-tight insulation.
- To prevent air flow through interior insulation and the associated risk of water vapour condensation, attention must be paid to air tightness and its practical feasibility.
- The connection areas of the ceilings/floors to the exterior wall require detailed planning (thermal bridges). The severing of historical ceiling and floor constructions (abutments) must be excluded.
- Aggregates conforming to the material are to be used (e.g. mineral aggregates for lime plasters) and the plaster thickness is to be as close as possible to the original plaster.
- In case of removal of historic plaster surfaces that characterise the room, the new plaster surface must either be as similar as possible to the original character or, if necessary, a new surface design must be conceived in agreement with the Federal Office for the Protection of Monuments.

The measures to thermally improve the exterior walls of the Martinek Barracks were checked and verified by the computer-assisted thermal simulation. These include mineral insulation on the inside (e.g. calcium silicate boards) with a thickness of 5 cm and insulation on the attic side of the top floor ceiling with a thickness of 20 cm (e.g. mineral wool insulation boards).

[15] (Bundesdenkmalamt Hofburg, 2011, S. 13)

The installation of interior insulation in the corridor areas must be coordinated with the existing ceiling and wall elements worthy of preservation. Any temporary removal and re-installation after the mineral interior insulation has been installed must be coordinated with the Federal Office for the Protection of Monuments.

8.2.4 Thermal refurbishment of the windows

The historic windows of the Martinek Barracks are designed as box-type windows. Windows in strictly listed buildings can be treated in various ways. The two most common methods are, on the one hand, a pure renovation of the existing windows and thus an improvement of the air tightness but not of the thermal insulation. On the other hand, the glass structure of the inner sashes of the box-type windows can be replaced with modern double-pane thermal insulation glass. With this method, U-values comparable to new buildings of up to 0.9 W/m²K and g-values of about 55% can be achieved.
However, due to the higher weight of these panes, considerable reinforcements and adaptations of the inner sashes are necessary. Subsequent widening of the glass rebates is not justifiable in most cases from a preservation of view. Instead, gluing on to achieve higher rebate thicknesses should be aimed for. However, like the entire renovation of the windows, this is often time-consuming and therefore cost-intensive.
The determination of the respective HWB_{SK} in the existing building stock with 5 cm internal insulation and existing windows or with renovated windows shows that the internal insulation has a significantly higher effect on the HWB than the renovation of the windows. Therefore, in addition to the technical consideration of the possibilities, it must also be economically examined whether a renovation of the windows is cost-optimal. This assessment can only be the result of a holistic consideration.

9 Economic assessment

In the last few years anergy networks, water-based heating respectively cooling networks which manage the energy transport approximately to surrounding temperature have been more often discussed (Götzl *et al*., 2017; Schrammel *et al*., 2019; Ruesch and Haller, 2017 and Schmidt *et al.*, 2017) and demonstrated (Gautschi, 2016 and Vetterli, 2014) as future-oriented systems for a sustainable supply of heating and cooling services. The advantages of anergy networks are diverse and vary from extremely low-loss energy respectively anergy transport to corresponding networks, the possible benefit of for example industrial heat loss with low temperature level, the possible heating and cooling storage in geothermal BHE storages with great capacity to load compensation between heating and cooling loads within the network and the supply of virtually free services as “Free Cooling“.

In Switzerland the number of realised pilot and demonstration plants increases continuously. Examples are the LTHC grids Naters (room heating with heat source groundwater), the Genève lac nations project (office building cooling with water of the lake Geneva) or the ETH Zurich, Hönggerberg (major project with several geothermal BHE fields and dynamic development potential), the Suurstoffi area in Rich/Rotkreuz (zero-emission-project with geothermal BHE fields, PV and car-free mobility concept) (Vetterli, 2014 and Hans Abicht AG, 2016), or the family home cooperative Zurich (geothermal BHE fields). Research and progress reports mostly refer to aspects of system technology and operational management in detail. Usually empirically based information about economic figures as specific heating and cooling production costs, payback periods etc. are not publicly available.

As strongest economic constraint Gautschi (2016) mentions the competition with fossil energy carriers especially natural gas and the high investment costs of the plants in particular the costs of the installation of the anergy network as well as the geothermal BHE fields. The same author names the intersection of the cost comparison method between the option heating with fuel / cooling with electricity and the option heating and cooling with anergy network and geothermal BHE fields with 12 years for a +3 %/a energy price scenario. For the option natural gas respectively with an increasing calculation interest rate this period clearly lengthens.

Based on the experiences of the existing pilot and demonstration plants the economically feasible system analysis in the project SANBA is made on the basis of two different approaches. A top-down approach on the basis of network figures and a micro-data-based bottom-up approach on the basis of the capital value method are compared and also complemented.

Figure 53: Views of the listed existing buildings in the area of the Martinek military camp in Baden near Vienna. Pictures: Peter Biermayr.

The essential system components of the research object are residential buildings, service buildings, geothermal BHE storage, water-based technical storage, the central heat loss source, decentralised heat pumps as well as a 2-piped anergy network. Typical temperatures of the heating flow range in winter from 7 to 12°C and in summer from 12 to 22 °C. The respective temperature difference to the return amounts to approximately 4 to 5 K.

The basic data for the modelling and system analysis in the project SANBA have been empirically collected in regard to the existing buildings, the qualities of a central heating source and in regard to the hydrogeological and thermotechnical qualities of the underground. In January 2020 in the company grounds of the NÖM AG an exploratory drilling of -150 metres was drilled and expanded as experimental BHE. The results confirm the suitability of the underground for the planned heating and cooling storage.

9.1 Top-down evaluation approach through network figures

As handy framework condition for a profitable operation of anergy networks Gautschi (2016) indicates a density of thermal energy of 3 MWh/(a*m_{route}) for predominant heat use respectively a by 30 % or 50 % lower value with combined heat and cooling use. These figures have been clearly surpassed by the above quoted projects ETH Zurich with 6 MWh/(a*m_{route}) heating usage plus 5 MWh/(a*m_{route}) direct cooling and the family home cooperatives Zurich with 5 MWh/(a*m_{route}) heat supply plus 2,5 MWh/(a*m_{route}) direct cooling whereby these projects may be classified as potentially profitable in regard to the figures of a top-down approach.

Further starting-points for an economic system analysis in the project SANBA are provided by the already concluded research projects GEOSOL (Biermayr *et al*., 2013) and DEGENT-NET (Götzl *et al*., 2017) whereby in project DEGENT-NET findings could already be gained within the frame of specific case examples in Vienna and Salzburg.

In regard to the classical high temperature heating networks as is the case with urban district heating or biomass local heat supply, for a rapid evaluation of the economic feasibility figures are commonly used

for the specific power density and the specific work density of the network. The minimal densities typically are 1 kW/m_{route} respectively 1,5 MWh/(a*m_{route}) whereas the actual requirements always have to be defined project specifically on the basis of definite planning documents.

Now the displayed figures already reveal a strategic problem of anergy network projects: On the one hand, planners will aim at highly efficient building structures within the frame of renovations and new building projects in order to allow for an energy efficiency in the total system which is as high as possible (low energy figures of the building plus low temperature heat distribution system).

On the other hand, a certain energy turnover is necessary for an economic operation of the anergy network. However, in this respect great economic opportunities are in the additional cooling supply for the cooling of buildings, in the dense structures of new buildings, in the integration of partially energetically restorable buildings with a high heat demand (for instance monument protection), as well as in the application of suitable business models.

The network figures for the three evaluated SANBA-scenarios are summarized in Table 17. If you take the above documented framework conditions for an economically successful operation of the system into account there is few hope for the scenario MINI whereas the scenarios MIDI and MAXI show promising figures.

Table 17: Network figures for the three SANBA-scenarios.

Figures in the SANBA-scenarios	MINI	MIDI	MAXI
Density of thermal energy [$MWh_{th}/(a*m_{route})$]	1,6	4,9	5,4
Density of thermal power [kW_{th}/m_{route}]	0,8	1,7	2,1

The calculation of the network figures can already be made in an early project phase after establishing the network topology and determining the heating and cooling loads respectively the annual useful energy demand for heating and cooling of buildings. However, this top-down approach may rightly be criticized as “vague“ because of the relatively low information depth. It is nevertheless suitable and empirically sufficiently verified to be used as a method for a rapid evaluation of rough system designs.

9.2 Bottom-up assessment approach on the basis of the capital value method

A detailed economic system analysis was accomplished in SANBA on the basis of the classical capital value method. The definition and investigation of all cost data including the consideration of learning and scaling effects caused a noticeable effort which may be reduced in practice through aggregation of components and a corresponding tender of system boundaries. The system boundaries have been defined for the calculation with technical limits of the thermal energy system.

However, the purely formally given accuracy of the method is put into perspective through a great number of assumptions which have to be made for the calculations. Here, the uncertainty rests with long-term projects with low discounting especially in the area of divergent developments of deposits and payments (compare electricity price prediction vs. development of heating and cooling prices) respectively likewise in the area of re-investments. In the course of the system analysis the economic robustness of the system may indeed be tested through a variation of essential and critical parameters but the uncertainties which arise due to the long period of calculation cannot be eliminated in doing so. Anyhow, this circumstance is not due to the innovative energy system in SANBA but is rather a general property of projects with lots of investments with long operating life.

In order to illustrate specific results of the profitability calculation which are comparable outside the scenarios the documented assumptions in Table 18 have been made for further illustrations.

Table 18: Assumptions and basic parameter values for the following presentation of results

Adequate target rate	3.0 % (variable)
Rising prices (inflation)	1.5 % (general, unspecific)
Electricity price	100 €/MWh (mere energy price, no fixed and power components; variable)
Reference date t_0	year after completion = full use
Building phase (planning, construction)	max. 4 a (scenario MAXI)
Operational phase	40 a (passive components), 20 a (active components)
Heat price (heating)	60 €/MWh (mere energy price)
Heat price (process water)	80 €/MWh (mere energy price)
Cooling price (Room cooling)	100 €/MWh (mere energy price)
Anergy price (Heat loss)	1 €/MWh (mere energy price)
Subsidies	Not considered

Taking into account the scenario specific micro-cost data for planning, investments, operation, renovation, re-investments and the corresponding payments the following illustrated results arise.

Figure 54 shows an absolute and relative comparison of the costs in the three investigated scenarios, divided into the essential system components. The cost structure shows that with an increasing project size the costs portion of the geothermal BHE storage equally increases while the costs portion for

“miscellaneous“ (planning services, obligatory industrial management, maintenance contract for energy centres, operating expenses for anergy) decreases.

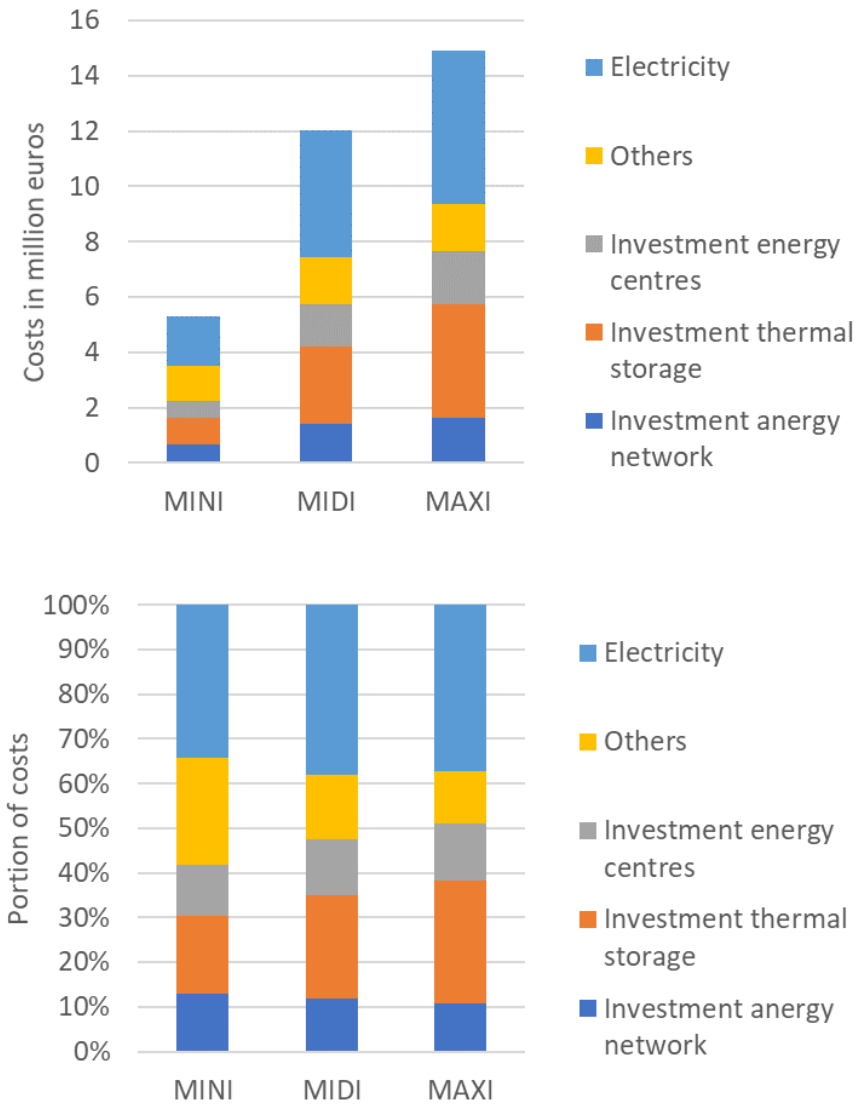

Figure 54: Comparison of the absolute (above) and relative (below) costs of the investigated SANBA scenarios

In Figure 55 the discounted flowing of the deposits and payments for the scenarios MINI and MAXI are illustrated. It becomes apparent that although there are similar relations in the operation phase between deposits and payments this is not the case in regard to the relation between investments and payments. As a result, this imbalance leads to a critical overall economy of the MINI scenario.

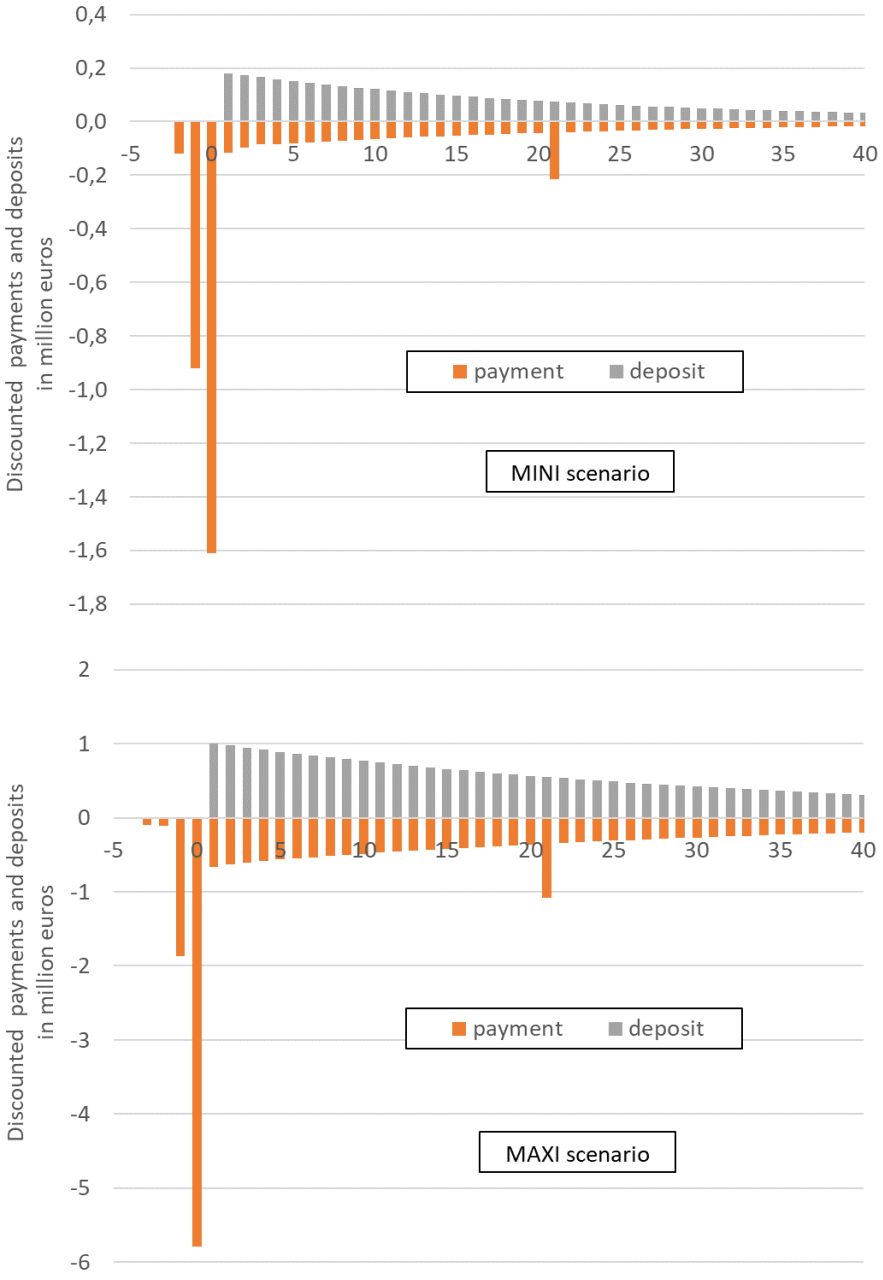

Figure 55: Dynamic development of the deposits (above) and payments (below) in the scenarios MINI and MAXI over the total project duration.

Figure 56 shows the capital values of the various scenarios dependent on calculation interest rate (abscissa) and electricity price (parameters of the family of curves). A positive capital value stands for an economically successful constellation under the respective circumstances while a negative capital value stands for a corresponding economic loss.

Consequently, in the MINI scenario there exists only a very small solution space for parameter constellations that make an economically successful project possible. Appropriate solutions would require a calculation interest rate of maximally 2,3 % (corresponds to the maximal internal interest rate)

and a maximal electricity price of about 80 €/MWh (mere energy price!). The level of the calculation interest rate (for instance non-profit housing) may possibly be argued but not the required electricity price. If the scenario MINI should be realised in spite of the bad economic starting point, high subsidies have to be granted – possibly as not refundable investment grant.

In the MIDI and MAXI scenario, the economic situation of the energy system is completely different. In these scenarios positive capital values can be achieved under the assumption of realistically feasible parameters. The solution space for economically successful constellations is rather big in these two scenarios which also creates a free space for attractive business models for possible network operators, anergy suppliers or contracting-vendors.

These relations are also displayed in Figure 57 where the internal interest rate in dependency of the electricity price is illustrated for the three scenarios. In each case the area under the scenario-specific curve may be considered as solution space for economically successful parameter constellations. The MINI scenario displays - as explained above – a small and not realistically feasible area whereas the MAXI scenario offers the greatest scope. Consequently, the MAXI scenario is the economically most robust system design whereas you need to emphasize that the statements exclusively relate to the investigated thermal energy system of the quarters.

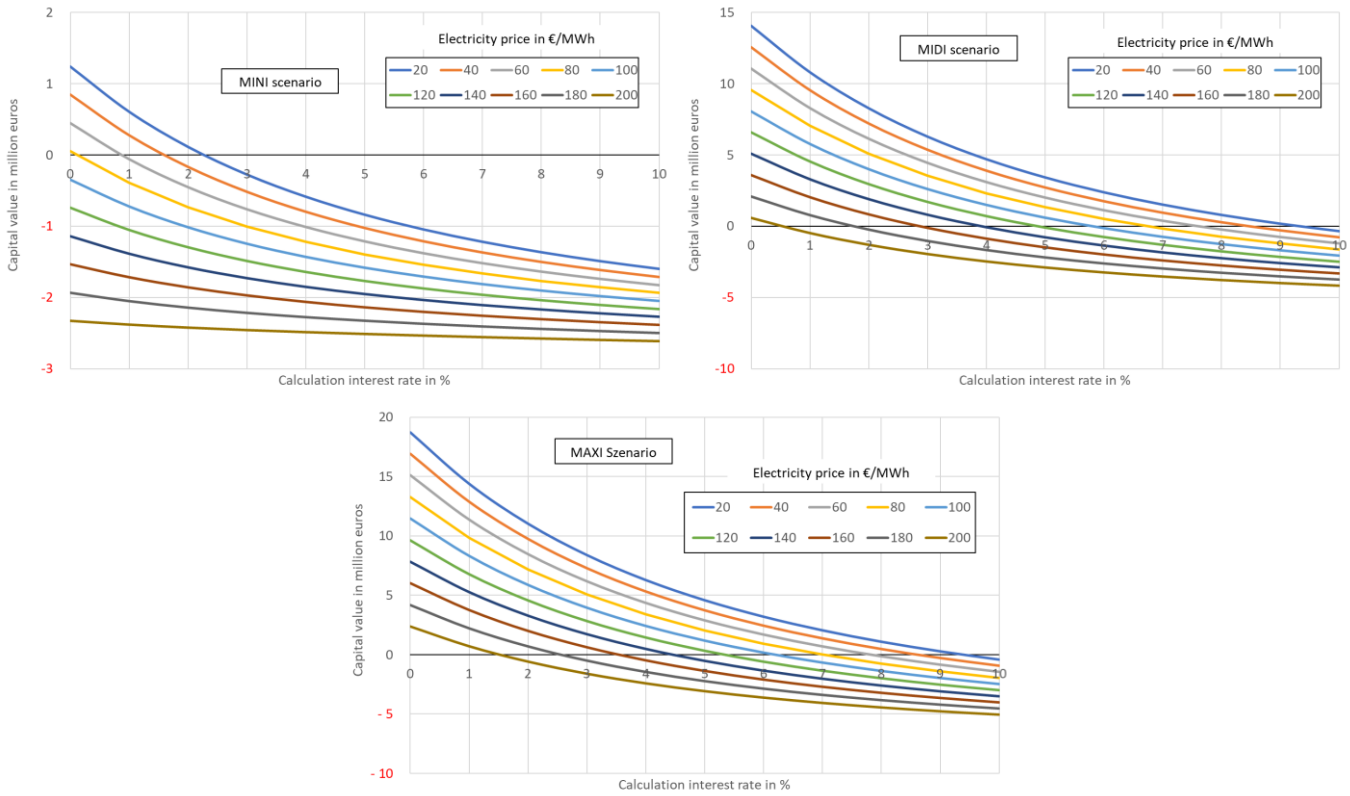

Figure 56: Capital values depending on the electricity price and the calculation interest rate for the investigated scenarios.

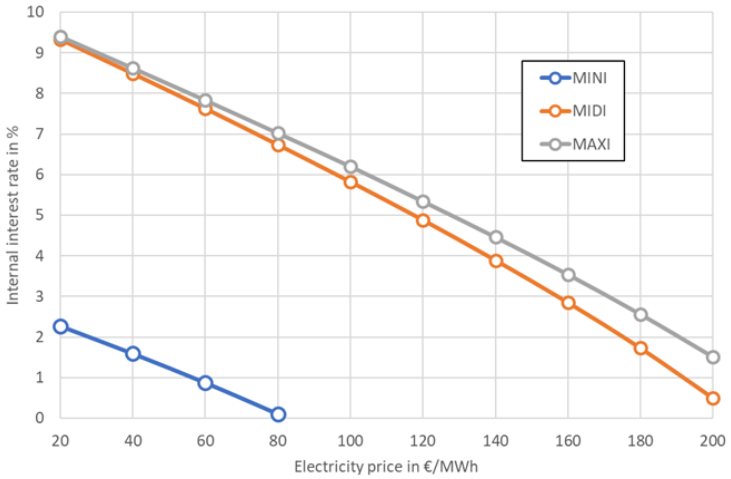

Figure 57: Internal interest rate depending on the electricity price.

9.3 Further qualitative aspects

9.3.1 Benefits of the grid feed

The heat emission of a grid feed (typically of a business enterprise or an industrial plant) into the anergy network has to have a calculable benefit without process technical risks. The attainable benefit also depends on the particular point in time when such a project is realized. If the potential grid feed is an established business the mobilizable short-term use is often reduced to a reduction for instance of the operating power of the back cooling. On the long term respectively with a simultaneous creation of an anergy network and the installations of the grid feed appropriate parts of installations of the grid feed may be economised.

However, in such a case the anergy network operator will have to give a guarantee for a minimum anergy consumption where obligatory agreements are made concerning the load profile and the temperature bandwidths of heating flow and return. Furthermore, in the investigated scenarios MIDI and MAXI a moderate feed-in tariff for the grid feed is also presentable whereas these earnings have lesser importance in comparison to other benefits.

9.3.2 Technical frame of the grid feed

In the course of the empirical surveys in the SANBA project it became apparent that the use of heat loss of cooling plants (for instance back cooling of refrigerating machines) is process technically significantly easier than the use of heat loss of sewage even if it has an attractive temperature level. The background is the temperature dependency of the dissolving power of the sewage and the tendency of precipitation of dissolved constituents during the cooling down. However, at this an intervention in existing plants is by far more difficult and cost intensive than a simultaneous planning and creation of an anergy network and operational plants. As a rule, appropriate sewage heat exchangers have to be provided with cleaning equipment to guarantee a continuous transmission power. The specific costs of such heat exchange installations are significantly higher than of heat exchangers which can for instance be implemented in water-based or brine-based recooling systems.

9.3.3 Investment costs for the anergy network

Calculations of the SANBA-project partner TU Vienna have shown that in case of an underground installation following the company standards of the pipe producer of non-insulated PE 100 PN 10 plastic pipes for the planned 2-piped anergy network (DN 160, wall thickness 9.5 mm) the short loss of heat between hot pipes and cold pipes on the one hand and the heat loss towards the surface of the earth on the other hand amount to below 1 % in comparison to the convectively transferred energy via the pipe. An of any kind whatsoever thermal insulation of the anergy network pipes exceeding the standard wall thickness of the material of the pipes and the bedding of the pipes in sand following the company standards is thus neither thermodynamically reasonable nor economically feasible.

A part from the material costs of the pipelines the laying expense has a great influence on the installation costs of the anergy network. Essential aspects are here the degree of freedom for the choice of the transmission route for a minimal route length (limitations through existing buildings, already used infrastructure routes, traffic routes etc.) as well as the working conditions for the installation (“green meadow“ versus inner-city). In this regard, in the case of the SANBA project there are mixed conditions whereas within the area of the barracks there are favourable conditions however, the connection of the dairy factory NÖM AG causes greater efforts (installation underneath sealed areas, crossing of a main road).

The requirements of the pressure resistance of the used plastic pipes are also a further cost factor. The requirements of the pressure resistance of the pipes result mainly from the topology of the anergy network whereby the pipe producers typically offer the standard classes PN 6, PN 10, PN 16 and PN 25. In the case of the SANBA project the pressure class PN 10 is planned as in spite of the great transmission route there is not any significant height difference.
The scale effects in regard to the used pipe diameter are very moderately marked and are negligible from DN 110. The background is that with constant pressure resistance with increasing nominal pipe diameter the wall thickness of the pipes also rises linearly which subsequently lead to almost constant service specific material costs of the various pipe diameters. As a result, the power specific price depends only on the temperature spreading between hot pipes and cold pipes, see Figure 58.

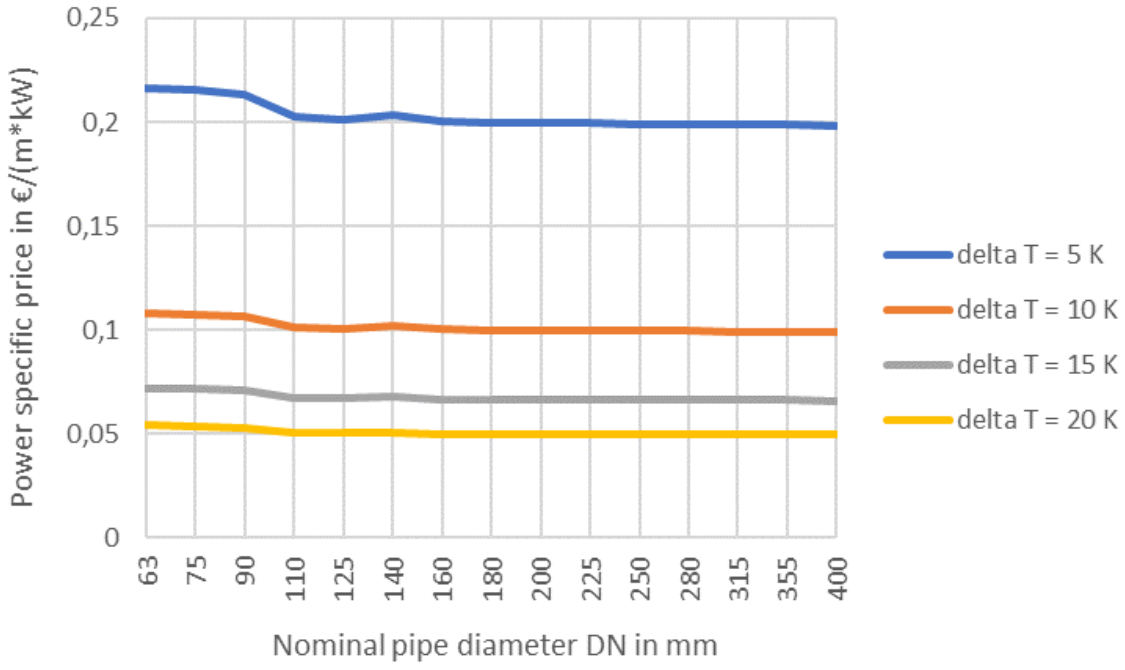

Figure 58: Service specific prices (excl. VAT) for various pipe diameters depending on the temperature spreading. Respectively for PE 100 PN10 SDR 17, 12 m off-the-peg, excl. closures etc.

The specific prices of rolled goods which are available in piece lengths of 100 m to maximum DN 160 are approximately 25 % higher than those of the off-the-peg goods. Through the reduction of the shaped pieces and the production effort for the welding etc. the use of rolled goods in sparsely structured network sections is economically feasible.

9.3.4 Scale effects in the energy centres

The absolute size of the anergy network planned in the SANBA project requires numerous energy centres which are the interface to the decentralized energy systems of the buildings or the building sections. The most essential component is either one or more heat pumps. The specific net prices of brine/water heat pump units dependent on the thermal nominal capacity per unit are illustrated in Figure 59. On the basis of the collected data, it can be presumed that a splitting up of the necessary power >40 kW per unit is a cost-efficient approach. Similar conditions can be observed with decentralized, water-based heat pumps whereby the limit of sinking prices per storage capacity is reached between 1000 to 2000 litres of storage capacity.

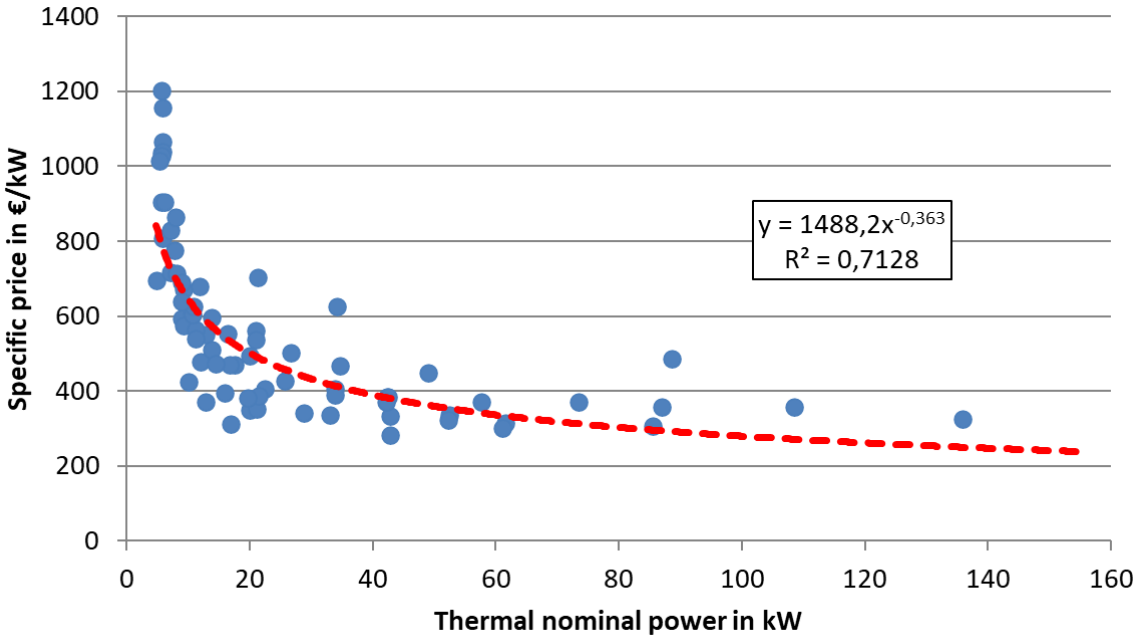

Figure 59: Power specific net price of brine/water heat pump units depending on the thermal nominal power.

Regarding the costs of maintenance and operations of technical components, the costs of appropriate maintenance contracts respectively the contractual prolongation of warranty periods are part of the profitability calculation which reduces the cost risk of potential investors or operators.

9.3.5 The influence of learning effects

The technical realisation of the energy system planned in the SANBA project is feasible with established, on the market available, technical components. The essential components are here geothermal BHE, heat pumps, pipelines, heat exchanger, water-based thermal storage systems as well as pumps and control systems. From the actual moment of planning to the potential moment of realisation no significant economic learning effects can be expected with all these components which might influence the statements regarding the profitability of the system. The situation is similar with the moment of re-

investment during the 40-year period under observation of the dynamic observation of profitability. As one cannot expect any significant technical learning effects like efficiency increase or reduced space requirements of components in the named key areas up to the moment of a potential realisation, any influence on profitability of the project is not expected from this part.

9.3.6 Failure reserve and redundancy

In the project SANBA strategies how to deal with system failures were equally discussed. Here scenarios are of particular interest which enlighten a short-term up to permanent failure of the industrial waste heat source at various load conditions of the anergy network. The time periods of the failure are hereby classified as hours, days, weeks and months up to years. Failures in the scale of hours up to days can be managed in heavy-load periods with the help of the system inertia and the performance of the geothermal energy storage. For longer failures lasting several weeks a network interface for the feeding of heat with a mobile container heating plant is provided at first and all the necessary structural measures for a rapid delivery and installation of such a heating plant are taken. Here the investment costs are very low (storage area, driveway, network interface). For the very unlikely case of a long-term or permanent failure of the heat source additional measures for the permanent construction of an air/water large heat pump installation are taken. For the given power requirement in SANBA a storage space the size of a 40-foot container including driveway is necessary. Moreover, the electrical power requirement, possible sound emissions etc. have to be taken into account during the planning. The construction and start-up of a suitable large heat pump installation with appropriately prepared infrastructure requires 4 to 8 weeks according to the producer.

Alternative concepts for the creation of a failure reserve respectively a redundancy in regard to the waste heat source as for example the prophylactic creation of a district heating or a natural gas connection have been investigated in the already quoted project DEGENT-NET (Götzl *et al*., 2017). Here it became apparent that the costs of appropriate connections respectively the power provision through the energy supplier causes high costs which have to be priced into the heat production costs of the system. This significantly increases the specific heat costs. The above illustrated solution equally covers all the failure scenarios and only causes marginal costs in the course of a project realisation.

9.3.7 Cooling of buildings

A strong point of the investigated anergy network in the project SANBA is the supply of coldness for the cooling of buildings. Basically, this coldness can be supplied as “Free Cooling“ through the existing geothermal energy storage as the summer temperatures in the cold pipe of the anergy network are suitable for the cooling of buildings. If appropriate facilities for the distribution of the coldness are created in the buildings or the existing heat distribution systems are suitable for distributing the coldness, the cooling of the building does not cause any further costs on the surface apart from the electric driving energy of possible pumps. However, in the course of a systemic analysis costs like the geothermal energy storage have to be included in the provisioning of coldness and a suitable heat and coldness rate has to be defined. Concerning this matter, it has already been shown in the project DEGENT-NET (Götzl

et al., 2017) that missing paragraphs or missing rating of coldness in anergy networks result in non-competitive heat prices which is also already expressed in the above quoted figures for the anergy network of Gautschi (2016).

9.3.8 Cost structure of anergy networks

Systems with anergy networks are very investment intensive. That is the main part of the relevant life cycle costs arises during the construction of the system. When comparing such systems with operating costs intensive systems as for example a heat supply based on natural gas including provisioning of coldness via compression cooling units the height of the chosen calculated interest rate has a great influence on the result of the comparison (for instance following the hereby used net present value method). Consequently, for an equally fair as well as serious comparison of systems a sensitivity analysis – at least regarding the calculation of the interest rate is indispensable. Further variations should also be conducted in regard to the underlying energy price scenarios.

In light of the national and international climate- and energy targets an evaluation of the avoided greenhouse-gas-emissions also has to take place in the course of the system comparison. This can either be taken care of in a separate emissions balance or it may be implemented in the economic evaluation via costs of CO_2-emissions. In the second case one has to critically mention that predictions in regard to CO_2-prices over a long service life of for instance 40 years are not reasonably feasible and a discounting of monetary CO_2 savings in the course of a dynamic profitability calculation do not really make sense.

10 Summary and conclusions

The project results clearly showed a high potential for an low-temperature heating and cooling grid at the area of the former military camp “Martine-Kaserne” with the waste heat from the NÖM and geothermal storage in borehole heat exchanger fields. The network can be operated economically regardless of future use. The results of the project are an important first step that contributes to the broader implementation of LTHC grids in Austria. It will enable both site screening and network design planning. The consortium has set itself the goal of supporting potential developers in realizing the LTHC grid in the "Martinek-Kaserne" in the near future.

In addition, positive proof of the feasibility of LTHC grids for protected buildings and / or buildings in need of renovation can lead to further application of these concepts in other barracks. The Federal Ministry for National Defense is one of the largest property owners in Austria and has many other military camps in Austria for which LTHC grids could be an interesting option for a sustainable energy supply in the future.

10.1 Summary of technical design of the LTHC grid

The technical design including the thermal-hydraulic simulation of all three scenarios have been proven to be possible. In the following, a summarizing energy flow diagram is discussed for the scenario MIDI.

Figure 60 shows the annual demand and supply flows to operate the case-specific LTHC grid. The left side shows the feeder flows and how the required energy for H, DHW, loading the BTES, and thermal losses are met. The right side shows the demand flows and how the supplied energy is used. The sum of the energy flows of the left and right sides are identical and are both 11154.2 MWh/yr. Thus, the energy balance of the overall system is met in each case. Approximately 2795.8 MWh_{th}/a are fed into the grid by the NÖM. The thermal energy demand for H and domestic hot water (8066.1 MWhth/a) is more than twice the energy demand for C (2814 MWh_{th}/a). The electricity required to operate ULTDH is 2507.9 MWh_{el}/yr, which is 22.5 % of the total demand/supply flows.

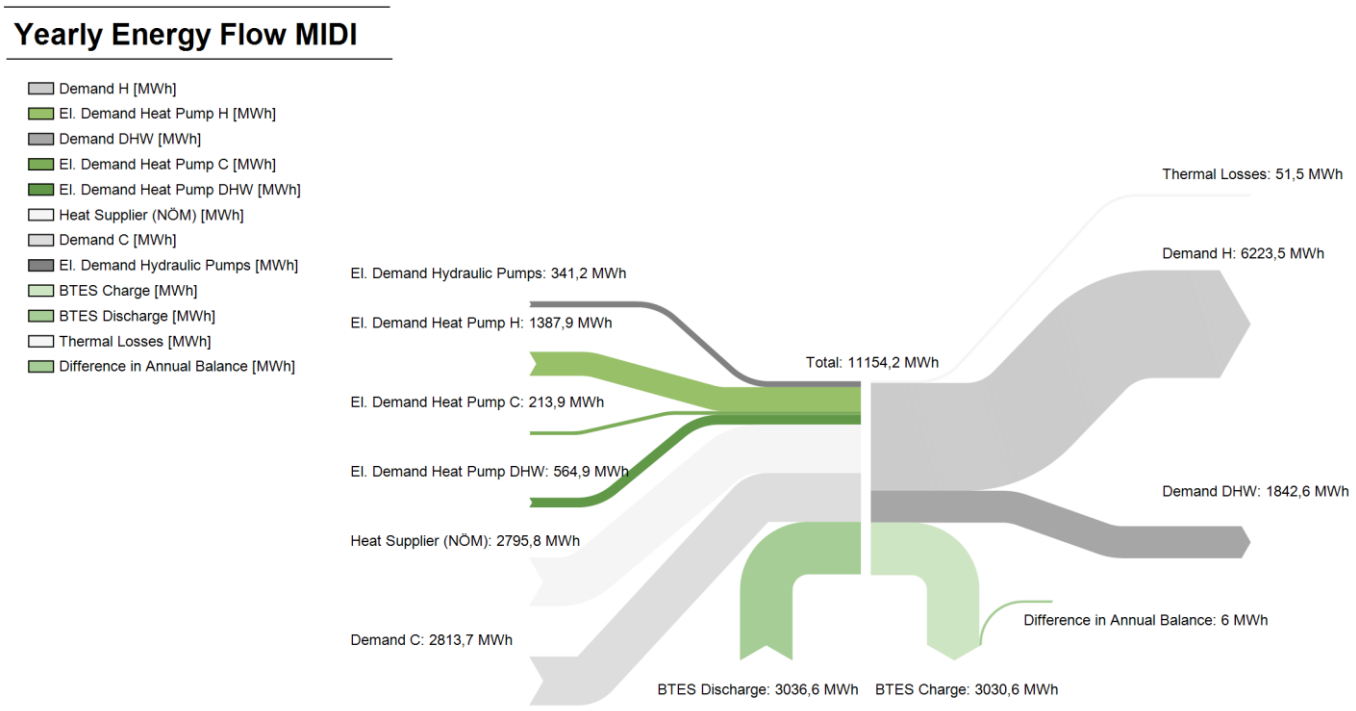

Figure 60: Sankey diagram - annual energy flows to operate the anergy network for scenario MIDI.

Since the BTES is part of the subsurface, no specific storage capacity can be assigned. Similar to residential geothermal storage with only one or two BHE, it is theoretically possible to continuously discharge the storage. However, the temperature of the soil, and thus the withdrawal capacity, decreases over the years until saturation occurs. Lower soil temperatures and the resulting lower flow temperatures of the connected heat pumps reduce the COP value. Nearly the same amount of energy must be charged and discharged at regular intervals. This keeps the temperature of the subsurface at a reasonable level over the long term to keep the system efficient and ensure long-term use of the BTES. Approximately 3030,6 MWh_{th}/yr, representing 27 % of total demand/supply flows, is charged and discharged in the BTES in an annual cycle. The BTES is not fully balanced to zero. It is discharged by 6 MWhth/yr more than it is charged. In addition, it is possible to discuss the calculated heat losses and reduce them by varying pipe parameters, such as material, diameter, or insulation. Due to the short residual times of water in the pipe network, the heat losses are low, amounting to 51,5 MWhth/a, which is 0,5 % of the total demand/supply flows. One of the main reasons for the extraordinarily low heat losses is fluid temperatures in the pipe network that are close to the ambient temperature.

10.2 Summary of the available waste heat of the NÖM dairy

The analysis of the NÖM dairy has shown that about 19 % of the final energy used (gas and electricity) can be decoupled as low-temperature heat. This is much more than required to supply the LTHC grid. The exact breakdown of the individual plants with temperature range and exergetic share in the respective waste heat flow can be seen in Table 19.

Table 19: Low temperature waste heat compared to energy input (gas and electricity), detailed results broken down by process.

Plant	Low temperature waste heat compared to energy input [%]	Temperature level [°C]	Exergy share of waste heat [%]
Cooling system product logistics	7,3	23 - 40	3 - 8
High pressure air generation	1,6	25 - 50	6 - 11
Steam boiler	4,0	60 - 70	13 - 17
Heat recovery storage tank	1,1	70 - 75	16 - 19
Waste water (reference 25°C)	5,3	27 - 34	5 - 7
Total	19,4		

10.3 Economic Summary and Conclusions

The identified economic success factors in the SANBA project for heating and cooling supply on the basis of LTHC grids are:

- The determination of figures for the density of thermal power and thermal energy creates the possible assessment of the profitability in an early planning phase for anergy networks – as well as conventional heating networks.
- The economic analysis with figures and the capital value method show a good convergence of results.
- The heat output of a feed-in (for example industrial plant) to the anergy network has to have a calculable benefit for the feed-in without process technical risk for the key business.
- From the point of view of the feed-in the heat consumption through the anergy network has to be reliable and continuous.
- Process technically the benefit of heat loss from cooling systems is by far easier than the benefit of heat loss from wastewater (dissolving power, precipitation).
- The investment costs for the anergy network have to be minimized. As a rule, the use of non-insulated, underground plastic tubes is economically as well as thermodynamically reasonable.

- For the sizing of the energy centres and their components you need to take care of the optimal benefit of scale effects.
- Economic learning curves concerning the system components will hardly influence the profitability of the anergy networks in the following decades.
- Investment costs or contract costs with an external heat supplier for a redundant heating source have to be minimized. However, structural arrangements for the short-term, medium-term and long-term failure of the central heating source have to be made.
- Free cooling is not free of cost. The users have to be charged for the cooling supply in the interest of the overall economy.
- Anergy networks have high investment costs. When comparing these systems to heating and cooling supply systems with mostly operating costs the calculation interest rate has a great influence on the result.
- A comparison of anergy networks with energy systems for the use of fossil energy is not reasonable because of the national, international and global targets for the upcoming decades as fossil energy is no longer an option.

In the concrete SANBA project economically attractive and robust scenarios have been identified. These solution approaches enable the integration of the monument protected existing buildings into a sustainable energy system. The system benefits from industrial low temperature heat loss in an anergy network with geothermal heat storage. The investigated location is especially suitable for the realisation of an internationally remarkable pilot- and demonstration plant.

11 Literature

Amt der NÖ Landesregierung, Gruppe Wasser. (2012). *Wärmepumpen und Grundwasserschutz - Planung, Bau und Betrieb*. St. Pölten : Amt der NÖ Landesregierung, Gruppe Wasser.

Bauer, D. (2018). *Zur thermischen Modellierung von Erdwärmesonden und Erdsonden-Wärmespeichern.* Stuttgart: Universität Stuttgart.

Biermayr et al. (2013). *Erfolgsfaktoren für solare Mikrowärmenetze mit saisonaler geothermischer Wärmespeicherung (GEOSOL).* Endbericht zum Forschungsprojekt im Forschungs-programm Sparkling Science, gefördert vom BM für Wissenschaft und Forschung.

BMLFUW, Abteilung IV/3 Nationale und internationale Wasserwirtschaft. Erhebung der Wassergüte in Österreich gemäß Gewässerzustandsüberwachungsverordnung (GZÜV) BGBl. I Nr. 479/2006, i.d.g.F. s.l. : Ämter der Landesregierungen.

Bothe, D. (2016). *Modellierung und Simulation von weit verzweigten, vermaschten Netzen für thermische Energie und Gas.* Wien: TU Wien.

Brix, F. und Plöchinger, B. (1982). *Blatt 76 Wiener Neustadt. Geologische Karte der Republik Österreich 1: 50,000*. Wien : Geologische Bundesanstalt.

Brix, F. und Plöchinger, B. (1988). *Erläuterungen zu Blatt 76 Wiener Neustadt. Geologische Karte der Republik Österreich 1: 50,000*. Wien : Geologische Bundesanstalt.

Bundesministerium für Nachhaltigkeit und Tourismus, Abteilung I/8: Wasserlegistik und -ökonomie. (2018). *Wasserrechtsgesetz1959 - idF BGBl. I Nr. 73/2018*. Wien : Bundesministerium für Nachhaltigkeit und Tourismus.

Claesson, J., & Javed, S. (2019). Explicit Multipole Formulas for Calculating Thermal Resistance of Single U-Tube Ground Heat Exchangers. *Energies*.

Claesson, J., & Javed, S. (2019). Explicit Multipole Formulas and Thermal Network Models for Calculating Thermal Resistances of Double U-pipe Borehole Heat Exchangers, Science and Technology for the Built Environment.

Ćorić, S. und Hohenegger, J. (2008). *Quantitative analyses of calcareous nannoplankton assemblages from the Baden-Sooss section (Middle Miocene of Vienna Basin, Austria).* Geol. Carpathica, 59, 5, 447—460.

DHI-WASY GmbH. Simulation package FEFLOW. [Online] [Zitat vom: 12. 01 2021.] http://www.feflow.info.

Diersch, H.-J. G. und Perrochet, P. (2009). *On the primary variable switching technique for simulating unsaturated-saturated flows*. Berlin : FEFLOW White Papers Vol. I, DHI-WASY GmbH.

Diersch, H.-J. G., et al. (2010). *Finite element formulation for borehole heat exchangers in modelling geothermal heating systems by FEFLOW*. Berlin : FEFLOW White Papers Vol. V, DHI-WASY GmbH.

EDTMAYER. *NÖM, Dampfkesselanlage*. [Online] [Zuletzt abgerufen am: 09. 11. 2021] https://edtmayer.at/de/referenzen/dampfkesselanlage-noem

eHYD Hydrographischer Dienst: "Karte der Hydrographie Österreichs". [Online] [Zitat vom: 07. 05 2019.]

https://ehyd.gv.at/.

Elster, D., et al. (2016). *Erläuterungen zur geologischen Themenkarte Thermalwasser in Österreich 1:500.000. - 296*. Wien : s.n.

Energielexikon: *Brennwertkessel*. [Online] [Zuletzt abgerufen am: 21.01.2020.] https://www.energie-lexikon.info/brennwertkessel.html

Fuchsluger, M., et al. (2017). DEGEN-NET. *Dezentrale geothermale Niedertemperatur-Wärmenetze in urbanen Gebieten. Endbericht*. Wien : Klima- und Energiefonds.

Gautschi, T. (2016). *Anergienetze in Betrieb*. Vortrag vom 29.01.2016 in Zürich, Amstein + Walthert.

Gegenhuber, N. (2007). *Interpretation der faziellen und hydrogeologischen Verhältnisse des Raumes Baden/Bad Vöslau aufgrund von Bohrlochmessungen und seismischen Profilen*. Magisterarbeit. Leoben : Montanuniversität Leoben.

Gmeindl, M., Niederbacher, P. und Dunkel, C. (2014). *Einreichprojekt zur wasserrechtlichen Bewilligung eines wasserwirtschaftlichen Förderversuches am Standort Gst.- Nr. 1077/2, EZ 2371, KG 4035 Bad Vöslau – Technische Beschreibung und hydrogeologische Standortbeurteilung.* s.l. : Technischer Bericht, Projekt NÖM AG, Brunnenfeld Bad Vöslau.

Gmeindl, M., Niederbacher, P. und Dunkel, C. (2013). *Orientierende Beurteilung des Grundwassernutzungspotenzials am Standort des bestehenden Brunnenfeldes – Datenauswertung Bestand und Empfehlungen zur Vorgehensweise*. s.l. : Technischer Bericht, Projekt NÖM AG, Brunnenfeld Bad Vöslau.

Götzl, G., et al. (2012). *Die Nutzbarmachung geothermischer Grundlagenforschung für das Land Niederösterreich (Thermalwassermodell Hochscholle südliches Wiener Becken)*. Endbericht. Wien : Geologische Bundesanstalt.

Götzl et al. (2017). *Dezentrale geothermale Niedertemperatur-Wärmenetze in urbanen Gebieten (DEGENT-NET)*. Publizierbarer Endbericht zum Klima- und Energiefonds/FFG Forschungsprojekt Nr. 853649.

Hans Abicht AG. (2016). *Energiekonzept Suurstoffi Rotkreuz*. Präsentation vom 11.04.2016, Hans Abicht AG, Zug.

Huber, D. (2020). *Modellierung, Simulation und Analyse von verschiedenen Rohrsonden-Typen zur Nutzung geothermischer Energie.* Wien: TU Wien.

Huber, D., Illyés, V., Turewicz, V., Hoyer, S., Götzl, G., & Ponweiser, K. (2021). *Novel District Heating Systems*: *Methods and Simulation Results*. Energies.

Huber, D., Illyés, V., Turewicz, V., Hoyer, S., Götzl, G., & Ponweiser, K. (2021). *Thermal Energy Grid Simulation (TEGSim) for Smart Urban Regions*, 9th Eur. Conf. Ren. Energy Sys. 21-23 April 2021, Istanbul, Turkey.

Kiefer, K., Farnung, B. und Müller, B. (2018). *Degradation in PV Power Plants: Theory and Practice, Fraunhofer ISE*. 36th European PV Solar Energy Conference and Exhibition, Marseille.

Klein, P. und Küpper, H. (1985). *Zur Kenntnis der hydrogeologischen Situation von Bad Vöslau (Wiener Becken, Niederösterreich).* Wien : Jb. Geol. B.-A., 127, 633 – 637.

Kröll, A. und Wessely, G. (1993). *Wiener Becken und angrenzende Gebiete: Strukturkarte – Basis der tertiären Beckenfüllung 1:200.000*. Wien : Geologische Bundesanstalt.

Land Niederösterreich: "*NÖ Atlas*". [Online] [Zitat vom: 07. 05. 2019.] http://www.noe.gv.at/.

Malm, F. (2013). *Bestimmung thermischer Untergrundparameter in Erdwärmesondenfeldern und Evaluierung tiefenaufgelöster Thermal Response Tests durch thermohydraulische Modellierungen*. Mainz : Dissertation im Promotionsfach Geologie/Paläontologie am Fachbereich Chemie, Pharmazie und Geowissenschaften der Johannes Gutenberg-Universität Mainz.

MIKE Powered by DHI. MIKE Powered by DHI. *FEFLOW - Modelling geothermal energy and heat transport processes*. [Online] [Zitat vom: 12. 05. 2020.] https://www.mikepoweredbydhi.com.

Nagler, J. (2018). *Design criteria for GCHP-systems with seasonal storage (Anergienetze).* Wien: TU WIen.

Österreichischer Wasser- und Abfallwirtschaftsverband (ÖWAV). (2009). *ÖWAV-Regelblatt 207 - Thermische Nutzung des Grundwassers und des Untergrunds - Heizen und Kühlen*. Wien : s.n.

Pervesler, P., Uchman, A. und Hohenegger, J. (2008). *New methods for ichnofabric analysis and correlation with orbital cycles exemplifiedby the Baden-Sooss section (Middle Miocene, Vienna) Geol. Carpathica*, 59, 5, 395-409.

Project GeoPLASMA-CE. (2017). *JOINT REPORT ON CHOSEN APPROACHES AND METHODS FOR CALIBRATION (D.T3.5.1).* s.l. : Interreg Central Europe.

Quaschning, H. (1998). *Höhere Flächeausbeute durch Optimierung bei aufgeständerten Modulen, 13*. Symposium Photovoltaische Solaranlagen, Staffelstein.

Rögl, F., et al. (2008). *The Middle Miocene Badenian stratotype at Baden-Sooss (Lower Austria). Geol. Carpathica*, 59, 5, 367—374.

Ruesch, F., and Haller, M. (2017). *Potential and limitations of using low-temperaturedistrict heating andcooling networks for direct cooling of buildings*. Elsevier, Energy Procedia 122 (2017) 1099-1104.

Sanner, B., et al. (2005). *Thermal Response Test – Current Status and World-Wide Application. Antalya, Turkey*: Proceedings World Geothermal Congress 2005.

Schmidt, D. et al. (2017). *Low Temperature District Heating for Future Energy Systems.* Elsevier, Energy Procedia 116 (2017) 26-38.

Schnabel, W. (1997). Blatt 58 Baden. *Geologische Karte der Republik Österreich 1: 50,000*. Wien : Geologische Bundesanstalt.

Schrammel et al. (2019). *DeStoSimKaFe Konzeptentwicklung & gekoppelte deterministisch/stochastische Simulation und Bewertung Kalter Fernwärme zur Wärme- & Kälteversorgung*. AEE INTEC, Gleisdorf.

Schweizerischer Ingenieur- und Architektenverein. (2010). *SIA-Norm 384/6 Erdwärmesonden*. Zürich : SIA Zurich.

Stadtgemeinde Baden bei Wien: "*Die Infrastruktur*". [Online] [Zitat vom: 26. 04. 2019.] http://www.baden.at/de/unsere-stadt/umwelt/wasserwerk/infrastruktur.

Umweltbundesamt. *Altlastenkataster*. [Online] [Zitat vom: 27. 05. 2020.] https://secure.umweltbundesamt.at/altlasten/?servicehandler=publicgis.

V. e. V. (2013). *VDI - Wärmeatlas*, Berlin, Heidelberg: Springer.

Verein Deutscher Ingenieure e.V. (2016). VDI 4640 Blatt 5: *Thermische Nutzung des Untergrunds - Thermal Response Test.* Düsseldorf : Beuth Verlag GmbH.

Vetterli, N. (2014), *Monitoring Suurstoffi-Areal Rich/Rotkreuz – Dynamik und Optimierung einer*

thermischen Vernetzung (Anergienetz). Hochschule Luzern, Poster im Auftrag der Zug Estates AG.

Villalva, M.G., Gazoli, J.R. and Filho, E.R. (2009). *Comprehensive Approach to Modeling and Simulation of Photovoltaic Arrays*.

Wagreich, M., et al. (2008). *Probing the underground at the Badenian type locality: geology and sedimentology of the Baden-Sooss section (Middle Miocene, Vienna Basin, Austria). Geol. Carpathica*, 59, 5, 375—394.

Wessely, G. (2006). *Niederösterreich*. 416. Wien : Geologische Bundesanstalt.

Wessely, G. (1983). *Zur Geologie und Hydrodynamik im südlichen Wiener Becken und seiner Randzone. Mitt. Geol. Ges*., 76, 27 – 68. Wien : s.n.

Wessely, G., et al. (2007). *Geologie und Paläontologie von Bad Vöslau (Niederösterreich).* Jb. Geol. B.-A., 147, 419 – 448. Wien : s.n.

12 Contact data

Dr. Edith Haslinger
AIT Austrian Institute of Technology GmbH, Center for Energy
Giefinggasse 4, 1210 Vienna, Austria
Tel.: +43 50550-3608
Mobile: +43 664 8251128
https://www.ait.ac.at

Edith Haslinger, Robin Friedrich, Veronica Vana, AIT Austrian Institute of Technology GmbH
Veronika Turewicz, Gregor Götzl, Geologische Bundesanstalt
Karl Ponweiser, Viktoria Illyés, David Huber, Technische Universität Wien
Andreas Hammer, Montanuniversität Leoben
David Stuckey, Philipp Stern, Institute of Building Research & Innovation
Peter Biermayr, ENFOS

Gerhard Bartak, NÖM AG
Gerfried Koch, Stadt Baden
Richard Niederbrucker, geohydrotherm GmbH
Franz Vogl, David Bauernfeind, beyond carbon energy

13 Annex

13.1 Geoscientific site evaluation

13.1.1 Geoelectric (DC) resistivity profiles

Locations of the two geoelectric DC resistivity measurement profiles and results of the measurement along the profiles: [1] shallow gravel-based aquifer; [2] clay and marl dominated zone and [3] a zone of increasing resistivity indicating higher sand contents or conglomerates:

(1) Location of the geoelectric DC resistivity measurement profiles

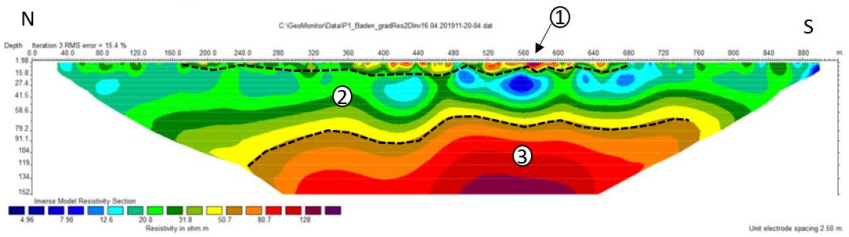

(2) Results of the resistivity measurement along profile 1

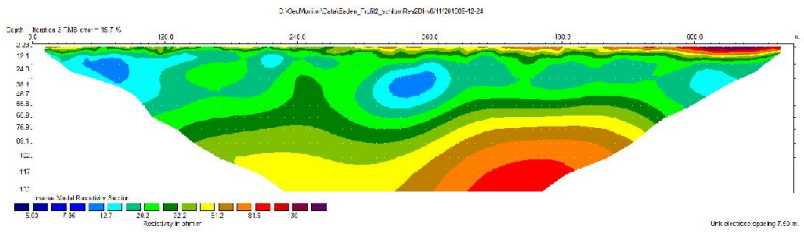

(3) Results of the resistivity measurement along profile 2

13.1.2 Profile sections used as data sources for the elaboration of the 3D model

Profile section from Bad Voeslau (Wessely, et al., 2007):

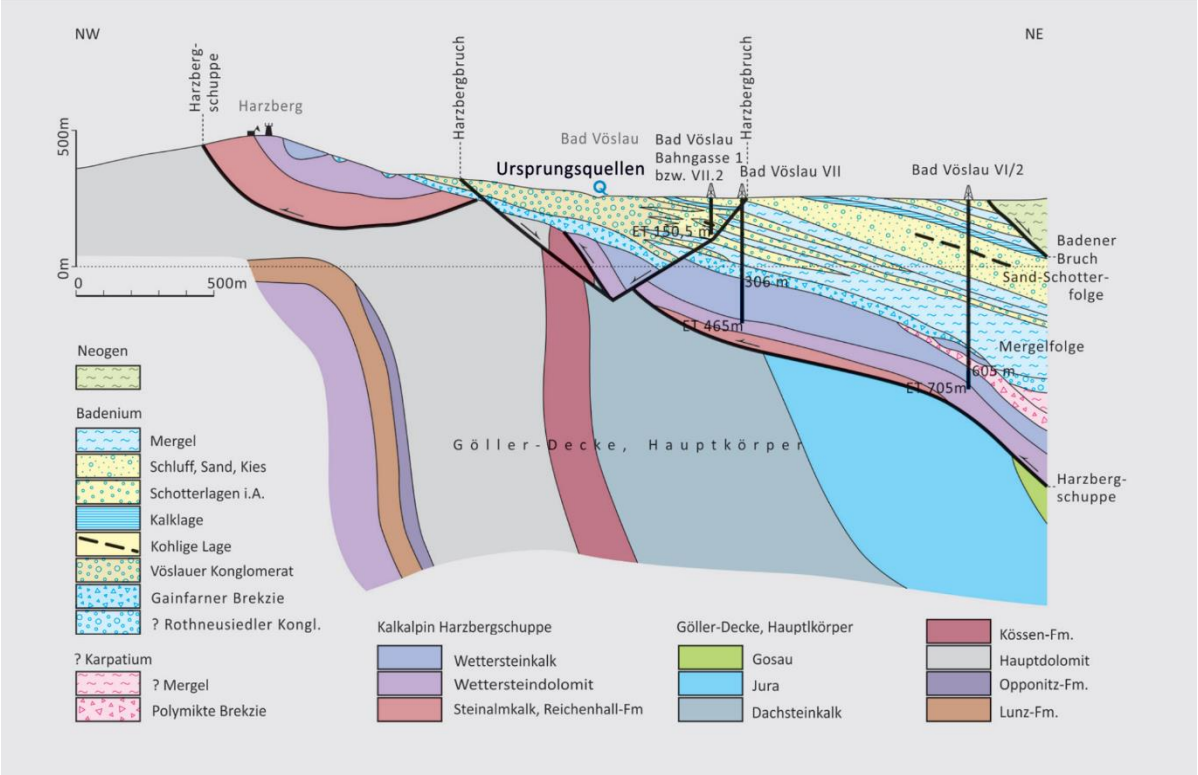

Profile section in the South (Wessely, 1983):

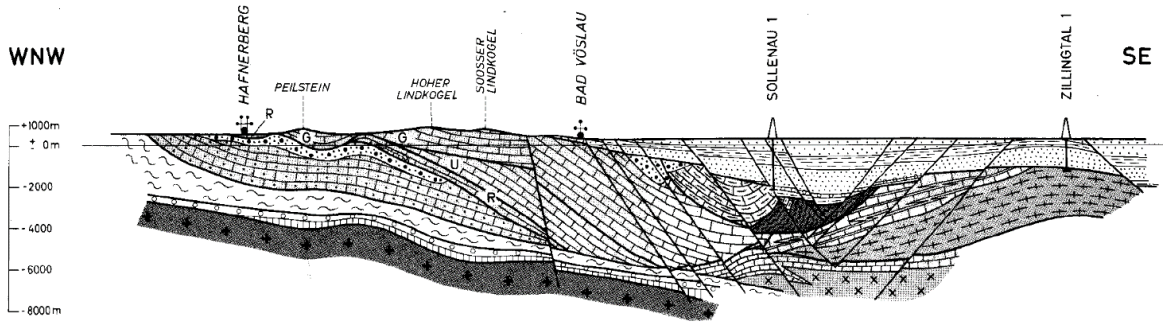

Profile section in the North (Wessely, 1983):

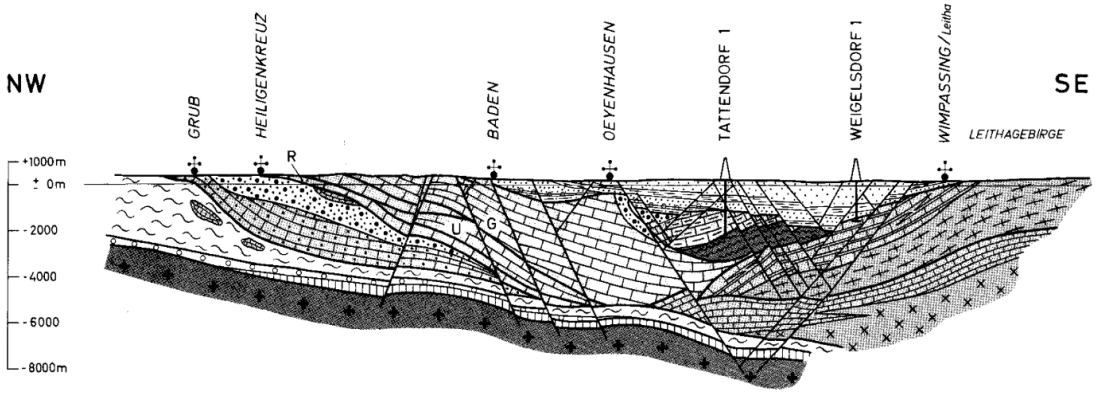

13.2 Energetic evaluation of the scenarios

13.2.1 MINI

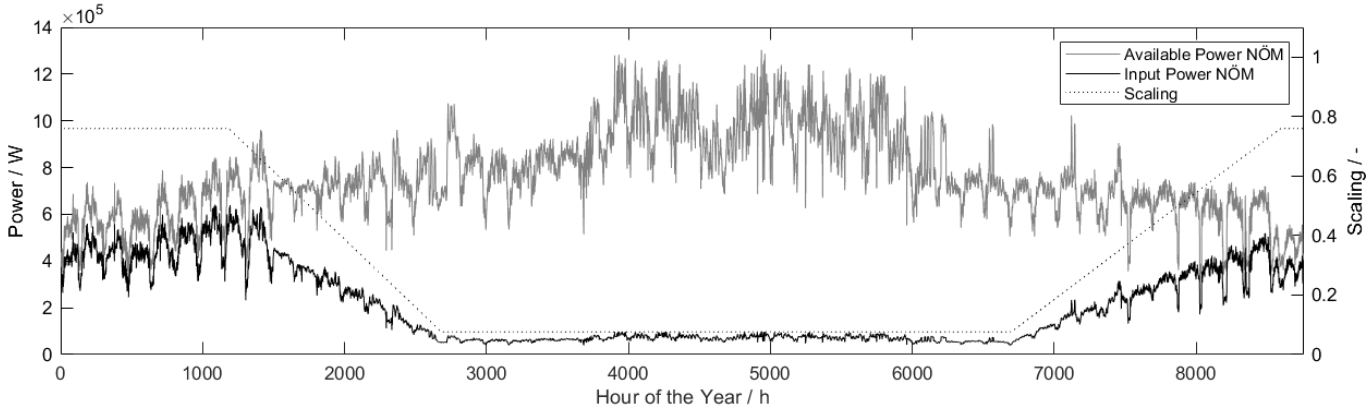

Figure 61: Power provided by NÖM, scaling, and the actual power fed into the anergy grid for scenario MINI.

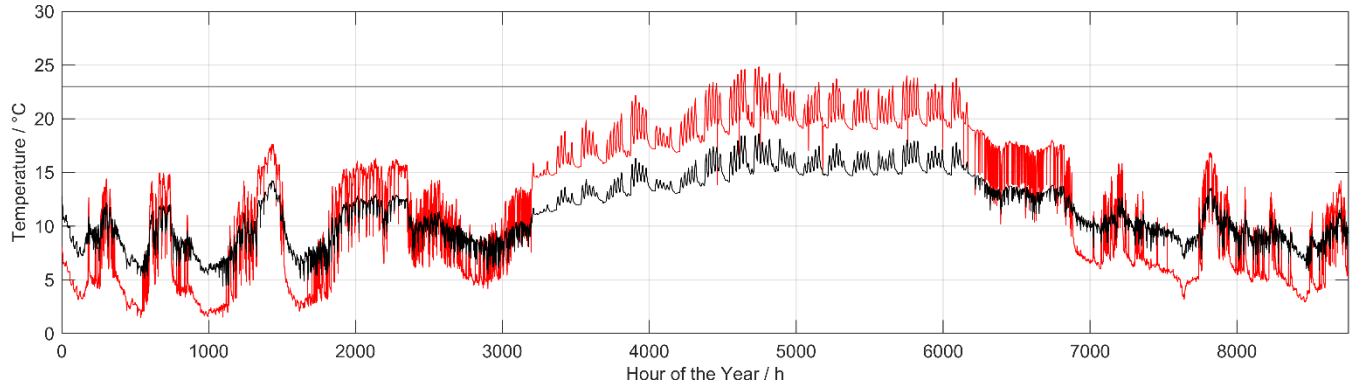

Figure 62: Average inlet and outlet temperature of the fluid into the BTES for scenario MINI.

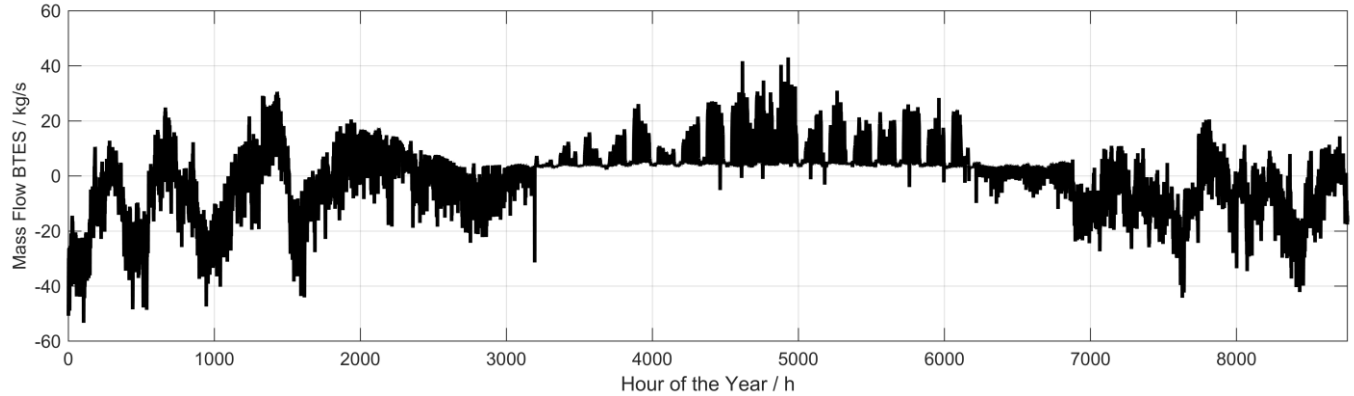

Figure 63: Mass flow at the inlet or outlet of the BTES for scenario MINI.

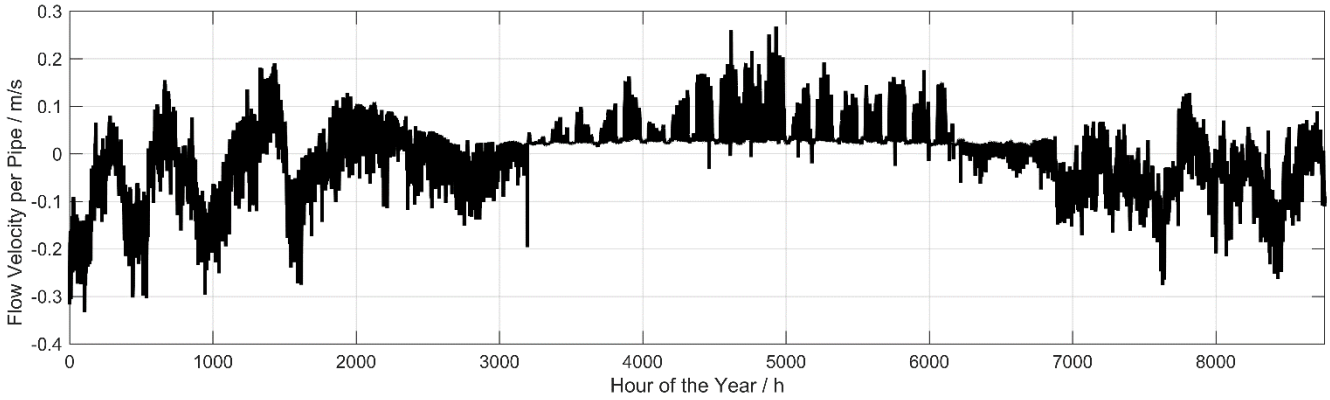

Figure 64: Flow velocity in a pipe of the BTES for scenario MINI.

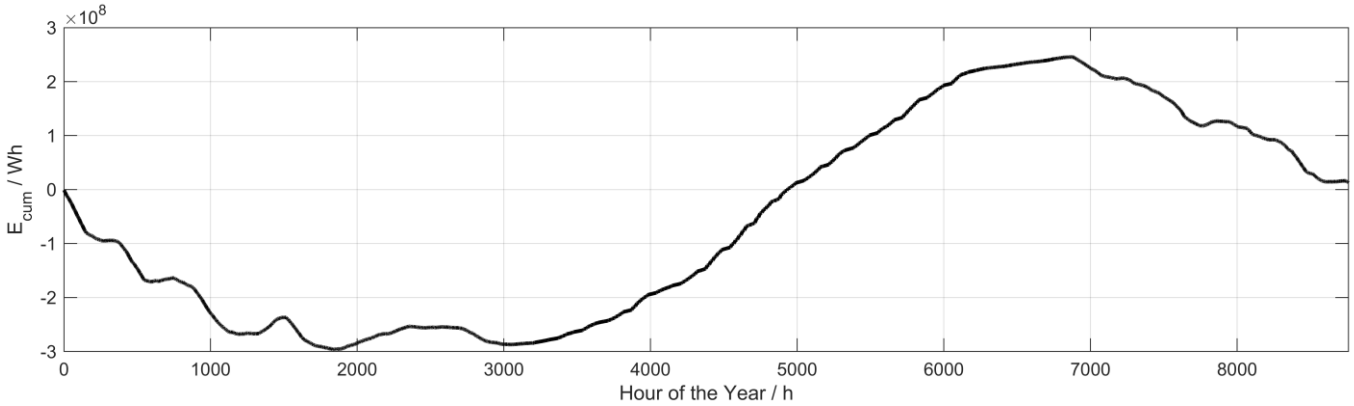

Figure 65: Cumulative energy in the BTES for scenario MINI. Unloading of the BTES at negative gradient and loading at positive gradient.

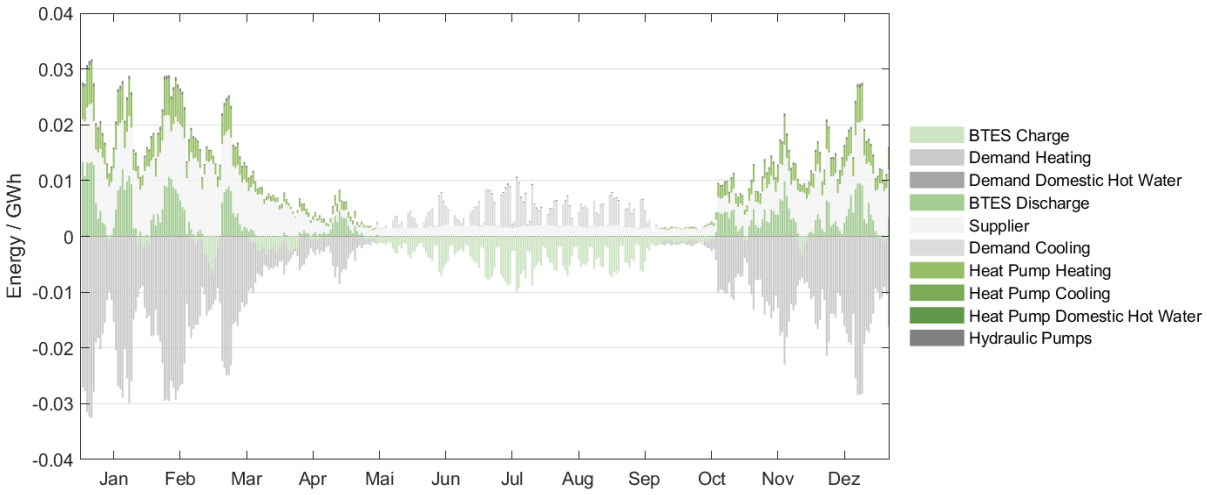

Figure 66: Energy flows of the anergy grid in daily resolution for scenario MINI.

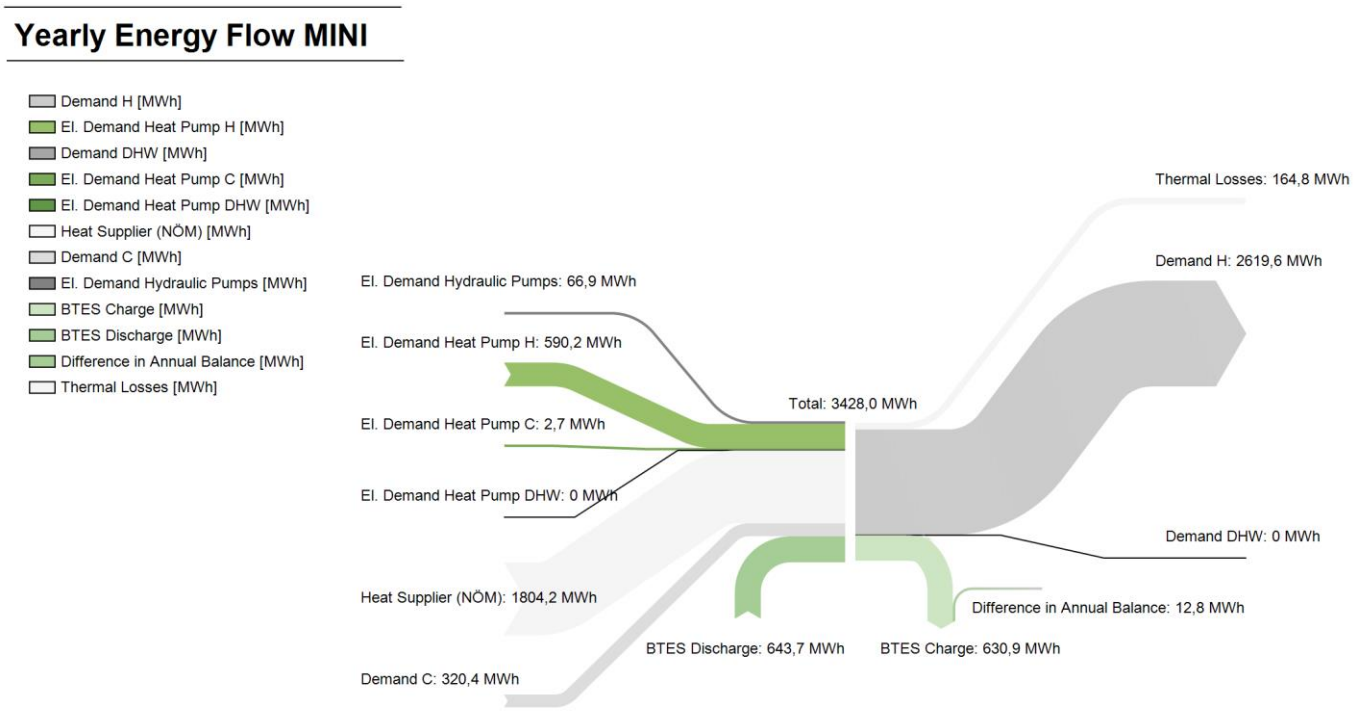

Figure 67: Sankey diagram - annual energy flows to operate the anergy network for scenario MINI.

13.2.2 MIDI

Low-temperature waste heat

The evaluation of waste heat potential revealed that four main sources of waste heat are available: hot wastewater, compressed air generation, refrigeration, and steam generation. Since the available waste heat far exceeds the required energy, waste heat is used exclusively from refrigeration generation. The measured supply temperature at the chillers connected to the refrigeration generation varies between 32 and 36 °C depending on the season. The measured temperature difference between supply and return is about 4-5 K. ULTDH networks can also take advantage of this temperature level, which is very close to the ambient temperature. The average waste heat capacity of the chillers is 1692 kW. If all the available waste heat is fed in, the temperature of the BTES and the pipe network will rise so much that FC is no longer possible. Therefore, only a fraction of the waste heat potential from the coolers is needed. However, by feeding the waste heat into the ULTDH network, the dairy cannot do without the coolers. On the one hand, because not all of the available energy can be used, and on the other hand, because the continuous production of dairy products requires high reliability of the cooling systems.

Figure 68 shows the actual power fed into the dairy. During the cooling season, approximately from hour 3400 to 6200, the available power input is much lower. This allows the temperature in the BTES and the piping system to be reduced to the point where mainly FC can be used.

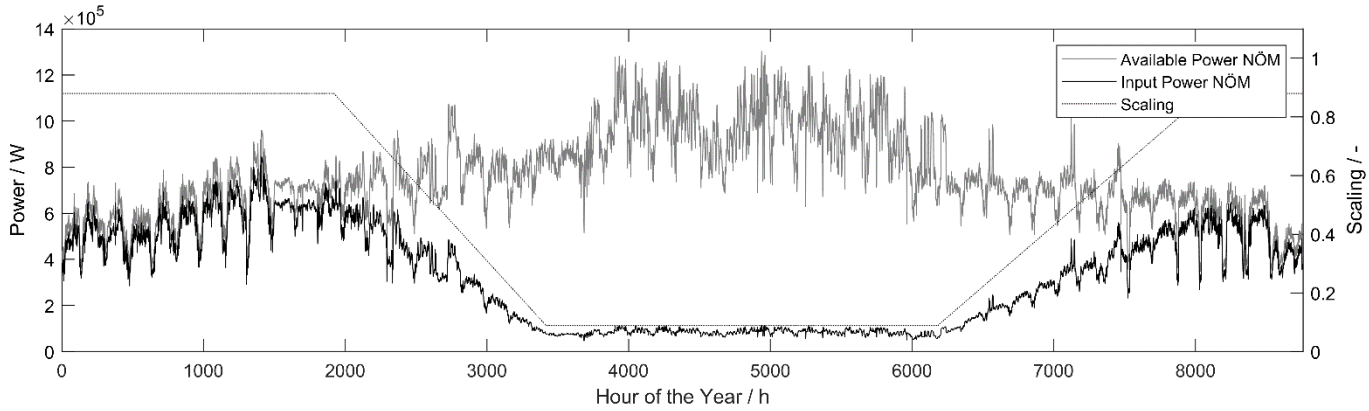

Figure 68: Power provided by NÖM, scaling, and the actual power fed into the anergy grid for scenario MIDI.

Dynamic behavior

Since the simulation calculates temperatures, pressures, and velocities at each node, much more information can be found in the curves in addition to the highest and lowest values. For example, Figure 69 shows the inlet temperature into the BTES in red and the average outlet temperature in black for one year. From hours 1 to 1400, it can be seen that the outlet temperature is higher than the inlet temperature, which means that discharging occurs in winter. The opposite is true in summer when the BTES is loaded. It is easy to see that the average temperature increases in summer and reaches its highest value. In winter, the BTES cools down significantly. Since the cooling load is predominant in summer and the excess heat from the buildings is stored in the BTES, the low-grade industrial waste heat can be reduced to a minimum. The horizontal line in Figure 69 at a temperature of 23 °C represents the boundary between FC and AC. When the return temperature to the pipe network is below 23 °C, the required cooling demand can be met very efficiently by FC. At higher return temperatures, heat can still be extracted from the rooms to be cooled, but the upper-temperature limit of 23 °C ensures the necessary living comfort.

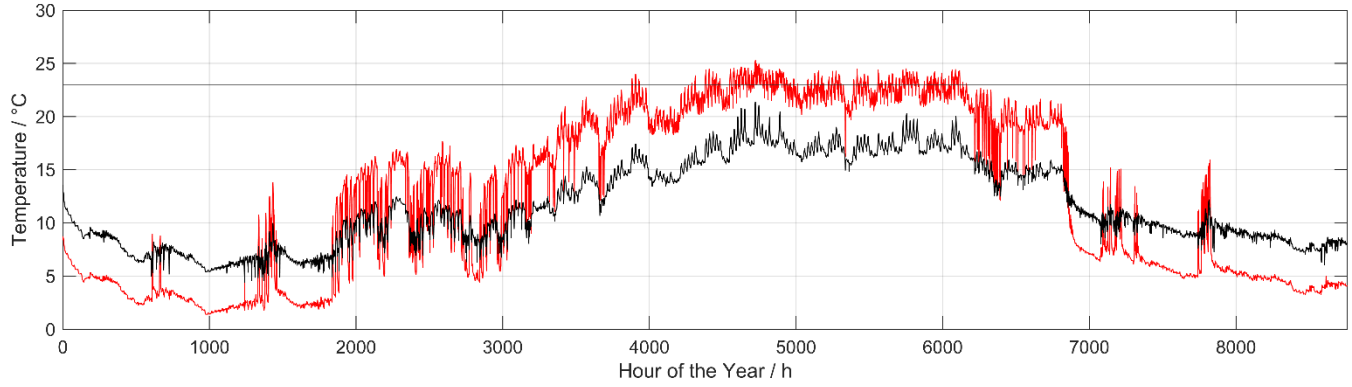

Figure 69: Average inlet and outlet temperature of the fluid into the BTES for scenario MIDI.

The BTES is charged a few times during the heating period at hourly 750, 1400, 7200, and 7800, which is reflected in a positive sign of the mass flow and flow velocity, respectively, in Figure 70 and Figure 71. The changing sign of the mass flow is due to the complex interaction of low heat demand and high

amounts of energy injected by the NEG. The transitional seasons in spring and fall are characterized by frequent changes in loading and unloading and fluctuating supply temperatures. The highest mass flows are required in summer when cooling demand and grid temperatures are high.

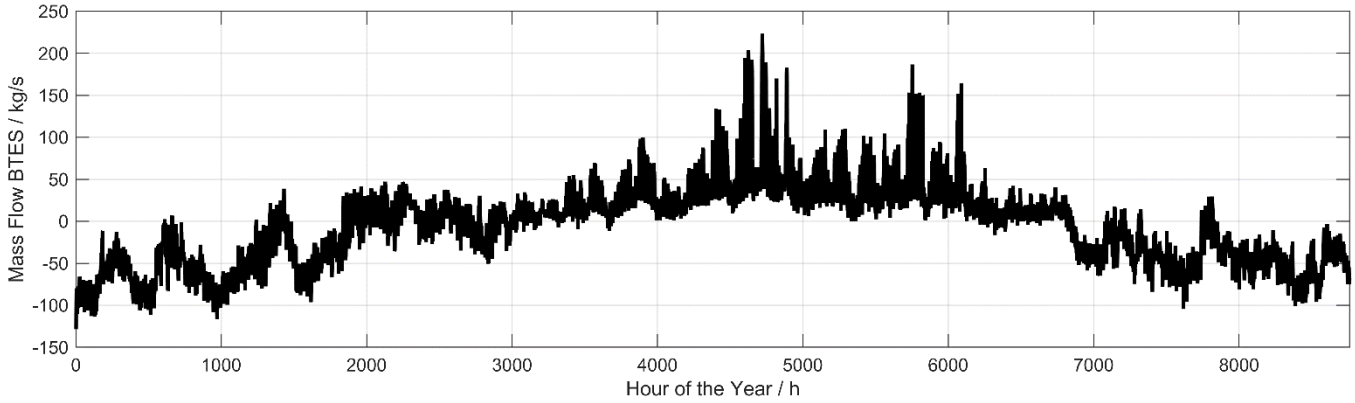

Figure 70: Mass flow at the inlet or outlet of the BTES for scenario MIDI.

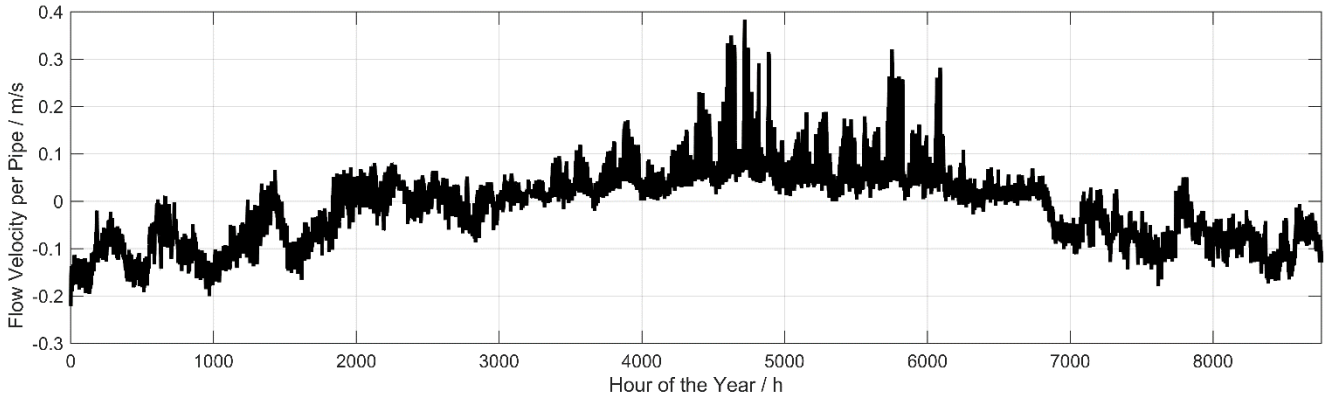

Figure 71: Flow velocity in a pipe of the BTES for scenario MIDI.

The aggregated energy of the BTES shows a steady trend near the ideal sinusoid, see Figure 72. A negative slope means that the BTES is being discharged, and a positive slope means that it is being charged. Thus, the BTES is charged during the cooling period between hours 1800 and 6800 and discharged during the rest of the time - the heating period. The BTES can only be used as a seasonal thermal store for a longer period of time if the same amount of energy is discharged during the heating period as is charged during the cooling period. In this scenario, the BTES is operated at almost perfect balance.

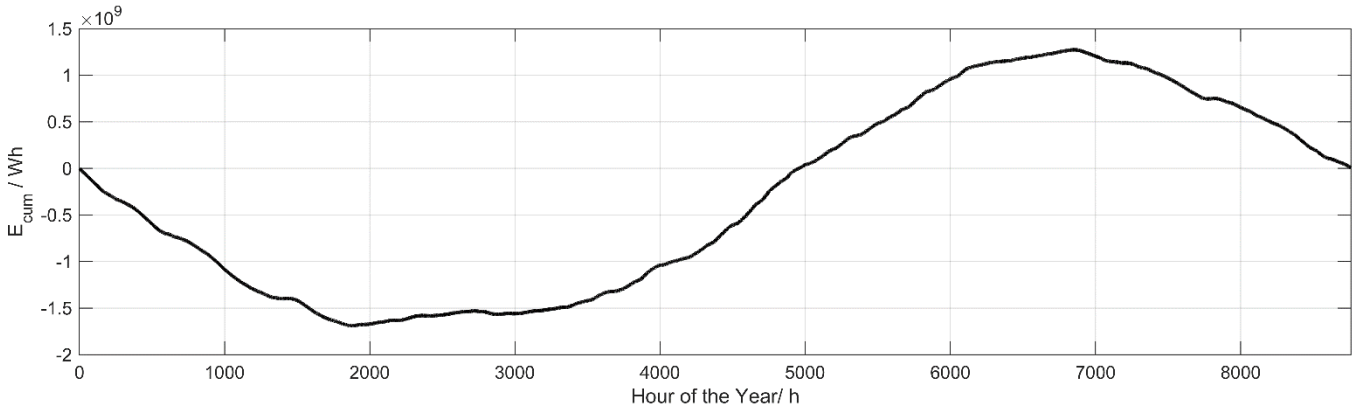

Figure 72: Cumulative energy in the BTES for scenario MIDI. Unloading of the BTES at negative gradient and loading at positive gradient.

Share of AC and FC

A maximum permissible indoor temperature of 26 °C was assumed when simulating the cooling demand of the buildings. The maximum allowable indoor temperature may exceed eight hours per year to dampen any peak loads. Table 20 provides an overview of the prosumer´s cooling demand. Compared to the existing buildings with a maximum of two stories, some of the newly constructed buildings (V12_1, V13_1, V13_2, and V14_1) are up to five stories high. The large GFAs are reflected in high cooling requirements. The proposed new buildings in Scenario MIDI alone account for 71.2% of the total cooling demand. Specific cooling demand depends on geographic location, building structure, the ratio of window area to façade area, and building use, among other factors. In the category Gastro, Event, Shop, the specific cooling demand is highest with an average of 37.43 kWh/a/m2. The specific cooling demand is generally higher for new buildings than for existing buildings. The reason for this is the higher proportion of windows in the facade area in new buildings from the MIDI scenario, 10% compared to 30%.

Table 20: Prosumer cooling demand for scenario MIDI, duration of the cooling period, and whether provided by AC or FC.

Prosumer	E^C	e^C	p^C	t^{FC}	t^{AC}	t^C
-	MWh_{th}/a	$kWh_{th}/a/m_2$	%	h	h	h
V11_1	23,33	6,30	0,8	1401	1147	2548
V12_1	466,01	15,53	16,6	1047	1955	3002
V03_1	71,44	5,21	2,5	606	1877	2483
V13_1	581,63	26,44	20,7	2365	1543	3908
V13_2	219,18	14,61	7,8	841	2146	2987
V14_1	734,90	27,22	26,1	1747	241	1988
V05_1	72,75	19,50	2,6	1196	195	1391
V04_1	177,27	39,88	6,3	2346	163	2509
V04_2	155,48	34,98	5,5	2343	164	2507
V02_2	78,74	6,43	2,8	1204	301	1505

V02_1	177,27	14,45	6,3	1192	312	1504
V01_1	58,01	5,11	2,1	1238	258	1496

Whether a prosumer is cooled with AC or with FC depends exclusively on the supply temperature in the pipe network. As shown in Figure 73, prosumers V11_1, V12_1, V03_1, V13_1, and V13_2 are supplied with FC to a maximum of 60%. In contrast, prosumers V14_1, V05_1, V04_1, V04_2, V02_2, V02_1, and V01_1 are cooled by AC for more than 80%. On the one hand, the reason is the generally longer cooling period of prosumers V11_1, V12_1, V03_1, V13_1, and V13_2, see Table 20. Towards the end of the cooling season, the BTES is already too warm to cool buildings with FC. On the other hand, in the area where prosumers with very high cooling demand (V12_1, V13_1, V13_2) are located, the water in the pipe system is heated quickly. Therefore, prosumers with low cooling demands (V11_1, V03_1) near prosumers with high cooling demands are no longer adequately cooled with FC, see Figure 73. It can be concluded that prosumers with small cooling loads can be cooled less effectively with FC next to prosumers with high cooling loads. This often results in financial disadvantages for prosumers with small cooling loads due to higher electricity costs for reversible heat pump operation. In contrast, however, the position of the prosumer cannot be changed in most cases.

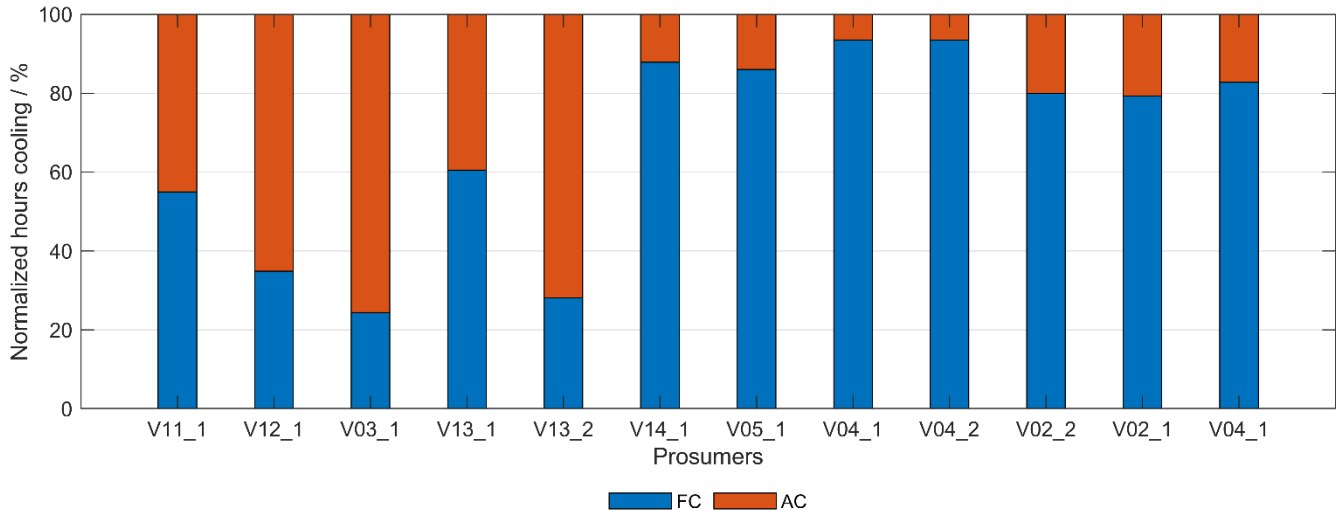

Figure 73: Normalized share of FC and AC for the considered prosumers in scenario MIDI.

Energy flows

Together with other parameters, such as configuration and number of ETS, grid topology, size of BTES, and waste heat costs, these results allow an economic evaluation of the investigated power system. Figure 74 shows the electrical and thermal energy flows of the studied use case in daily resolution. Negative bars indicate the demand flows of the overall system and include the energy demand for heating, hot water production, and loading the BTES. Positive bars show the supply flows of energy due to unloading of the BTES, injection of waste heat, cooling, and the electrical energy for the heat pumps and circulators. The magnitudes of the demand and supply flows are identical except for the thermal

losses. It is easy to see that the energy demand during the heating period is mainly covered by the discharge of the BTES and by the additional energy supplied by the NEOC. During the cooling period, the required cooling energy is provided almost exclusively by loading the BTES. The energy supplied by the NEG is reduced to a minimum during this period. In addition, it is easy to see that the demand for electrical energy increases on days with high cooling loads by switching on the reversibly operating heat pumps.

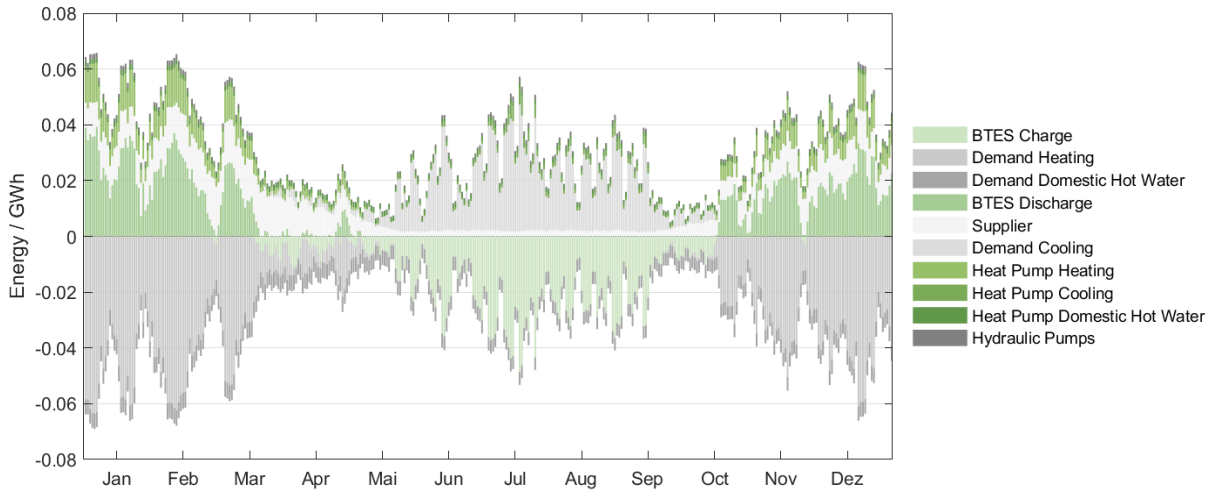

Figure 74: Energy flows of the anergy grid in daily resolution for scenario MIDI.

13.2.3 MAXI

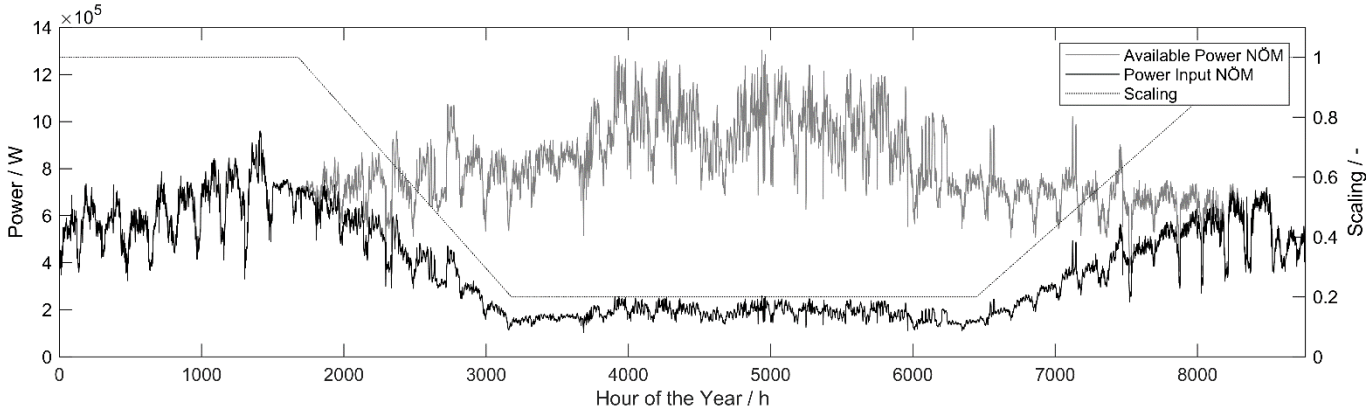

Figure 75: Power provided by NÖM, scaling, and the actual power fed into the anergy grid for scenario MAXI.

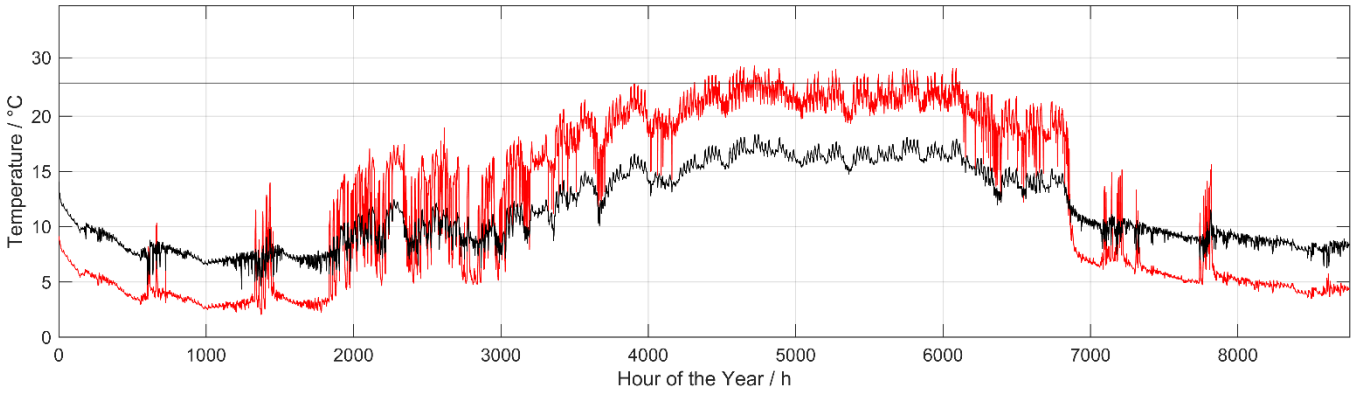

Figure 76: Average inlet and outlet temperature of the fluid into the BTES for scenario MAXI.

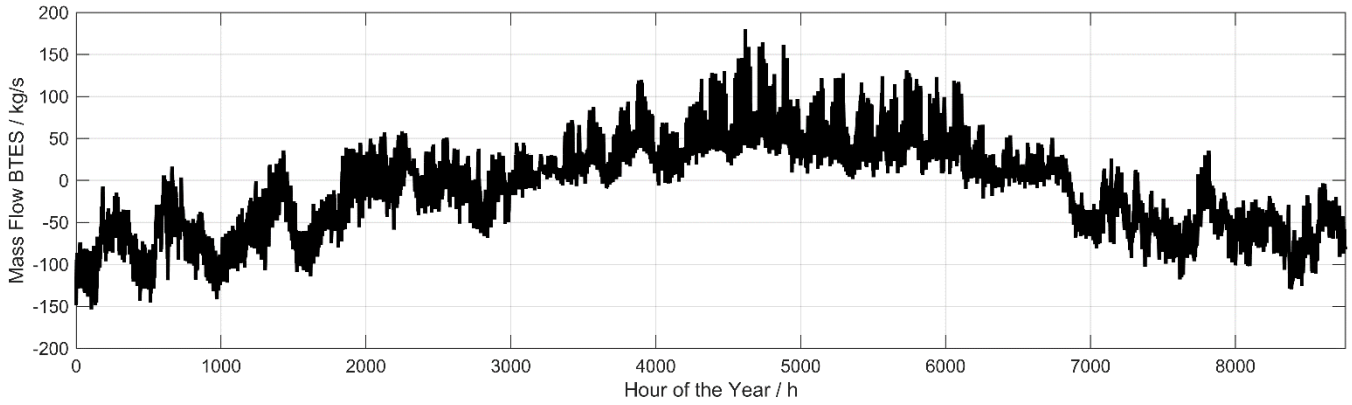

Figure 77: Mass flow at the inlet or outlet of the BTES for scenario MAXI.

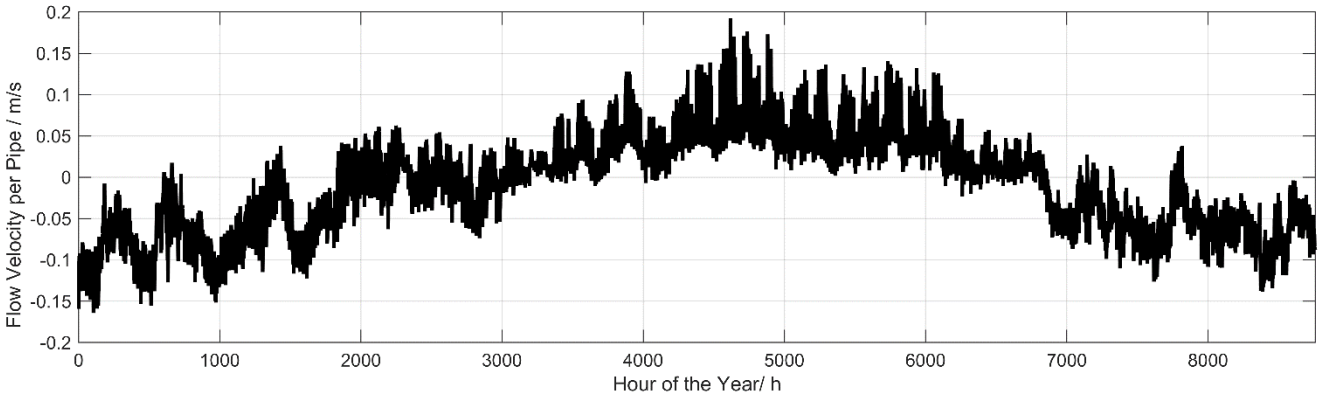

Figure 78: Flow velocity in a pipe of the BTES for scenario MAXI.

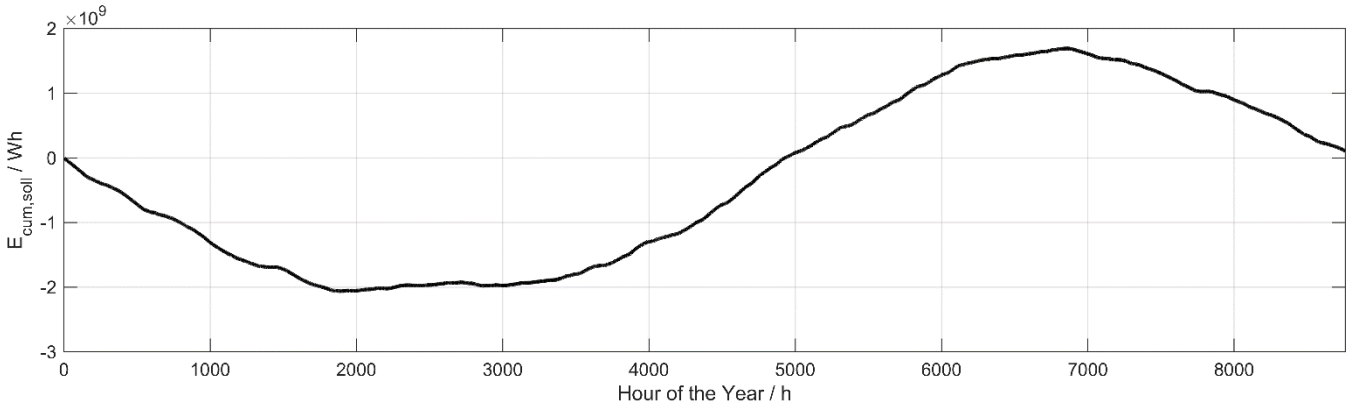

Figure 79: Cumulative energy in the BTES for scenario MAXI. Unloading of the BTES at negative gradient and loading at positive gradient.

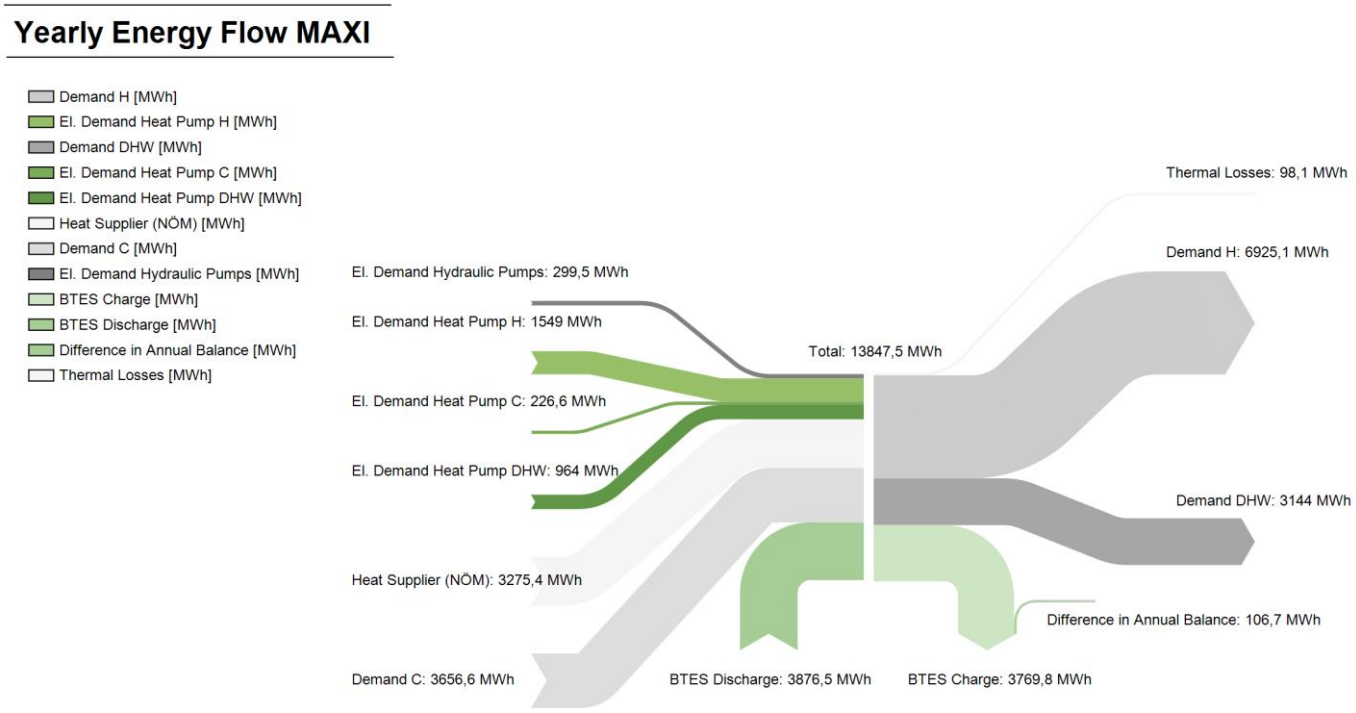

Figure 80: Sankey diagram - annual energy flows to operate the anergy network for scenario MAXI.

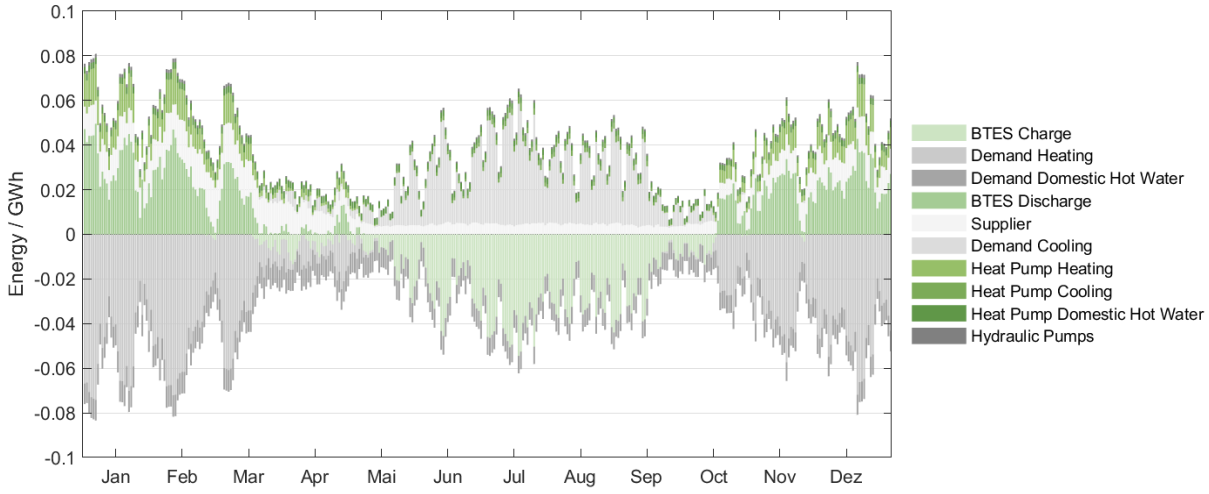

Figure 81: **Energy flows of the anergy grid in daily resolution for scenario MAXI**.

14 List of Figures

Figure 1: Illustration of the general concept of a low-temperature heating and cooling grid 8
Figure 2: Satellite view of the “Martinek Kaserne” and the NÖM dairy plant 9
Figure 3: Pictures of the interior of the buildings and the outside area. 11
Figure 4: Locations of water facilities 15
Figure 5: Geological cross section at the Martinek former military camp in Baden 17
Figure 6: Location and results of the DC resistivity measurement at the Martinek military camp 18
Figure 7: 150 m flush drilling and 30 m core drilling drilled at the site of the NÖM plant 19
Figure 8: Cross section 1 and 2 of the elaborated hydrogeological 3D model. 20
Figure 10: Evaluated depth-dependent thermal conductivities and lithological profile 22
Figure 10: Temperature profiles of the underground 23
Figure 13: 3D subsurface model 25
Figure 14: Relative deviations between the simulation results of the tool and FEFLOW 26
Figure 15: Inlet temperature into the BTES for one operating year of the MINI scenario 26
Figure 16: The resulting outlet temperatures of the programmed tool and FEFLOW 28
Figure 17: Simplified heat load capacities and mass flow for each borehole heat exchanger 29
Figure 18: Vertical sections of the subsurface model in the tenth simulation year 30
Figure 19: Grid plan of three scenarios, left: MINI, middle: MIDI, right: MAXI 33
Figure 20: Subareas relevant for scenario development - MINI 34
Figure 21: Breakdown by usage category for scenario MINI 35
Figure 22: Development-relevant subareas for scenario MIDI 35
Figure 23: Breakdown by usage category for scenario MIDI 36
Figure 24: Development-relevant subareas for scenario MAXI 37
Figure 25: Breakdown by usage category for scenario MAXI 38
Figure 26: Overview of the identified waste heat potentials 39
Figure 27: Temperature curve of the two wastewater streams from the CIP processes 40
Figure 28: Curves of the heat output and the exergy factor for the wastewater 41
Figure 29: Boiler plants for process steam generation 42
Figure 30: Trend of heat output from Off-gas stream July 2018 to June 2019 43
Figure 31: Changes of the energy or exergy level from steam production to wastewater. 43
Figure 32: Ultrasonic flow measurement at the cold brine line (left) and the warm brine line (right). 44
Figure 33: Trend of heat output and exergy factor of fresh products logistics FRILO 45
Figure 34: Illustration of the available heating power and its exergetic part. 47
Figure 35: Measurements on the HDD systems: Atlas Copco (left) - LMF (right) 48
Figure 36: Profile of heat output of high-pressure compressed air systems for the year 2019. 49
Figure 37: Sankey diagram to illustrate the exergy or anergy flow of a compressed air system. 49
Figure 38: Circuit diagram of a PV cell / diode model 50
Figure 39: Suitable roof surfaces of the NÖM dairy 50
Figure 40: PV performance profiles for the location of the NÖM dairy in Baden 51
Figure 41: Flowchart of the thermal-hydraulic calculation scheme for one hydraulic calculation step 55

Figure 42: RCM for a segment of the pipe network and the surrounding soil 57
Figure 43: RCM for a segment of a 2U pipe BHE and the surrounding soil 58
Figure 44: Schematic hydraulic diagram of a fully equipped ETS and its main components 60
Figure 45: Schematic temperature curve down to a depth of 30 m for different seasons 63
Figure 46: Energy demand for heating and cooling of the three utilization scenarios 67
Figure 47: Aerial photograph of the ensemble with marking of the object 24 69
Figure 48: Damage patterns in different indoor spaces.....71
Figure 49: Damage to ceiling and walls due to moisture ingress 72
Figure 50: Cellar room with considerable water ingress.....73
Figure 51: Damage to parquet flooring 73
Figure 52: Interior with considerable moisture damage.....74
Figure 53: Orthophoto of the barracks site with designated area of monument protection 79
Figure 54: Aerial view with buildings approved for demolition 79
Figure 55: Views of the listed existing buildings in the area of the Martinek military camp 84
Figure 56: Comparison of the absolute and relative costs of the investigated SANBA scenarios.....87
Figure 57: Dynamic development of the deposits and payments in the scenarios MINI and MAXI 88
Figure 58: Capital values depending on the electricity price and the calculation interest rate 90
Figure 59: Internal interest rate depending on the electricity price. 90
Figure 60: Service specific prices for various pipe diameters.....92
Figure 61: Power specific net price of brine/water heat pump units 93
Figure 76: Sankey diagram - annual energy flows to operate the anergy network for scenario MIDI. 97
Figure 62: Power provided by NÖM, scaling, and the actual power fed into the anergy grid MINI.....106
Figure 63: Average inlet and outlet temperature of the fluid into the BTES for scenario MINI. 106
Figure 64: Mass flow at the inlet or outlet of the BTES for scenario MINI.....106
Figure 65: Flow velocity in a pipe of the BTES for scenario MINI.....107
Figure 66: Cumulative energy in the BTES for scenario MINI. 107
Figure 68: Energy flows of the anergy grid in daily resolution for scenario MINI. 107
Figure 69: Sankey diagram - annual energy flows to operate the anergy network for scenario MINI. ...108
Figure 69: Power provided by NÖM, scaling, and the actual power fed into the anergy grid MIDI.....109
Figure 70: Average inlet and outlet temperature of the fluid into the BTES for scenario MIDI. 109
Figure 71: Mass flow at the inlet or outlet of the BTES for scenario MIDI.....110
Figure 72: Flow velocity in a pipe of the BTES for scenario MIDI.....110
Figure 73: Cumulative energy in the BTES for scenario MIDI. 111
Figure 74: Normalized share of FC and AC for the considered prosumers in scenario MIDI.....112
Figure 75: Energy flows of the anergy grid in daily resolution for scenario MIDI. 113
Figure 77: Power provided by NÖM, scaling, and the actual power fed into the anergy grid MAXI. 113
Figure 78: Average inlet and outlet temperature of the fluid into the BTES for scenario MAXI. 114
Figure 79: Mass flow at the inlet or outlet of the BTES for scenario MAXI. 114
Figure 80: Flow velocity in a pipe of the BTES for scenario MAXI.....114
Figure 81: Cumulative energy in the BTES for scenario MAXI.....115
Figure 82: Sankey diagram - annual energy flows to operate the anergy network for scenario MAXI. ..115
Figure 83: Energy flows of the anergy grid in daily resolution for scenario MAXI. 116

15 List of Tables

Table 1: Overview of the depth ranges and chosen thermal properties 27
Table 2: Categories for future utilization of buildings 31
Table 3: Energy demand of the existing building stock according to the energy certificate. 32
Table 4: Preliminary values of scenarios 32
Table 5: Building-specific data for scenario MINI 34
Table 6: Building-specific data for scenario MIDI 36
Table 7: Building-specific data for scenario MAXI 37
Table 8: Energy yields of the years 2016 and 2011 52
Table 9: Temperature differences and pinch point at the different heat exchangers 61
Table 10: Tiefenabhängige thermophysikalische Parameter des Untergrunds 63
Table 11: Constant thermophysical parameters of the subsurface 64
Table 12: Design strategies for the anergy network and its components 64
Table 13: Existing exterior wall construction 70
Table 14: Ceiling above upper floor of the existing building stock 70
Table 15: Ceiling above basement of the existing building stock 70
Table 16: Window stock 71
Table 17: Network figures for the three SANBA-scenarios. 85
Table 18: Assumptions and basic parameter values for the following presentation of results 86
Table 19: Low temperature waste heat compared to energy input (gas and electricity) 98
Table 20: Prosumer cooling demand for scenario MIDI 111